Design and Optimization of Dielectric Resonator Antenna Arrays Based on Substrate Integrated Waveguide Technology for Millimeter-Wave Applications

By

Mona Sabry Abdalla Abousheishaa

A Thesis Submitted in Partial Fulfillment

of the Requirements for the Degree of

Doctorate of Philosophy

in

Electrical and Computer Engineering

University of Ontario Institute of Technology

May, 2016

ABSTRACT

With the lower frequency bands heavily crowded, the millimeter wave (MMW) frequency band has attracted a lot of attention, offering a wide range of applications. It also introduces new challenges to the research community. Antennas and MMW circuits with compact size, low cost, high efficiency, and low loss are much needed to meet the new requirements of these applications.

This research focuses on the design and optimization of dielectric resonator antenna (DRA) arrays based on substrate integrated waveguide (SIW) technology, which has been proven to be promising for MMW applications. The objectives include both the development of highly efficient computer aided design and optimization techniques, and the development of new designs based on the SIW-DRA technology.

Toward these objectives, an efficient and accurate circuit model is developed first. A previously reported structure of DRA array is investigated based on two different slot orientations. The total mutual coupling between antennas is firstly extracted and modeled as a two port S-parameters. Two different methods are used to extract the total mutual coupling due to the difference of the slot configurations. Next, a new and fully adjustable model for the mutual coupling is developed for DRA array, resulting in a flexible circuit model allowing the design parameters to be varied. A comparison with full wave simulation and measurement results proves that the circuit model can be used as an efficient design and optimization tool.

The model is further verified through a new design of SIW-series fed DRA parasitic array, in which an additional parasitic DRA is added on both sides of each active element to improve the gain. The antennas are fed using longitudinal slots on SIW. Due to the configuration of the antenna elements, there is strong mutual coupling between the antenna elements. The good agreement between the electromagnetic (EM) simulated and circuit model results for this design further proves the efficiency of the model.

Next, a new design of an eight-element SIW middle fed series rectangular DRA array with 45° linear polarization is developed. The implicit space mapping (ISM) technique is applied for the optimization of the complex structure. The new circuit model plays an important role in the optimization method serving as the coarse/surrogate mode, and a full wave solver is used as the fine model. Parameters in the surrogate model are divided into pre-assigned parameters and design parameters. In each iteration, the pre-assigned parameters are extracted so that the fine model and surrogate model outputs match. The design parameters are then re-optimized and fed to the fine model. As demonstrated with this DRA array design, the optimization approach combining the developed circuit model with ISM technique is highly efficient. Only three iterations are needed to reach an optimized solution for such a complex structure.

The optimized design has been fabricated using a low cost Printed Circuit Board (PCB)-based technology for validation of both performance of the design and modeling techniques. The comparison between the simulated and the measured results shows very good agreement.

To

My grandmother's flowery and sensational memory, to my dearest parents, and family in Egypt, to my loving husband, and to my lovely children.

Acknowledgments

First, I would like to thank God for his blessing and for giving me wonderful family, whose love, encouragement and support have been my source of inspiration. I am eternally grateful to all of them for the sacrifices they have made so that I can reach this important goal of my life.

I would like to express my heart-felt thanks to my supervisor Dr. Ying Wang, whose insights and invaluable advices have helped me reach this special milestone. I would also like to present my deepest gratitude to her for her supervision and keen support throughout the duration of this research.

I would like to express my sincere thanks to Dr. Wael Abdel-Wahab, who is always willing to help, has patiently answered so many of my questions, and provided invaluable help with the measurements.

I wish to express my sincere gratitude to all members of the Department of Electrical, Computer, and Software Engineering for a warm and friendly environment.

Special and warmest thanks from my heart to my loving husband Tamer for his encouragement, patience, and support, especially during the past five years. I also want to express appreciations to my beloved son Moustafa and little angel Nour, for their emotional support and understanding that help me through this journey.

Last but not least, I would like to thank my loving family in Egypt for their prayers, support, and patience with me during difficult times.

Table of Contents

List of Figures

List of Tables

List of Acronyms

Abbreviation	Abbreviation
ADS	Advanced Deign System
CPW	Coplanar Waveguide
DIG	Dielectric Image Guide
DRA	Dielectric Resonator Antenna
EIRP	Effective Isotropically Radiated Power
EM	Electromagnetic
FEM	Finite Element Method
HFSS	High Frequency Structural Simulator.
ISM	Implicit Space Mapping
LP	Linear Polarization
MMW	Millimeter Wave
PCB	Printed Circuit Board
PE	Parameter Extraction
RWG	Rectangle Waveguide
RF	Radio Frequency
SIC	substrate Integrated Circuit

SIW	Substrate Integrated Waveguide
SLL	Side Lobe Level
SM	Space Mapping
SoS	System-on-Substrate
VSWR	Voltage Standing Wave Ratio

Chapter 1

Introduction

1.1 Motivation

Millimeter wave (MMW) covers frequency range from 30 GHz to 300 GHz. Systems operating at MMW frequency bands have a wide range of applications, and offer many advantages over those operating at the lower frequency bands. For example, compared to microwave imaging system (3 – 30 GHz), MMW systems are more compact and offer better spatial resolution. For wireless communications, compared to the heavily crowded lower frequency bands, MMW systems are capable of massive data rate. At the same time, it also introduces new challenges to the research community. For instance, conductor loss become significant for metallic components as the frequency increases, which degrades the overall efficiency of the system. Antennas and MMW circuits with compact size, low cost, high efficiency, and low loss are much needed to meet the new requirements of these applications.

In recent years, there has been extensive research on the dielectric resonator antennas (DRAs) due to the fact that they have no conductor loss, and are easy to fabricate in this frequency

range [1]. Besides high radiation efficiency, DRAs also offer compactness, light weight, low cost, and wide bandwidth. There are different methods for feeding DRAs such as transmission line, coaxial probe, microstrip line, coplanar waveguide, and substrate integrated waveguide.

Substrate integrated waveguide (SIW) technology shows a promising approach for the fabrication of compact, low-loss, and low cost components, circuits, antennas and complete systems at microwave and millimeter-wave band. The interest in SIW technology is increasing in the last decade. It allows integration of passive and active components, and antennas in a single substrate, thus avoiding transitions and reducing losses and parasitic effects. For example, entire wireless systems can be integrated using SIW technology, according to the system-on-substrate (SoS) technique. SIW is a good choice for feeding the DRAs operating at millimeter wave band. Using SIW as the feeding structure minimizes the conductor loss compared to other traditional feeding networks. It is a closed guiding structure that keeps the excitation fields inside, which subsequently enhances the overall antenna radiation efficiency. The SIW consists of two solid conductor planes, separated by a dielectric substrate, with conductor sidewalls realized by rows of metalized through-plated vias, and it can be fabricated by a standard printed circuit board (PCB) technology [2].

The SIW and the DRAs are an excellent candidate for millimeter-wave applications when combined together [3]. This combination has achieved high gain antennas and arrays with high radiation efficiency.

The difficulty in the fabrication of antenna array, especially in the millimeter wave frequency range due to the small size, requires that the design to be carefully simulated and optimized. Design and optimization of an antenna array usually rely on accurate yet time

consuming full wave electromagnetic (EM) simulations, which can be challenging due to the size and complexity of the entire structure. Circuit models, on the other hand, are generally fast and much less computationally intensive, but without the required accuracy. The well-known space mapping (SM) techniques has been proven to be very effective in the optimization of different types of radio frequency (RF)/microwave circuits, in which design optimizations involve combination of precise EM models and fast coarse/surrogate models. However, the coarse model is dependent on the specific design and not readily available, especially for complex structures such as antenna arrays. New development in technology is putting demand on modeling and optimization techniques for first pass success.

1.2 Contributions

This research focuses on the design and optimization of dielectric resonator antenna (DRA) arrays based on substrate integrated waveguide (SIW) technology for millimeter-wave applications. The objectives include both the development of highly efficient computer aided design and optimization techniques, and the development of new designs based on the SIW-DRA technology.

Toward these objectives, an efficient and accurate circuit model is developed first. A previously reported structure of SIW series fed DRA array is investigated based on two different slot orientations, namely transverse and longitudinal slots. The total mutual coupling between antennas is firstly extracted and modeled as a two port S-parameters. Two different methods are

used to extract the total mutual coupling due to the difference of the slot configuration. Next, a new and fully adjustable model for the mutual coupling is developed for DRA array, resulting in a flexible circuit model allowing the design parameters to be varied. Comparison with full wave simulation and/or measurement results proves that the circuit model can be used as an efficient design and optimization tool.

The model is further verified through a new design of SIW-series fed DRA parasitic array. Parasitic elements are usually used to increase bandwidth or improve the gain [4], by placing parasitic elements on one side of the active element. In this design, an additional parasitic DRA is added on both sides of each active element. The antennas are fed using longitudinal slots on SIW. Due to the configuration of the antenna elements, there is strong mutual coupling between the antenna elements. The good matching between the simulated and circuit model results for this design further proves the efficiency of the model.

Next, a new design of an eight-element SIW middle fed series rectangular DRA array with 45° linear polarization is developed. We propose to apply implicit space mapping (ISM) technique for the optimization of the complex structure, which combines a coarse/surrogate model and a full wave solver as the fine model. In general, quality of the coarse model is very important for the performance of space mapping optimizations. The new circuit model plays an important role in the optimization method serving as the coarse/surrogate mode. Parameters in the surrogate model are divided into pre-assigned parameters and design parameters. In each iteration, the pre-assigned parameters are extracted so that the fine model and surrogate model outputs match. The design parameters are then re-optimized and fed to the fine model. As demonstrated with this DRA array design, the optimization approach combining the developed circuit model with ISM technique is

highly efficient. Only three iterations are needed to reach an optimized solution for such a complex structure with EM simulations showing a max impedance bandwidth of 2 GHz and a max gain of 15 dBi.

And finally, the optimized design is fabricated using a low cost PCB-based technology for validation of both performance of the design and modeling techniques. A maximum gain of 13 dBi has been achieved. It is further shown that by reducing the distance between the two middle elements around the center feeding slot, the side lobe level (*SLL*) can be improved from -10 dB to -12 dB. The comparison between the simulated and the measured results of the optimized design shows good agreement considering fabrication tolerances and connector losses.

Some of the results of the research work from this thesis have been published in the following refereed journal and conferences.

[1] M. Abdallah, Y. Wang, W. Abdel-Wahab, and S. Safavi-Naeini, "A Tunable Circuit Model for the Modeling of Dielectric Resonator Antenna Array," *IEEE Antennas and Wireless Propagation Letters*, vol. 15, pp. 830-833, 2016.

[2] M. Abdallah, Y. Wang, W. Abdel-Wahab, and S. Safavi-Naeini, "Modeling of Substrate Integrated Waveguide Series Fed Dielectric Resonator Antenna Array with Longitudinal Slots Excitation," *IEEE Antennas and Propagation Society International Symposium (APS/URSI)*, Vancouver, BC, Canada, July 19-24, 2015.

[3] M. Abdallah, Y. Wang, W. Abdel-Wahab, S. Safavi-Naeini, and J. Liu, "A Simple Circuit Model Including Mutual Coupling for Dielectric Resonator Antenna Array," *IEEE Antennas and Propagation Society International Symposium (APS/URSI)*, pp.1944-1945, Memphis, TN, July 6-11, 2014.

1.3 Outline

This dissertation is divided into five chapters.

Chapter 1 presents a brief introduction, explaining the motivation, objectives, and contributions of this work.

Chapter 2 discusses the relevant background by reviewing the literature in the areas of substrate integrated waveguide, dielectric resonator antenna, and space mapping. It covers firstly the SIW technology, implementation and propagating modes in SIW, SIW design guidelines, and losses in SIW. Secondly, a general overview of the DRA is presented with some details about different types of DRAs, DRA excitation methods, and recently work of SIW-based DRA. Thirdly, an introduction to SM, including basic concepts of SM, SM classifications, and SM algorithm, is given.

In Chapter 3, we present the development of the fully adjustable circuit model including mutual coupling for DRA array through three main sections: SIW-series fed DRA array configuration using transverse slots; SIW-series fed DRA array configuration using longitudinal slots; and SIW-series fed DRA parasitic array configuration using longitudinal slots. An example of a 4-element array is studied for each configuration. The simulation results using the circuit model and full wave solver are compared to validate the proposed modeling technique for each configuration. Comparison is also made with the experimental results for the DRA array with transverse slots.

Chapter 4 presents a new design of SIW middle fed series rectangular DRA array with 45° linear polarization. The space mapping technique is applied for the optimization of the structure. The circuit model developed in Chapter 3 is used as the coarse model. High optimization efficiency is demonstrated using an 8-element array, for which the design specification is met within three optimization iterations. For validation, this design is fabricated using the optimized design parameters obtained by SM. At the end of this chapter, the antenna measurement results are discussed and compared to the simulation results.

We conclude with chapter 5, which provides highlights of our results and contributions, and a summary of aspects that can be further investigated for future work.

Chapter 2

Literature Review

2.1 Substrate Integrated Waveguide (SIW) Technology

The conventional rectangular waveguide technology has been playing an important role in microwave and millimeter wave circuits and systems. It possesses important advantages, such as low loss, high Q-factor and high power handling capability. However, rectangular waveguides are bulky and difficult to be integrated in microwave and millimeter wave integrated circuits. A new generation of high-frequency integrated circuits called Substrate Integrated Circuits (SIC) has been developed [2]. This technology allows for both the planar and non-planar circuits to be integrated in different platforms. In particular, the new technology of substrate integrated waveguide (SIW) makes it possible to realize the waveguide characteristics in substrate integrated microwave and millimeter wave circuits [5]. Much research has proved that substrate integrated waveguide can be a

good candidate for the future generation of microwave and millimeter wave components and antennas.

2.1.1 Implementation and Propagating Modes in SIW Structure

The SIWs are rectangular waveguides consisting of two solid conductor planes, separated by a dielectric substrate, with conductor sidewalls realized by rows of metalized through-plated vias. The SIW structure is designed by choosing the spacing between the vias (*s*), all with the same diameter (*d*), to support guided wave propagation with minimum radiation loss. The amount of field leakage outside the waveguide should be sufficiently small. The width of the waveguide is calculated by the desired cut-off frequency of the dominant mode (TE_{10}). Figure 2.1 shows the common parameters of SIW; waveguide width, via diameter, and via spacing as W_{SIW}, *d*, and *s*, respectively [6]. The substrate height is *h*.

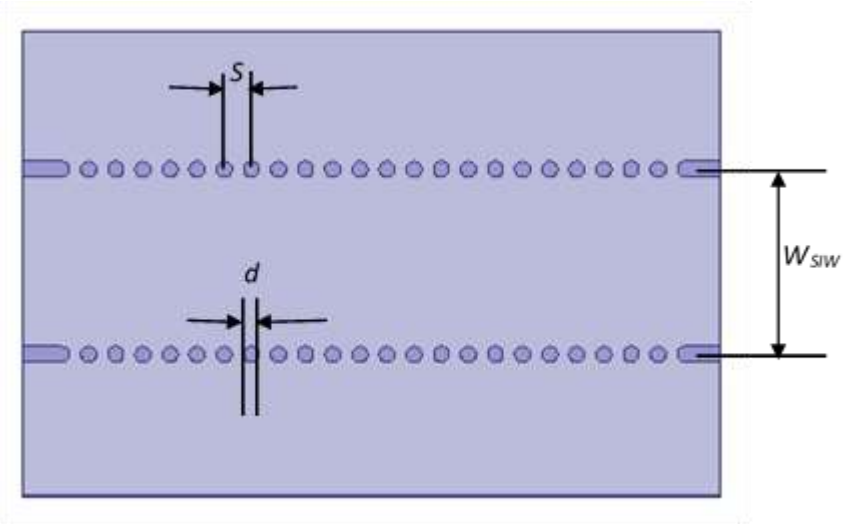

Figure 2.1 The geometry of the SIW: waveguide physical width, W_{SIW}, via spacing, *s*, and via diameter, *d* [6].

The rectangular waveguide has two main types of propagating modes depending on the absence of the electric field and the magnetic field components in the direction of propagation. In the transverse electric (TE) modes, there are no electric field components in the direction of propagation, while the transverse magnetic (TM) modes have no magnetic field in the direction of propagation. The TM modes require longitudinal current along the sides of the waveguide to propagate, while the TE_{mn} modes require the same surface currents for efficient propagation only for $n \neq 0$. It is necessary to connect the metalized vias with a good conductor material to protect the surface currents required for the propagation of TM and TE_{mn} modes, where $n \neq 0$ [6]. Only TE_{m0} modes are supported in an SIW structure with vias due to the discontinuous structure of the sidewall. The cutoff frequency for a solid rectangular waveguide (RWG) with a dielectric material can be calculated using equation (2.1).

$$f_c = \frac{C}{2\pi\sqrt{\varepsilon_r}}\sqrt{\left(\frac{m\pi}{a}\right)^2 + \left(\frac{n\pi}{b}\right)^2} \tag{2.1}$$

where a and b are the waveguide width, and height, respectively [7]. C is the speed of light, and ε_r is the relative permittivity. It is known that when a SIW works only in the dominant mode, the E-field is of a maximum value at the vertical center plane along the propagation direction, so the center plane can be considered as an equivalent magnetic wall.

2.1.2 Mapping from RWG to SIW

Substrate Integrated Waveguide (SIW) with via sidewalls is equivalent to a rectangular waveguide of similar width if a correction factor for the center-to-center via

spacing is taken into account. The cut-off frequency for the first two TE_{m0} modes of an SIW, using the width correction

$$f_{c(TE10)} = \frac{Co}{2\sqrt{\varepsilon_r}} \cdot \left(W_{SIW} - \frac{d^2}{0.95s} \right)^{-1} \tag{2.2}$$

$$f_{c(TE20)} = \frac{Co}{\sqrt{\varepsilon_r}} \cdot \left(W_{SIW} - \frac{d^2}{1.1s} - \frac{d^3}{6.6s} \right)^{-1} \tag{2.3}$$

It is proven that the dispersion characteristics of the SIW are the same as those of its equivalent RWG if the equivalent width W_{SIW} of the SIW is given by

$$W_{SIW} = a_{eff} + \frac{d^2}{0.95s} \tag{2.4}$$

where a_{eff} is the effective width of the RWG. This width is given by experiments and simulations results based on measuring the phase difference of the two guided wavelength and comparing the first two modes of the SIW with those of an equivalent RWG filled with the same dielectric. A more accurate empirical equation was proposed to calculate the effective SIW width considering the ratio of d/W_{SIW}, where *s* is sufficiently small [6]. The effective width is calculated by equation (2.5), and is valid when $s/d > 3$ and $d/W_{SIW} < 1/5$. Once a_{eff} *is* calculated, equation (2.1) may be used to accurately determine the SIW cut-off frequency [6].

$$a_{eff} = \left(W_{SIW} - 1.08\frac{d^2}{s} + 0.1\frac{d^2}{W_{SIW}} \right) \tag{2.5}$$

In [9], it is shown that the SIW and its equivalent rectangular waveguide have the same insertion loss using the Finite Element Method (FEM). Furthermore, an equation was derived in [10] using the Method of Lines to calculate the effective width of SIW as

$$a_{eff} = \xi_1 + \frac{\xi_2}{\frac{s}{d} + \frac{(\xi_1 + \xi_2 - \xi_3)}{\xi_3 - \xi_1}} \tag{2.6}$$

$$\xi_1 = 1.0198 + \frac{0.3465}{\frac{W_{SIW}}{s} - 1.0684} \tag{2.6.a}$$

$$\xi_2 = -1.1183 - \frac{1.2729}{\frac{W_{SIW}}{s} - 1.2010} \tag{2.6.b}$$

$$\xi_3 = 1.0082 - \frac{0.3465}{\frac{W_{SIW}}{s} + 0.2152} \tag{2.6.c}$$

For the higher order modes of SIW, the dispersion characteristics are similar to its equivalent RWG. On the other hand, there is a small difference in the equivalent width between the higher order modes and the fundamentals mode [11].

2.1.3 SIW Design Guidelines

Design rules are given in [12]. There are suitable values for both the ratios of d/λ_c and s/λ_c. At these values, the SIW is equivalent to RWG which has no leakage losses and no band gap in the bandwidth. In [13], these ratios are given as ${}^{s}/_{\lambda_c} \leq 2d$ and $s \leq 2d$ within the operating range of frequency and based on the fundamental TE_{10} mode. Firstly,

the waveguide width should be chosen to excite the dominant mode, where the first two modes to propagate are TE_{10} and TE_{20}. A good choice is to consider $f_{c(TE_{10})} = \frac{f_{o(SIW)}}{1.5}$, where $f_{o(SIW)}$ is the operating frequency of the SIW. The ratios *s/d and d/*W_{SIW} are chosen to be small to keep the overall losses at minimum levels. Secondly, the SIW rectangular waveguide effective width a_{eff} is calculated as

$$a_{eff} = \frac{1}{2.f_c(TE_{10}).\sqrt{\epsilon_{rs}.\mu}} \tag{2.7}$$

From (2.7) and (2.5), the physical width of SIW can be obtained using (2.8) where ε_{rs} is the relative permittivity of the substrate material.

$$W_{SIW} = \frac{3}{4f_o(SIW)\sqrt{\mu\varepsilon_{rs}}} + 1.08\frac{d^2}{s} - 0.1\frac{d^2}{W_{SIW}} \tag{2.8}$$

2.1.4 Losses in Substrate Integrated Waveguide

There are three types of losses in SIW; metallic loss (α_c), leakage loss (α_L) and dielectric loss (α_d), and the overall loss $\alpha = \alpha_c + \alpha_L + \alpha_d$ [14]. The losses increase when the vias are getting smaller and further away from each other. The periodic length (*s*) affects the energy that may propagate outside the two arrays of the vias and this is called leakage loss or radiation loss. If the ratio of $s/d \leq 2.5$, the attenuation constant α_L is smaller than 1dB/m [14].

For a given cut-off frequency of the TE_{10} mode, the dielectric and conduction loss for SIW with width W_{SIW} can be determined as [15]

$$\alpha_d = \frac{{k_o}^2 tan\delta}{2\beta} \tag{2.9}$$

$$\alpha_c = \frac{R_m}{a_{eff}\eta\sqrt{1-\frac{{k_c}^2}{{k_o}^2}}}\left[\frac{W_{SIW}}{b}+2\frac{{k_c}^2}{{k_o}^2}\right] \quad (2.10)$$

where

$k_o = w\sqrt{\mu\varepsilon} = 2\pi/\lambda$ is the wave number

β is the propagation constant of the waveguide

tanδ is the dielectric loss factor

$k_c = 2\pi/\lambda_c$ is the cutoff wave number

λ_c is the TE_{10} cut off wave length

η is the intrinsic Impedance.

b is the height of the substrate

For a frequency range from 10-300 GHz, the dielectric substrates of relative permittivity between 2 and 13 can be used in the design of SIW components, causing a dielectric loss factor of 10^{-3} to 10^{-4}. The conduction losses due to the finite conductivity of the metal decreases when the metal vias are large and closely spaced. On the other hand, the dielectric losses is slightly affected by the vias diameter and spacing. In [6], some conditions are listed to minimize the overall losses as $\frac{s}{d} \leq 2.5$ and $\frac{d}{W_{SIW}} < \frac{1}{8}$. One of the important advantages for SIW compared with traditional planar structures, such as MSL and CPW, is that, at high frequency, the overall loss decreases, whereas for the other

structures, it increases [16]. Therefore, the SIW can replace these traditional planar structures in millimeter-wave applications.

2.2 Antennas Overview

Antennas are one of the most important parts of any wireless communication systems to guarantee successful transmission and receiving of information. Due to this important role, the antenna research has grown rapidly in the last decades. The IEEE definition of an antenna is “That part of a transmitting or receiving system that is designed to radiate or receive electromagnetic waves” [17]. It provides a transition between free space and waveguides [18].

This section provides a summary of the most important parameters to be considered in antenna design, and an overview of dielectric resonator antennas (DRAs) due to a number of their attractive characteristics for millimeter-wave applications.

2.2.1 Important Parameters of Antennas [18-21]

- Polarization

Polarization is the variation of the electric field in direction and magnitude with time. Polarization may be linear, circular or elliptical according to the shape of the curve. Linear and circular polarizations are special cases of elliptical polarization, when the ellipse becomes a straight line or circle, respectively.

- Input Impedance and VSWR

Input impedance is defined as the impedance at the antenna's terminals or "the ratio of the voltage to current at its terminals". If interconnecting transmission line and the antenna is not matched to each other, a standing wave is initiated along the transmission line. The Voltage Standing Wave Ratio (VSWR) is defined by the ratio of the maximum voltage to the minimum voltage along the line.

- Directivity

The directivity determines the radiation properties of the antenna. It is defined as the ratio of the maximum antenna radiation intensity in a specific direction in space to the radiation intensity of an isotropic source for the same radiated power

- Power Gain

The gain of the antenna is closely related to the directivity, but considering the losses in the antenna as well as its directional capabilities.

- Efficiency

The antenna efficiency is the ratio of directivity to gain. It takes into consideration all the losses at the input terminals and within the antenna structure.

- Effective Isotropically Radiated Power (EIRP)

The Effective Isotropically Radiated Power (EIRP) expresses the effective radiated power in a given direction. It is equal to the product of the effective power accepted by the antenna and the antenna gain.

- Radiation Pattern

The antenna radiation pattern is the graphical representation of the radiation characteristics of the antenna as a function of the spherical coordinates (θ, φ). In most cases, the radiation pattern is determined in the far field region for constant radial distance and

frequency. A typical radiation pattern is characterized by a main beam with 3 dB beamwidth and sidelobes at different levels.

- Half-Power Beamwidth

Beamwidth is a very important parameter, and is easily determined from its 2D radiation pattern. Beamwidth is the angular separation of the half-power points of the radiated pattern.

- Return Loss (RL)

It is a parameter which indicates the amount of power that is "lost" to the load and does not return as a reflection. Hence *RL* is a parameter to indicate how well the transmitter is matched to the antenna.

- Bandwidth

The bandwidth of the antenna can be defined with respect to different parameters. It is often considered as the range of frequencies over which the return loss is better than 10dB.

2.2.2 Dielectric Resonator Antenna (DRA)

As mentioned before, the millimeter wave applications need a specific criteria for the antenna used in this frequency range. The widely used microstrip patch antenna has been investigated and designed at the mm-wave frequencies for wireless communication systems [22, 23]. They can be easily printed on the same layer of metallization. The fabrication cost is low and integration with other planar circuits is easy. However, researches have proved that the conduction loss and the dielectric loss of microstrip antennas are high especially in large arrays. In addition to their high losses, they suffer

from a narrow bandwidth. On the other hand, dielectric resonator antennas show a good performance and overcome the drawbacks of microstrip antennas.

Dielectric resonator antenna (DRA) has been extensively studied over the past 30 years [1], [24]. It is fabricated from low-loss dielectric material [25]. The DRA offers attractive features such as low profile [26-30], compact size [31-33], low ohmic loss, and high radiation efficiency [34]. It does not suffer from surface-wave losses, and has wide impedance bandwidth compared to the microstrip antenna [35]. DRAs have been studied as suitable antennas for wireless communication applications [36]. DRAs can be used at millimeter frequency bands and is compatible with existing excitation methods [37], such as coaxial probe, microstrip transmission line, coplanar waveguide feed or aperture coupling. In addition, DRAs are compatible with Microwave Integrated Circuits (MICs) [38-42].

2.2.2.1 Types of DRAs

There are different shapes of DRAs, such as rectangular, cylindrical, spherical and hemispherical geometries [43-47]. The resonant frequencies of DRAs are proportional to its material properties, dimensions, and shapes [48, 49]. For rectangular DRAs, two of the three of its dimensions can be varied independently for a fixed resonant frequency, which offers more design flexibility [50-52].

2.2.2.2 DRA Excitation Methods

Different excitation techniques have been used to couple the energy to the DRA. The resonance can be tuned in a specific range of frequencies while slightly changing the

feed position with respect to the DRA. It should be positioned within the area with strong field, whether electric or magnetic.

- Aperture Slot

In this technique, the feed network is located below the ground plane to avoid unwanted radiations that can cause distortion and degrade the pattern shape. For TE_{111} mode of a rectangular DRA with a rectangular slot, the aperture needs to be placed in a DRA strong magnetic field area to achieve relevant coupling [53]. The slot at the centre behaves like magnetic current streaming parallel to its length and excites the magnetic fields in the DRA body, which causes broadside radiation pattern in the far field [54, 55]. This technique is particularly recommended for millimeter-wave applications.

- Coaxial Probe

The coaxial probe feed is a common and efficient technique, where the probe can be considered as a vertical electric current to achieve strong coupling to the DRA. The height and diameter of the probe controls the level of coupling. Different modes can be excited depending on the shape of DRA and probe location. To excite only TM modes, it is fed axially. For TM_{01} mode, the feed probe is expected to be located at the centre to act as a quarter wavelength monopole for its far field radiation patterns. On the other hand when HEM_{11} (TM_{110}) mode is required, the feed probe is located close to the peripheral boundary so as to yield broadside radiation patterns [55, 56]. This technique is particularly recommended at lower frequencies to minimize the fabrication problems, however it is equally efficient at higher frequencies.

- Microstrip Line

Direct couplings are the simplest methods, as it excites the magnetic fields in the DRA to produce the short horizontal magnetic dipole [57, 58]. The amount of coupling can be optimized by choosing a material with high dielectric permittivity constant. The coupled energy increases when high ε_r is chosen.

- Coplanar Feeds

Another example of dielectric resonator antenna excitation techniques is the Coplanar Waveguide (CPW). It is easy to fabricate and has a good matching with the solid state devices. The coplanar loop perfectly couples energy to the DRA, as the coupling level and the mode of excitation can be obtained by gradually moving the DR element over the loop [59, 60]. Required resonance frequency and radiation patterns can be achieved by shifting the loop from the edge to the centre.

- Dielectric Image Guide

In millimetre-wave applications, to avoid the conductor loss of conventional feeding structure, the dielectric image guide is one the best solutions. The dielectric image guide (DIG) is a low loss feeding structure that couples the energy to the DRA. As mentioned before, a higher permittivity value can be chosen to enhance the coupling level. DIG can be utilised as series feed to linear array designs [61-63]. On the other hand, the DIG suffers from radiation losses and also a transition to rectangular waveguide needs be designed to couple the power to DIG, which introduces more loss.

- Substrate Integrated Waveguide

Traditional planar feeding structures, such as microstrip line [55] and coplanar waveguide [60], suffer from conduction loss, especially in the millimeter-wave frequency

band. SIW has recently become an attractive excitation technique used to feed the dielectric resonator antennas due to its advantages such as low loss, low cost, and ease of integration with planar circuits [37].

The SIW has been used as a feeding technique for DRA in [64] through a narrow slot cut on the SIW broad wall. The antenna has been designed at TM_{110} mode, where the center frequency was at 18GHz, and it achieved a gain of 6dB. The same design has been applied to 60GHz in [65], where it is excited by half mode SIW (HMSIW). The measured gain was 5.5dB with a radiation efficiency of 90%. However the gain of the single element was low.

In the SIW fed DRA reported in [66-68], two different slot configurations were used as shown in Figure 2.2, where good performance was achieved. A parametric study for all antenna parameters has been done to optimize the coupling between the SIW and DRA in [67]. DRA single elements have been fabricated using a low cost multi-layer printed circuit board (PCB) technology for both longitudinal and transverse slots. A high radiation efficiency SIW-DRA array with *N*-elements, based on the two slot configurations are reported in [68]. Simple transmission line circuit model is developed to optimize the SIW-DRA array characteristics.

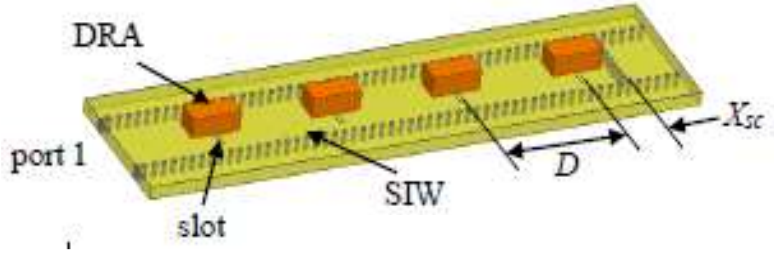

(a)

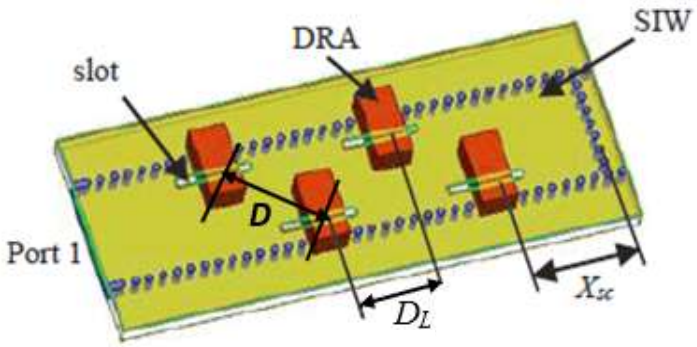

(b)

Figure 2.2 General configurations for SIW series fed DRA liner array, (a) using transverse slot, and (b) using longitudinal slot [68].

2.3 Space Mapping Optimization

In microwave/millimeter design, full wave electromagnetic (EM) simulation is essential to ensure first pass success due to its superior accuracy. However, full EM simulation is generally computationally intensive, which limits its applications in iterative design and optimization. Alternative thinking is to find a technique that combines the speed of circuit models, or surrogate models, and the accuracy of EM solvers. Space mapping (SM) is such a surrogate-based optimization method. The original space mapping

algorithm was initiated by Bandler *et al.* in 1994 [69]. Since then, there have been extensive research and applications of SM to EM optimization problems. [70-74].

SM can give unmatched efficiency when the problem can be molded in two different system models, namely the fine model and the coarse model, for the same physical system [75, 76]. The fine model is accurate but expensive to evaluate. The coarse model is faster but less accurate. The fine model is usually EM full wave solvers and the coarse models are circuit based models. The SM approach establishes the mapping between the two models, and updates the mapping or the coarse/surrogate model to better approximate the corresponding fine model [76]. Using this mapping in each iteration, most of the model evaluations can be directed to the fast coarse model [77]. It has been proven to be an efficient technique in many difficult engineering optimization problems.

2.3.1 The Optimization Problem

The optimization problem can be defined using two main vectors, $\boldsymbol{R_f}$ and $\boldsymbol{x_f}$ .The vector $\boldsymbol{R_f}: X_f \rightarrow R^m$ is the vector of m responses of the fine model, and $\boldsymbol{x_f}: X_f \subseteq R^n$ is the vector of n design parameters. Then, the optimization problem is formulated by the following equation [78]

$$\boldsymbol{x^*_f} = arg\left\{min_{x_f \in X_f}\, U\left(\boldsymbol{R_f}(\boldsymbol{x_f})\right)\right\} \tag{2.11}$$

where U is the objective function, and x^*_f is the optimal solution of the fine model. Space mapping suggests to find an accurate surrogate model $\boldsymbol{R_s}: X_s \times X_p \rightarrow R^m$, which is built from the coarse model $\boldsymbol{R_c}: X_c \rightarrow R^m$ and updated to align with $\boldsymbol{R_f}$. $X_s \subseteq R^n$ and $X_p \subseteq R^q$ refer to the design-parameter domain and the auxiliary preassigned parameter domain of the surrogate

model, respectively, while $X_c \subseteq R^n$ refers to the design parameters domain of the coarse model [79]. The surrogate model is updated at each iteration until the fine model result satisfies the design specifications.

2.3.2 SM Classifications

There are different types of SM that can be used depending on the complexity of the problem [80]. They can be generally classified into two categories, the explicit SM (ESM) and the implicit SM (ISM). The ESM includes four types; output SM (OSM), aggressive SM (ASM), trust region SM (RTSM), and hybrid SM (HSM).

ISM is one of the latest development of SM, which is an easy technique to implement [81]. Implicit space mapping (ISM) utilizes a set of auxiliary parameters $\boldsymbol{x}$. These auxiliary, or pre-assigned parameters, e.g. dielectric constant or substrate height, are not actual design parameters in the fine mode. They are extracted to match the coarse and fine model responses in each iteration. The resulting coarse model (surrogate) response $\boldsymbol{R_c(x_c, x)}$ is then re-optimized with respect to the coarse model design parameters, $\boldsymbol{x_c}$, to give $\boldsymbol{x_f = x_c^*(x)}$, where $\boldsymbol{x_f}$ is the prediction of the fine model design parameters. More details with the flow chart of ISM will be presented in chapter 4.

2.3.3 Space Mapping Algorithm

There are some key steps which are common in different types of SM, and can be summarized as following [78], [81, 82].

1) Select a coarse model suitable for the fine model.
2) Select a mapping process (original, aggressive SM, neural or ISM, etc.).

3) Optimize the coarse model (initial surrogate) with respect to design parameters $x_f = x_c^*$.
4) Simulate the fine model at this solution to find the fine model response $R_f(x_f)$.
5) Terminate if a stopping criterion is satisfied.
6) Apply parameter extraction (PE) using pre-assigned parameters or coarse model parameters.
7) Rebuild surrogate
8) Re-optimize the mapped coarse model (surrogate model) with respect to design parameters (or evaluate the inverse mapping if it is available).
9) Go to Step 4.

2.4 Conclusion

Millimeter wave applications have specific requirements for systems operating in this frequency range. MMW antennas and circuits with compact size, low cost, high efficiency, and low loss are much needed to meet the requirements of these applications.

Dielectric resonator antenna (DRA) offers attractive features required for MMW application. It shows a good performance and overcomes drawbacks of planar antennas, such as surface wave losses and narrow bandwidth. Moreover, it is fabricated from low-loss dielectric material, has low profile, compact size, low ohmic loss, high radiation efficiency, and is compatible with existing excitation methods, such as coaxial probe, microstrip transmission line, coplanar waveguide feed, and substrate integrated waveguide.

The technology of substrate integrated circuits allows for both the planar and non-planar circuits to be integrated. Although substrate integrated waveguide (SIW) has similar characteristics as conventional waveguides, it is compatible with planar and non-planar circuits, and has low cost, small size and small conduction loss. It has been proven that substrate integrated waveguide can be a good alternative for the future generation of microwave and millimeter wave components. The combination of SIW and DRA can be an excellent candidate for millimeter wave applications.

The difficulty of antenna array fabrication, especially in the MMW due to the small size, requires that the design be precisely simulated. Design and optimization of an antenna array usually depend on accurate yet time consuming full wave solvers, which can be challenging due to the size and complexity of the entire structure. Circuit models are fast and much less computationally intensive, but without the required accuracy. Space mapping (SM) is a powerful and unique optimization method that links the circuit model and the full wave solver. Application of SM to the design problem is not straightforward, as it requires the development of an efficient surrogate/coarse model. The objective of this research is to design, model, and optimize DRA arrays based on SIW technology for millimeter wave applications, with the help of highly efficient computer aided modeling and optimization techniques.

Chapter 3

Development of a Circuit Model Including Mutual Coupling for Dielectric Resonator Antenna Array

Design and optimization of an antenna array is usually performed through a parametric study using a full wave solver, which can be challenging due to the size and complexity of the entire structure such as dielectric resonator antenna (DRA) array backed by substrate integrated waveguide (SIW). In this chapter, a simple yet accurate circuit model is presented for modeling of SIW series-fed DRA array for two different slot configurations. The mutual coupling between antenna elements is taken into account in the new model, which has been ignored in earlier work. A single-element and a two-element antenna structures are simulated first using full-wave solver, HFSS. The mutual coupling between antennas is then extracted and subsequently plugged into the circuit model for the

antenna array. Millimeter-wave DRA arrays are used to validate the model. The S-parameters calculated using the model agrees well with the full-wave solver results.

The mutual coupling depends on the distance between antenna elements. The extracted coupling for a given structure does not apply if the distance varies. The next question is therefore how to model it so that the circuit model become flexible. To this end, a new adjustable model is developed, replacing the coupling data block with circuit models allowing optimizations of the design parameters.

Millimeter-wave DRA array examples are used to validate the model. The S-parameters calculated using the total extracted mutual coupling match with the new mutual coupling tunable model. And they both agree well with the full-wave solver results. Also, the reflection coefficient results of the four elements single port example agrees well with the previously published measured results [68]. The focus of this chapter is to develop a fast and accurate circuit model for the SIW series-fed DRA array, which includes mutual coupling between antenna elements. Some results from this chapter have been published in [83-85].

3.1 SIW-Series Fed DRA Array Configuration Using Transverse Slot

Figure 3.1 shows the structure of a 4 elements SIW-series fed DRA linear array (SIW-DRA array). The SIW, which supports the TE_{10} waveguide fundamental mode, is short circuited in one end. The antenna elements are separated by a distance, *D*, which is measured between the centers of the neighboring elements. The DRAs are excited through

the feed network, which consists of narrow slot cut on SIW broad wall. The optimized single element (SIW-DRA single element) in [68] is used as a building block for the *N*-element SIW-DRA array for the transverse slot orientation. *D* is an important parameter, as it defines the phase difference between any two elements, which has a direct effect on all the radiation characteristics of the antenna. Another important parameter is the distance from the center of the last element to the SIW short circuited end, X_{sc}, as shown in Figure 3.1. This parameter affects both the antenna input impedance and the phase difference. A good choice of these two parameters guarantees that the antenna elements can be placed in certain positions to obtain a designed phase distribution such as co-phase or linear phase excitation. For transverse slot orientation shown in Figure 3.1, *D* is approximately λ_g and X_{sc} is approximately $\lambda_g/2$, where λ_g is the guided wavelength of TE_{10} mode in the SIW, to achieve a co-phase SIW-fed DRA array excitation. The structure of SIW-DRA ensures that the slots are positioned where the maximum axial SIW currents occur and the excitation slot fields are in phase.

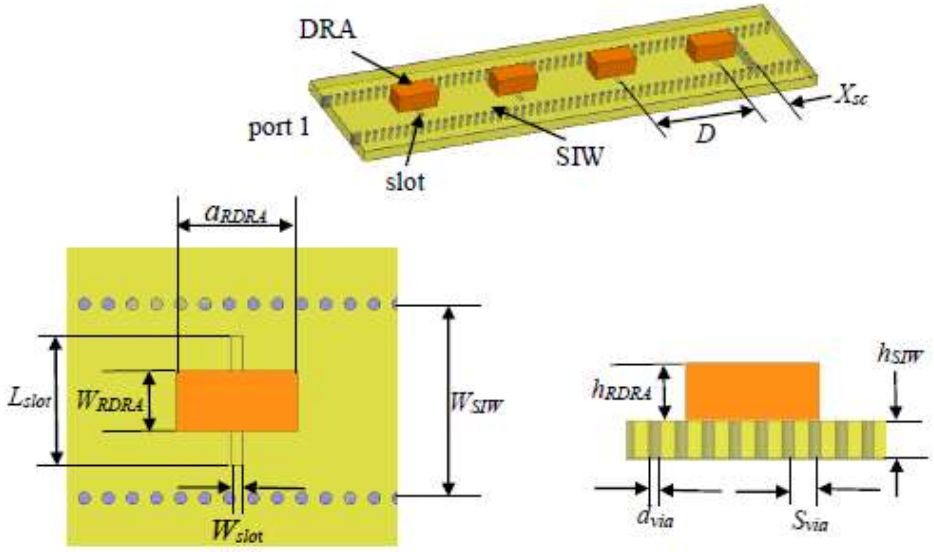

Figure 3.1 An example of a four-element SIW-DRA array fed by transverse slot [68]

In this design, DRAs are made of a dielectric material with ε_{RAD} =10.20 and dimensions of h_{RDRA} (thickness) = 1.27mm, a_{RDRA} (length) = 3.0 mm and W_{RDRA} (width) =1.50 mm. Each rectangular DRA element is excited by a narrow slot of length L_{slot}=3.2mm, and width W_{slot}=0.3mm. The SIW is made of two rows of metallic vias of diameter d_{via} =0.3 mm in a substrate, and two neighbouring vias are separated by s_{via}=0.6mm. The distance between the two rows are considered to be the width of the SIW, W_{SIW}=4.8mm. The substrate material, metalized on both sides, has a permittivity constant of ε_{SIW}=2.33 and a thickness of h_{SIW} = 0.7874mm. The SIW parameters are designed using the criteria described in [6], where the SIW equivalent rectangular waveguide width is given by (2.6a) to (2.6c) in chapter 2 [15].

3.1.1 Extraction of Mutual Coupling

The mutual coupling extraction methodology is outlined as follows.

Before a circuit model is constructed, a single element of SIW-DRA is first simulated using a full-wave solver, such as HFSS, to obtain the two-port S-parameters, $[S]_{single}$. The two ports are de-embedded to the center of the single element, where the references plane are defined. Next, the two-element structure in Figure 3.2(a), in which a PEC plane is inserted in the middle of the two DRAs, is also simulated using full wave solver. The PEC plane facilitates the extraction of the mutual coupling between antennas, which is modeled as a two-port S-parameters $[S]_{coupling}$. The equivalent circuit of the

structure in Figure 3.2(a) is shown in Figure 3.2(b). The impedance of the shorted circuited section of the SIW can be easily calculated as

$$Z_{SIW} = Z_o \tanh\left(\gamma . {}^{D}/_{2}\right) \tag{3.1}$$

in which γ is the propagation constant of the SIW and the characteristic impedance of the SIW, Z_0, is normalized and assumed to be 1 in the following calculations.

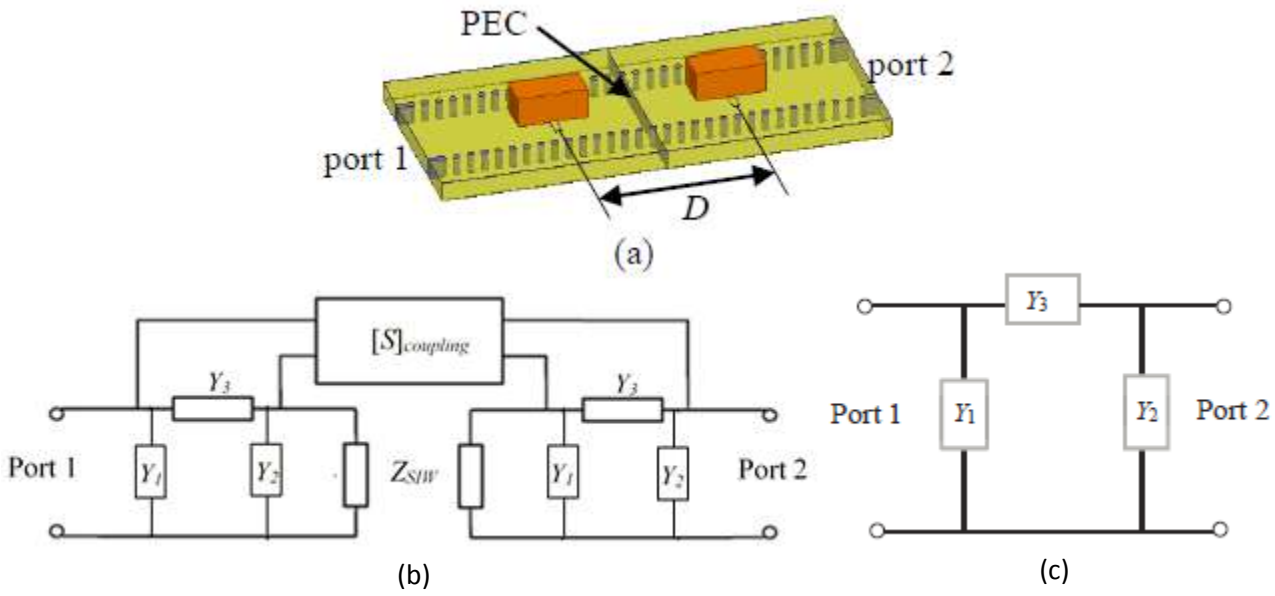

Figure 3.2 (a) Two-element SIW-DRA structures with PEC in the middle, (b) the circuit model, and (c) PI network of the single element.

The antenna element with the slot can be modeled as the *PI* two port network as shown in Figure 3.2(c) and it is calculated from the S-parameters of the single element of SIW-DRA, $[S]_{single}$. With known $[S]_{single}$ and Z_{SIW}, $[S]_{coupling}$ can be easily extracted through simple network analysis. Circuit model for the antenna array can be built using the building block shown in Figure 3.3, in which only two elements are shown. In Figure 3.3, each

dielectric resonator antenna is presented by its S-parameters, $[S]_{single}$. The SIW between the two antennas is modeled using a section of transmission line (T.L.) with the propagation constant γ. The mutual coupling between antennas is taken into account through $[S]_{coupling}$. Note that only couplings between adjacent antennas are considered. To build the circuit model for an array with *N* elements, the building block in Figure 3.3 needs to be repeated. The flexibility of circuit model can be further improved by replacing both the DRA data block, $[S]_{single}$, and the coupling data block, $[S]_{coupling}$, with circuit models, allowing optimizations of the design parameters, which will be shown in the next section.

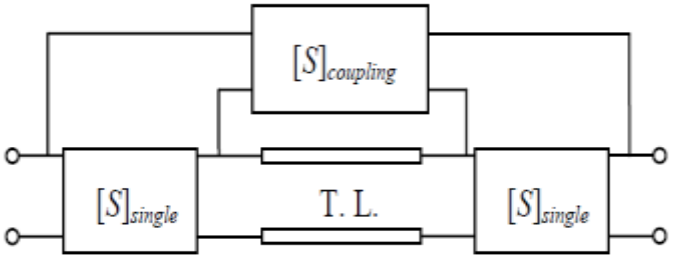

Figure 3.3 The build block for array circuit model.

3.1.2 Mutual Coupling Extraction Procedure

Before the extraction of mutual coupling, two EM simulations are performed: 1) a single element of SIW-DRA to obtain the two-port S-parameters $[S]_{single}$, and 2) a two-element SIW-DRA separated by *D*, where a PEC plane is inserted in the middle of the waveguide, to obtain the two-port S-parameters $[S]_{PEC}$. The following steps are then taken

to extract the S-parameters of the mutual coupling, $[S]_{coupling}$, based on the characteristics of the cascaded two ports network [7].

1 The S-parameters,$[S]_{PEC}$ is converted to ABCD parameter$[ABCD]_{PEC}$, and the left element of the *PI* network Y_1 is de-embedded firstly as follows:

   a. Y_1 is expressed as $[ABCD]_{Y1}$, where $[ABCD]_{Y1} = \begin{bmatrix} 1 & 0 \\ Y_1 & 1 \end{bmatrix}$

   b. The inverse of $[ABCD]_{Y1}$is obtained as $[ABCD]_{Y1}^{-1} = \begin{bmatrix} 1 & 0 \\ -Y_1 & 1 \end{bmatrix}$

   c. De-embed Y_1 from $[ABCD]_1$

$$[ABCD]_1 = [ABCD]_{Y1}^{-1} \cdot [ABCD]_{PEC} \cdot [ABCD]_{Y1}^{-1}$$

2 The shunt impedance Y_{sh} , which is the addition of Y_{SIW} and the right admittance of the *PI* network Y_2, should be de-embedded from $[S]_{PEC}$ as follows:

   a. Y_{sh} is obtained as $Y_{sh} = Y_2 + Y_{SIW}$, where $Z = {}^{1}/_{Y_{sh}}$

   b. Z is expressed as $[ABCD]_Z$,where $[ABCD]_Z = \begin{bmatrix} 1 & Z \\ 0 & 1 \end{bmatrix}$

   c. The inverse of $[ABCD]_Z$ is obtained as $[ABCD]_Z^{-1} = \begin{bmatrix} 1 & -Z \\ 0 & 1 \end{bmatrix}$

   d. De-embedded the shunt section from $[S]_{PEC}$

$$[ABCD]_2 = [ABCD]_z^{-1} \cdot [ABCD]_1 \cdot [ABCD]_Z^{-1}$$

3 Y_3 which is the center admittance of the *PI* network, and it is de-embedded from $[S]_{PEC}$ the same way as Y_1

   De-embedded the center impedance from $[ABCD]_2$

$$[ABCD]_{coupling} = [ABCD]_{Y3}^{-1} . [ABCD]_2 . [ABCD]_{Y3}^{-1}$$

3.1.3 Simulation Results

The SIW series-fed DRA array with four antennas as shown in Figure 3.1 is studied. The dimensions of the DRA and SIW are listed in section 3.2. The S-parameters of the mutual coupling are extracted following the steps described above for different values of the distance between antenna elements, *D*. The center frequency is at 33.87 GHz.

A. Two elements SIW series-fed DRA

For validation, a two port SIW-DRA structure with two antenna elements is simulated, which is similar to Figure 3.2(a) but without the PEC plane between antennas. The circuit model is the same as shown in Figure 3.3. The electromagnetic (EM) results using the full wave solver are compared to the circuit model results for different distances between the two elements, namely *D*=7mm, *D*=7.6mm, and *D*=8.2mm. For each *D* value, the previous steps are repeated to determine the total mutual coupling. Figure 3.4 to Figure 3.9 compare the S-parameters obtained using EM solver, the circuit model without taking into account the mutual coupling, and the proposed circuit model considering the mutual coupling effect, for different distances between the two antenna elements .

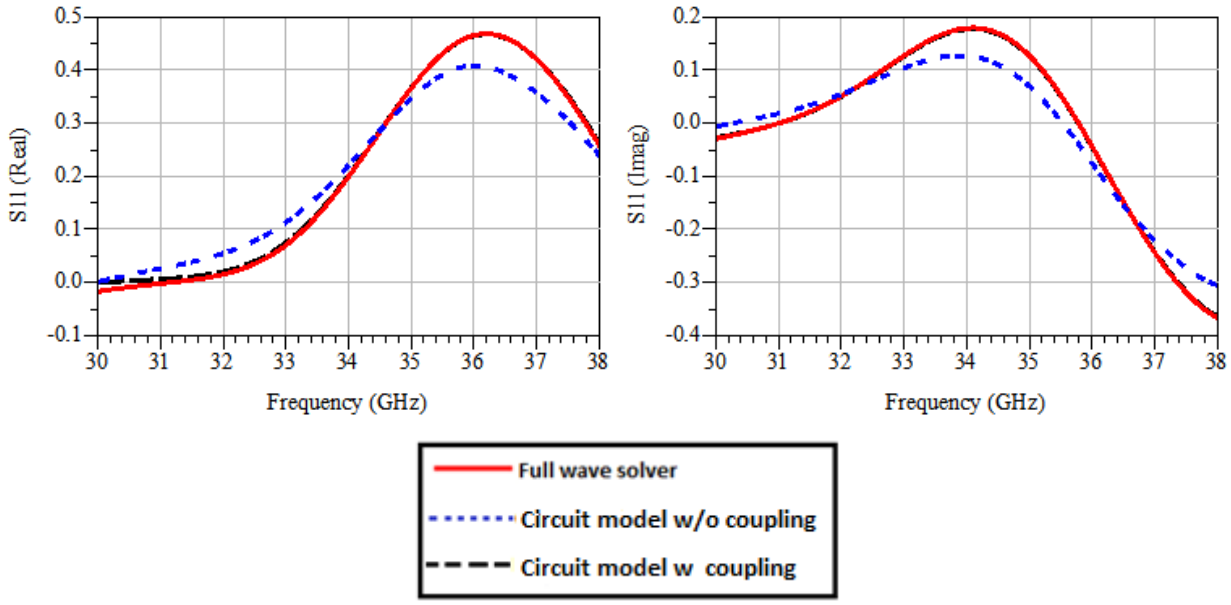

Figure 3.4 The S_{11} of the SIW-DRA structure with two elements. (D=7mm)

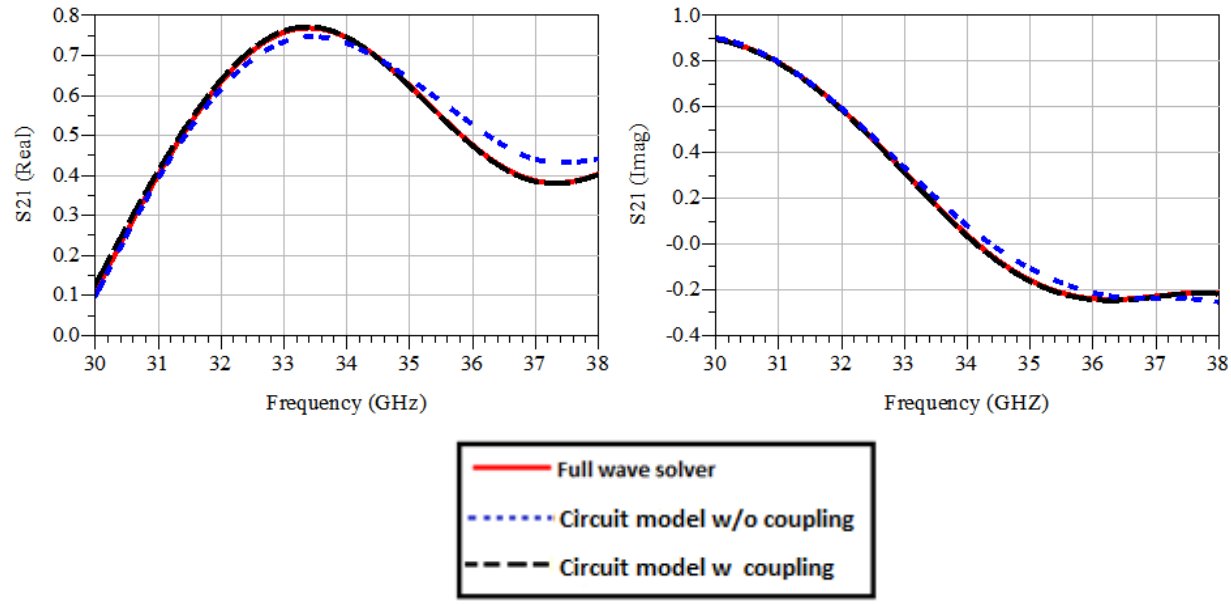

Figure 3.5 The S_{21} of the SIW-DRA structure with two elements. (D=7mm)

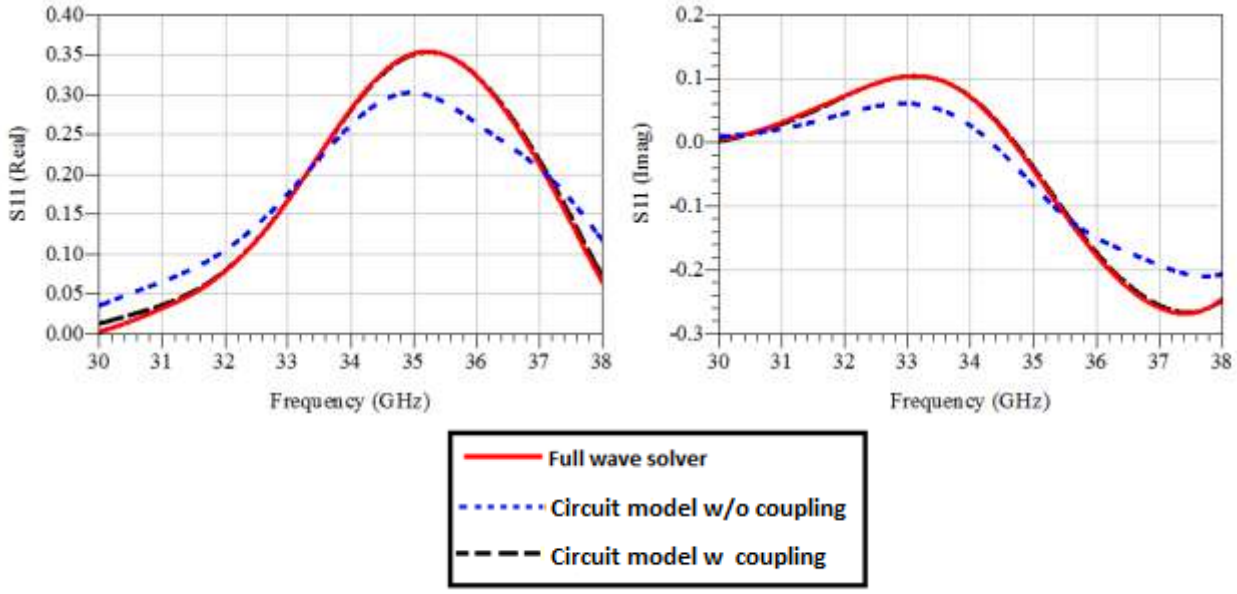

Figure 3.6 The S_{11} of the SIW-DRA structure with two elements. (D=7.6mm)

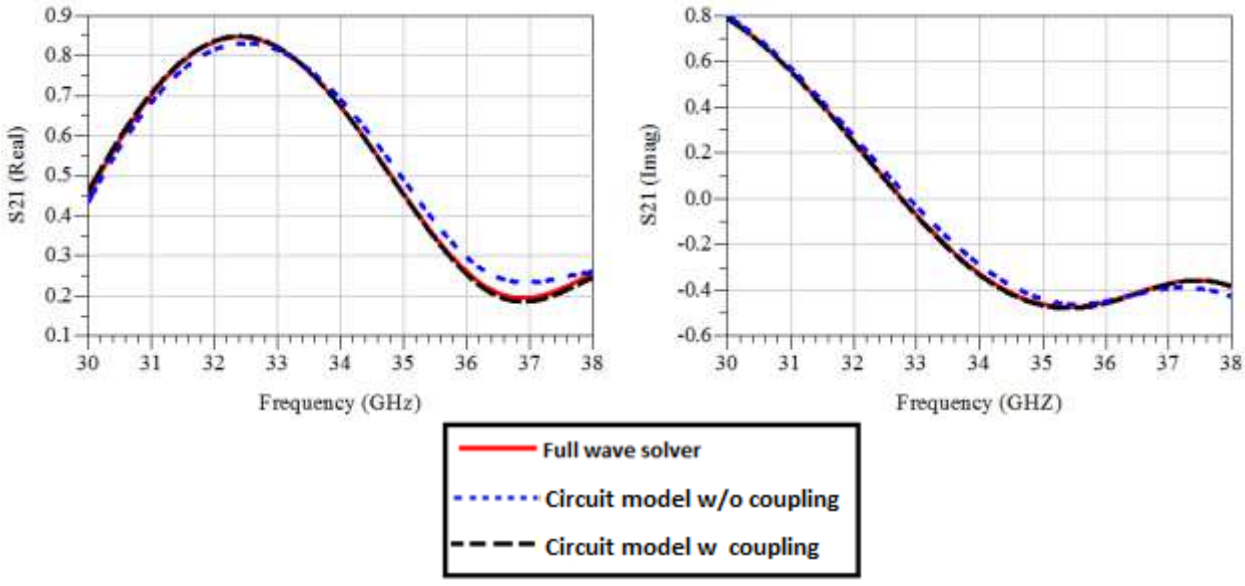

Figure 3.7 The S_{21} of the SIW-DRA structure with two elements. (D=7.6mm)

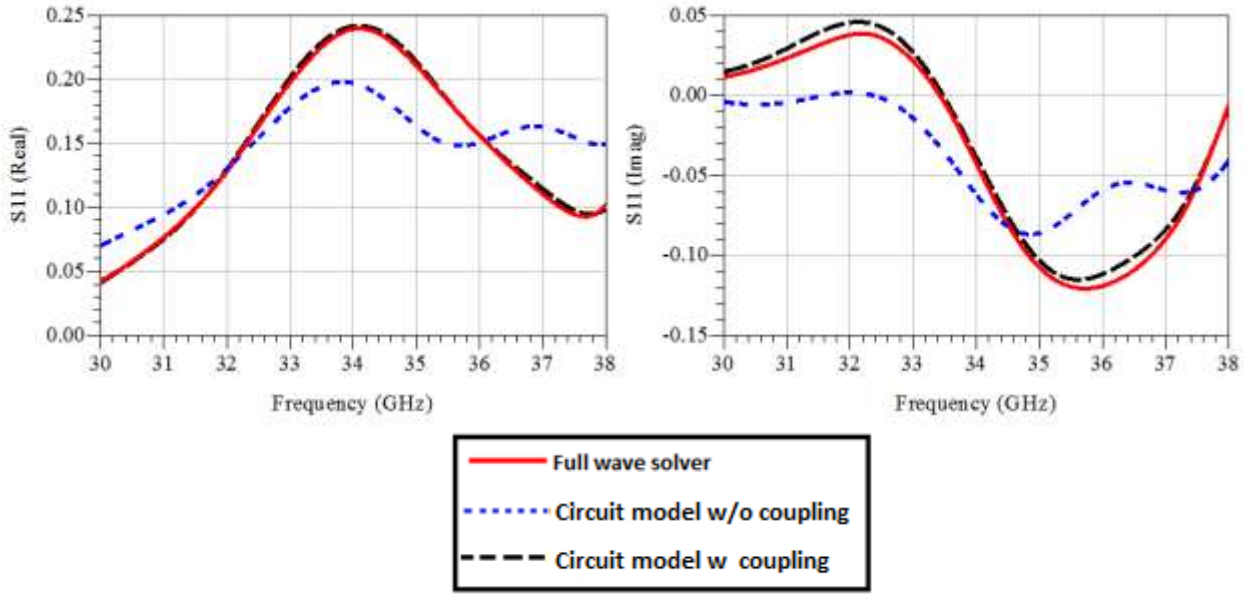

Figure 3.6 The S_{11} of the SIW-DRA structure with two elements. (D=8.2 mm)

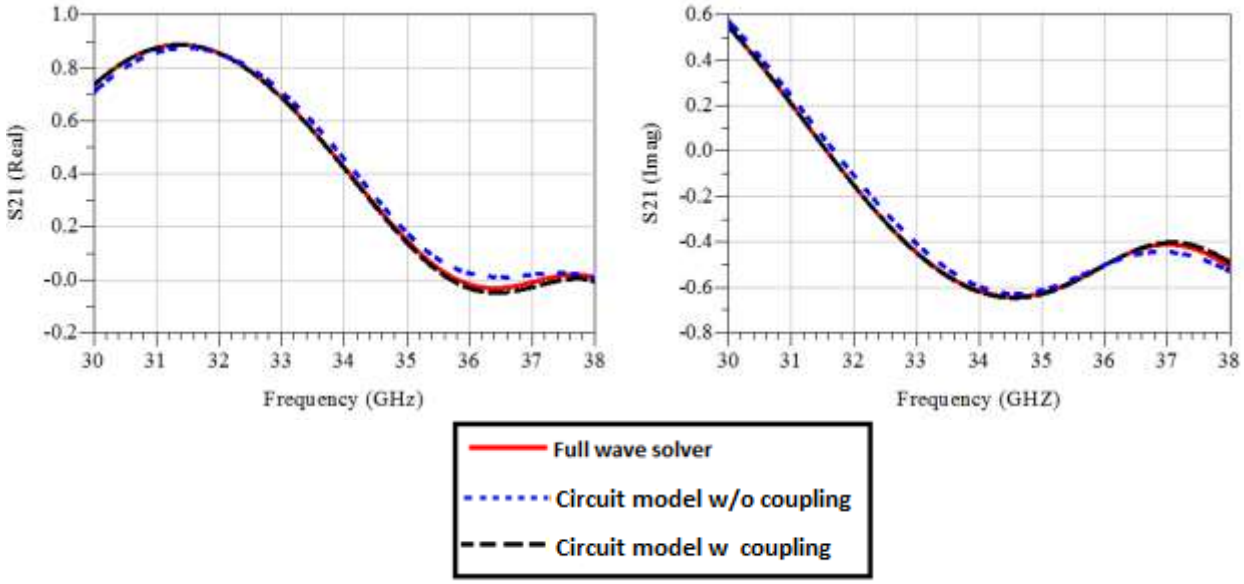

Figure 3.7 The S_{21} of the SIW-DRA structure with two elements. (D=8.2mm)

As shown in all three cases, the results show a good agreement between EM and the circuit model after adding the mutual coupling, while the circuit model without the mutual coupling is quite different from EM results.

B. Four elements SIW series-fed DRA array

This four-element SIW-DRA array with single port as shown in Figure 3.1 is investigated next. Firstly, a piece of SIW with one end short circuited is simulated in the full wave solver and compared to an ideal short-circuited transmission line. The length of the transmission line, X_{sc}, is measured from the center of the last element to the SIW short circuited end. The difference in the S-parameters for the SIW and the ideal short-circuited transmission line is compensated by adding a correction length ΔL to X_{sc} in the circuit model so the S-parameters of the EM model and circuit model agree to each other. Such a correction, or mapping from SIW to transmission line circuit model, will be shown in details in Chapter 4.

Two examples are simulated, in which D = 7.6mm and D = 7.2 mm, respectively. The short circuit length X_{sc} is set to be 2.5mm. The reflection coefficients are shown in Figure 3.10 and 3.11. It can be clearly seen that the simulated results using the full wave solver agrees very well with the proposed circuit model results considering the mutual coupling. On the other hand, the circuit model results without the mutual coupling is much less accurate.

i. D=7.6 mm and X_{sc}=2.5mm

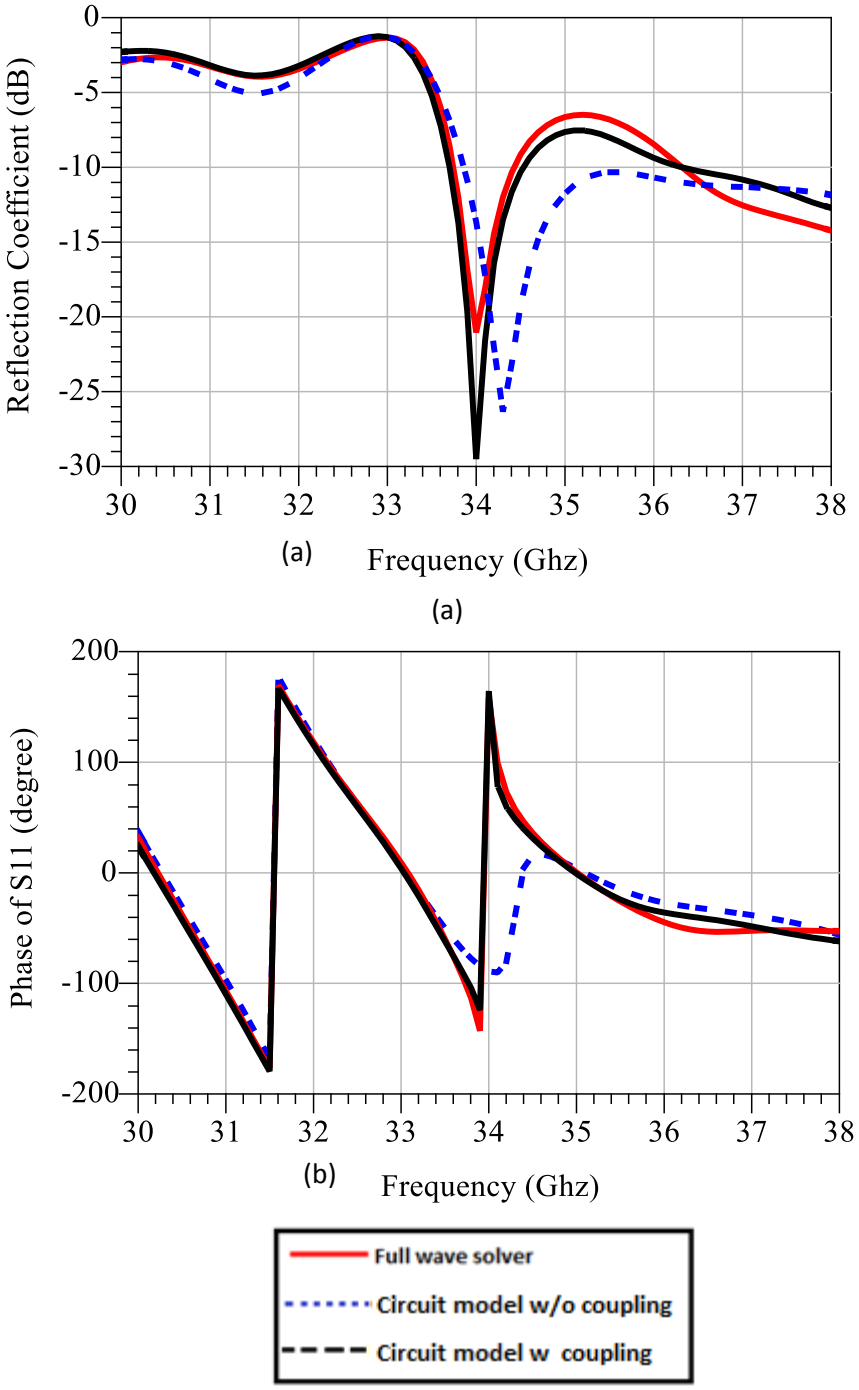

Figure 3.8 Four elements SIW-DRA array single port at D=7.6mm and X_{sc}=2.5mm. (a) Reflection coefficient (dB), and (b) phase of S_{11}.

ii. D=7.2 mm and X_{sc}=2.5mm

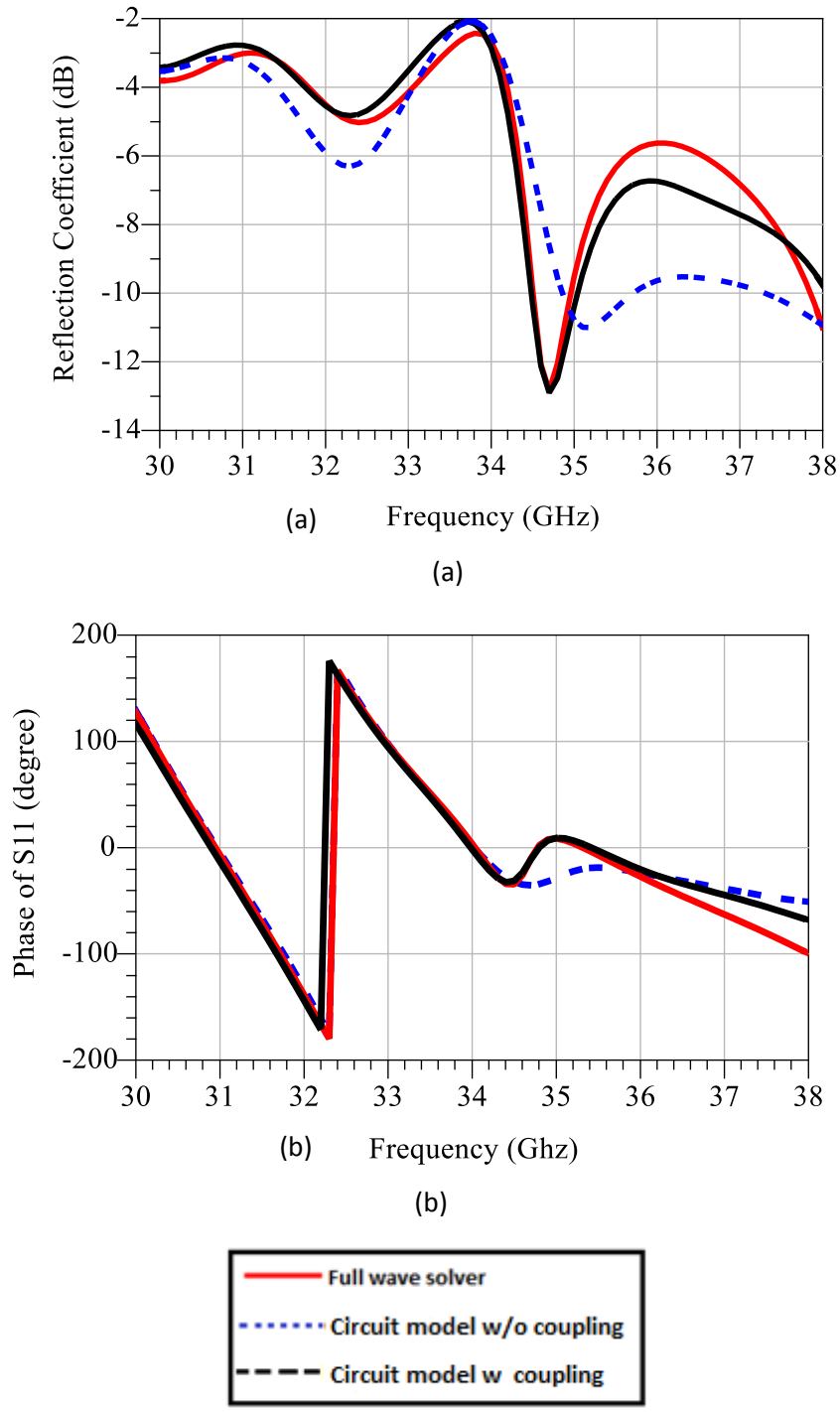

Figure 3.9 Four elements SIW_DRA array single port at D=7.2mm and X_{sc}=2.5mm. (a) Reflection coefficient (dB), and (b) phase of S_{11}

3.2 SIW-Series Fed DRA Array Configuration Using Longitudinal slot

In the previous section, a circuit model has been presented in for modeling SIW-DRA array fed by transverse slots. The mutual coupling is extracted and modeled as a two port network and then connected across two successive elements to improve the simulation accuracy for the antenna array. However, this model is not suitable for SIW-series fed DRA array using longitudinal slots due to the difference in the array structure.

In this section, a modified and improved circuit model is presented for modeling SIW-DRA array fed by longitudinal slots. Figure 3.12 shows the structure of a 4 elements SIW-series fed DRA linear array (SIW-DRA array), where narrow longitudinal slot cuts on the SIW broad wall are used to feed the DRAs [68]. The SIW, which supports the TE_{10} waveguide fundamental mode, is short circuited in one end. The antenna elements are separated by D_L, which is the distance between each two neighboring elements measured center to center. X_{sc} is the distance from the center of the last element to the short circuit end realized by vias. The initial values of D_L and X_{sc} are $\lambda_g/2$ and $3\lambda_g/4$, respectively, to achieve co-phase SIW series fed array excitation. The optimized single element (SIW-DRA single element) in [68] is used as a building block for the *N*-element SIW-DRA array for the longitudinal slot orientation. The structure of SIW-DRA ensures that the slots are positioned where the maximum SIW currents occur and the excitation slot fields are in phase. In this design, DRAs and SIW have the same dimensions, and are made of the same dielectric materials as the design mentioned in section 3.1. Only, the initial values of D_L and X_{sc} are different due to the change of the slot configuration.

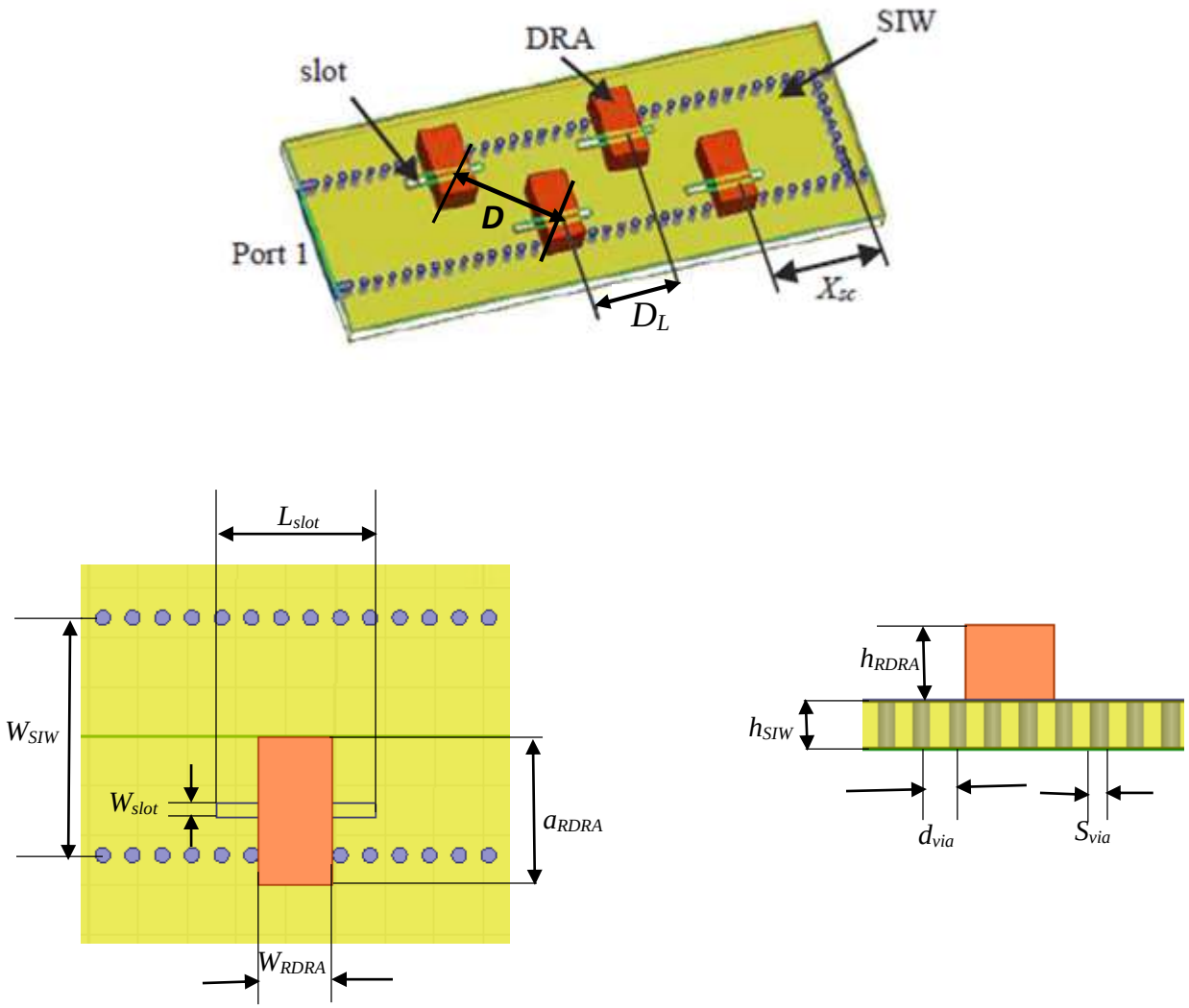

Figure 3.10 An example of a four-element SIW-DRA array fed by longitudinal slots [68]

3.2.1 Extraction of Mutual Coupling

The mutual coupling extraction methodology is outlined as follows, which is different from what is applied to the transverse slot. Before a circuit model is constructed, the basic cell of the array structure presented as a single element of SIW-DRA is first simulated using a full-wave solver, such as HFSS, to obtain the two-port S-parameters,

$[S]_{single}$. The reference planes are defined in the middle of a single element, and the two ports are de-embedded to the same plane. The single element can also be modeled as a "π" network as shown in Figure 3.20 (a) to facilitate the extraction of the coupling between elements. Next, the two-element structure in Figure 3.13(b), is also simulated using full wave solver, to obtain the two-port S-parameters for double elements structure, $[S]_{double}$, where the two ports are de-embedded to the center of each element. The SIW between the two antennas is modeled using a section of transmission line (T.L.) with the propagation constant γ.

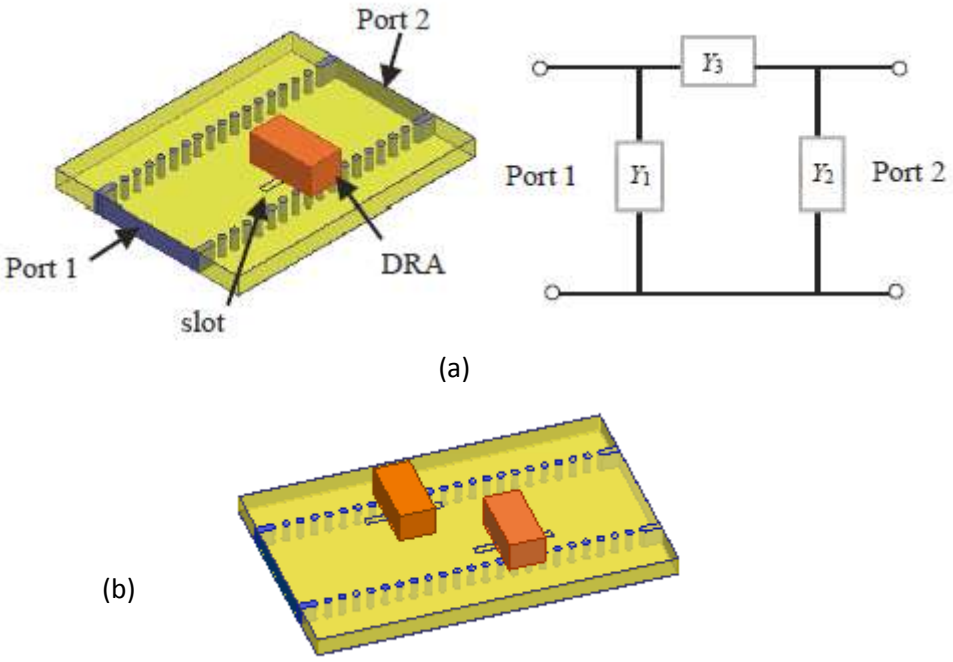

Figure 3.11 (a) A single module of SIW-DRA with longitudinal slot and its equivalent circuit as π network of the single element, and (b) the two-element SIW-DRA structure

The mutual coupling between antennas is taken into account through $[S]_{coupling}$. Note that only couplings between adjacent antennas are considered. The mutual coupling

in the case of longitudinal slots is found to be more accurately represented using the circuit model shown in Figure 3.14. The mutual coupling, expressed as a two-port network with S-parameters $[S]_{coupling}$, is shunt connected to each two successive elements. With known $[S]_{single}$ and $[S]_{double}$ from EM simulated single element, and two-element structures, respectively, $[S]_{coupling}$ can be easily extracted through simple network analysis using the circuit model shown in Figure 3.14. This model can then be used as building blocks to build the circuit model for an *N*-element array for a fast simulation of the array with improved accuracy.

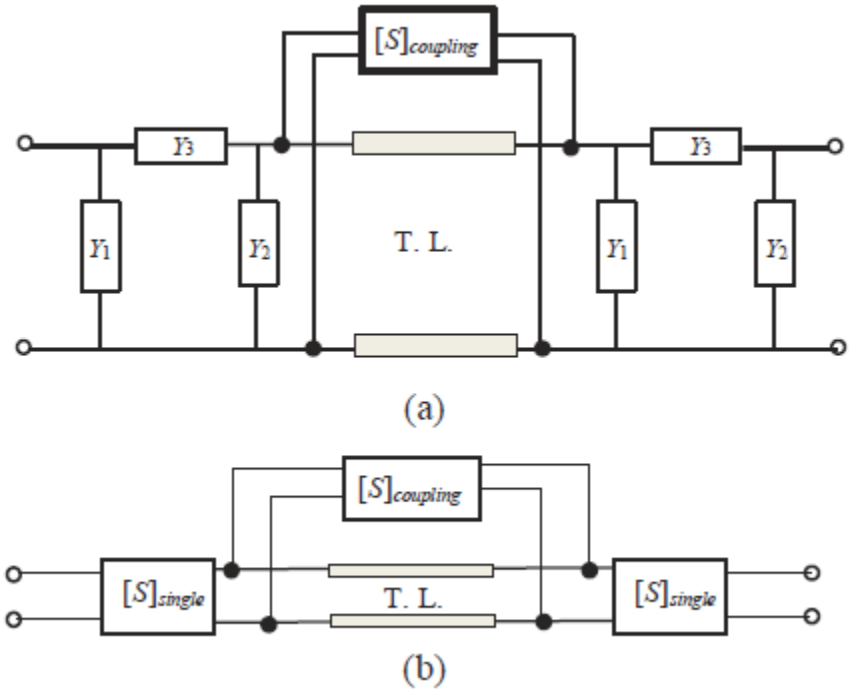

Figure 3.12 The circuit model of two-element SIW-DRA with single element modeled using (a) the π equivalent circuit, and (b) EM simulated S-parameters.

3.2.2 Mutual Coupling Extraction Procedure

As mentioned before, two EM simulations are performed: 1) a single element of SIW-DRA to obtain the two-port S-parameters $[S]_{single}$, and 2) a two-element SIW-DRA separated by D_L to obtain $[S]_{double}$. The following steps are then taken to extract the S-parameters of the mutual coupling, $[S]_{coupling}$, using the even-odd method and based on the characteristics of the cascaded two ports network [7].

1 Convert the S-parameters, $[S]_{single}$ to Y-parameters $[Y]_{single}$.

2 Find the admittances values Y_1,Y_2, and Y_3 of the *PI* two port network shown in Figure 3.14 (a) as follows:

a. $$Y_1 = Y_{11single} + Y_{12single} \tag{3.2}$$

b. $$Y_2 = Y_{22single} + Y_{12single} \tag{3.3}$$

c. $$Y_3 = -Y_{12single} \tag{3.4}$$

3 Apply the even-odd mode method to the S-parameters of the two elements SIW-DRA separated by D_L, $[S]_{double}$.

a. $$S_{11even} = S_{11double} + S_{12double} \tag{3.5}$$

b. $$S_{11odd} = S_{11double} - S_{12double} \tag{3.6}$$

4 Then, find the input impedance at the "even" and "odd" mode and convert it to the equivalent admittance.

a. $Z_{in-even} = \frac{1+S_{11even}}{1-S_{11even}}$; $Y_{in-even} = \frac{1}{Z_{in-even}}$

(3.7)

b. $Z_{in-odd} = \frac{1+S_{11odd}}{1-S_{11odd}}$; $Y_{in-odd} = \frac{1}{Z_{in-odd}}$

(3.8)

5 Calculate the coupling $[S]_{coupling}$ using even-odd mode method, as whole structure is symmetric and $[S]_{coupling}$ is shunt connected to each two successive elements as shown in Figure 3.14(a)

a. Calculate the admittance of the coupling at the even mode

$$Y_{in-even-coup} = \frac{1}{\frac{1}{Y_{in-even} - Y_1} - \frac{1}{Y_3}} - Y_2 - j\tan(\gamma . D_L/2)$$

(3.9)

b. Calculate the admittance of the coupling at the odd mode

$$Y_{in-odd-coup} = \frac{1}{\frac{1}{Y_{in-odd} - Y_1} - \frac{1}{Y_3}} - Y_2 + j\cot(\gamma . D_L/2)$$

(3.10)

Find the $[S]_{coupling}$

$$S_{11coup} = \frac{1-Y_{in-even-coup} \cdot Y_{in-odd-coup}}{(1+Y_{in-even-coup}) \cdot (1+Y_{in-odd-coup})} \quad ; S_{22coup} = S_{11coup}$$

(3.11)

$$S_{12coup} = \frac{Y_{in-odd-coup} - Y_{in-even-coup}}{(1+Y_{in-even-coup}) \cdot (1+Y_{in-odd-coup})} \quad ; S_{21coup} = S_{12coup}$$

(3.12)

3.2.3 Simulation Results

The SIW series-fed DRA array with four antennas as shown in Figure 3.12 is studied. The dimensions of the DRA and SIW are listed in section 3.1. The S-parameters of the mutual coupling are extracted following the steps described above for different values of the distance between antenna elements, D_L. The center frequency is at 38 GHz.

A. Two elements of SIW series-fed DRA

For validation, a two port SIW-DRA structure with two antenna elements as shown in Figure 3.13(b) is simulated. The circuit model is shown in Figure 3.14. The results for different distances between the two elements are shown below. The EM results using the full wave solver are compared to the circuit model results with and without considering the mutual coupling as shown in Figure (3.15) to Figure (3.17).

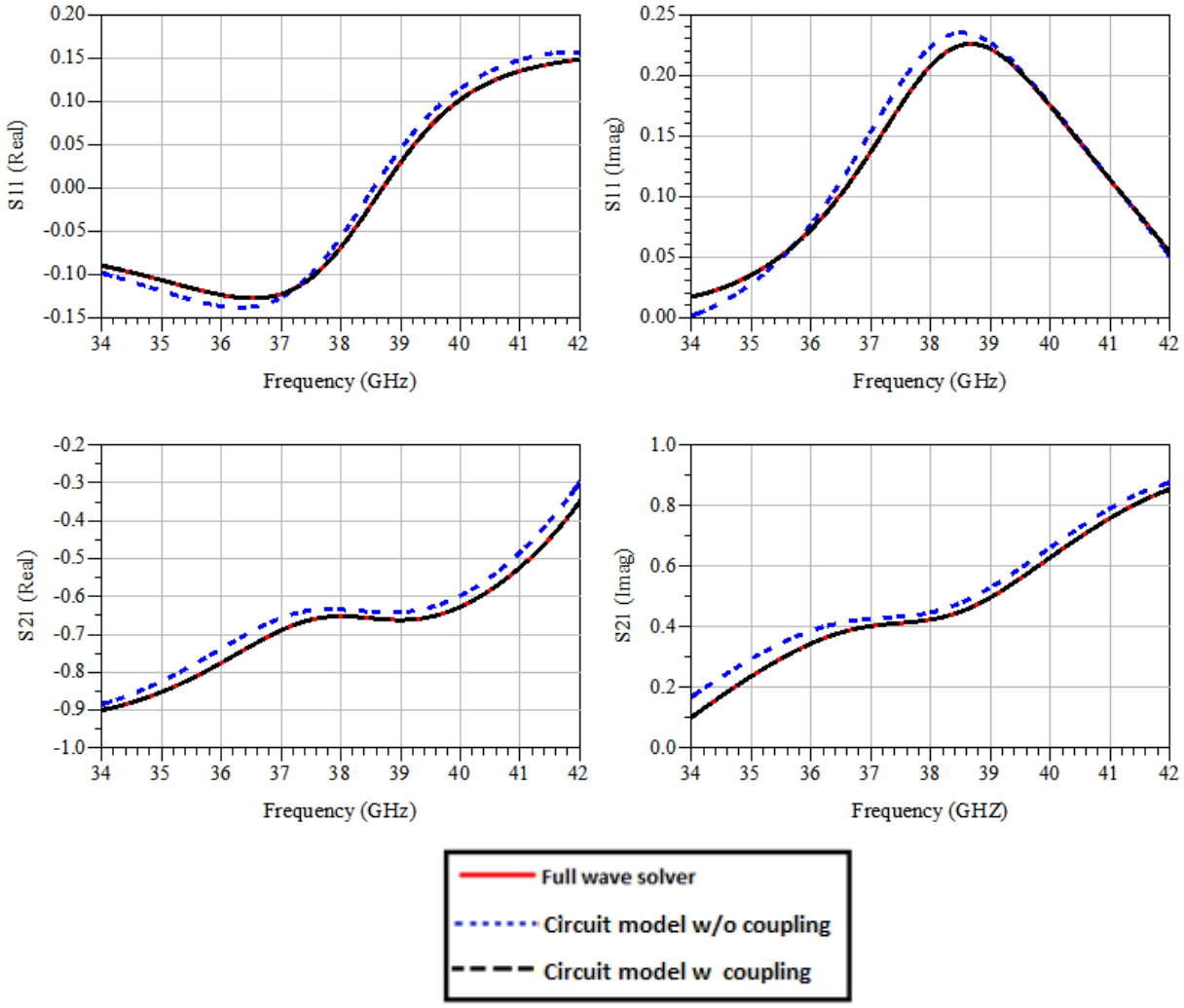

Figure 3.13 S-parameters of the SIW-DRA structure with two elements (D_L=3.5mm).

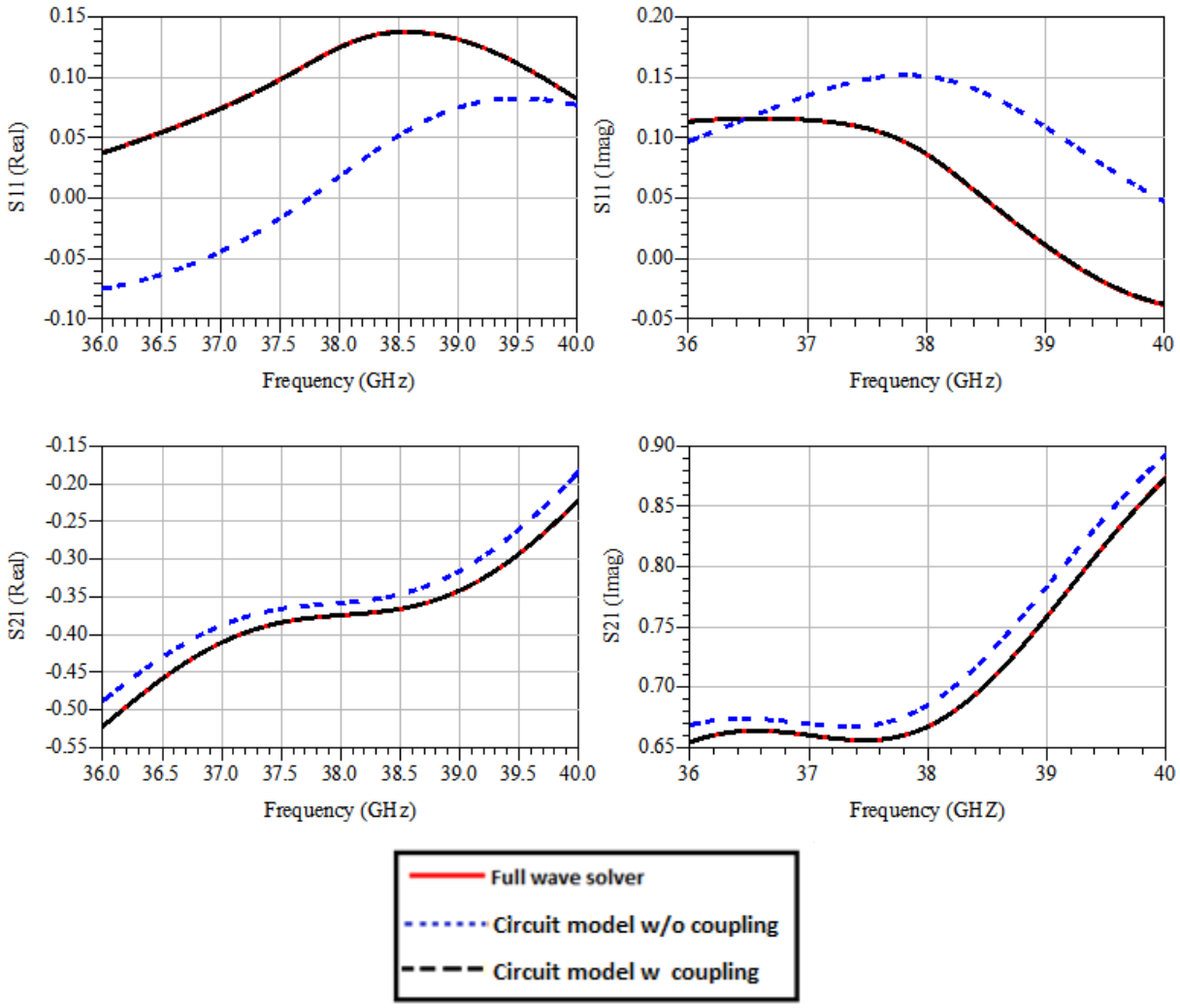

Figure 3.14 S-parameters of the SIW-DRA structure with two elements (D_L=4 mm).

As shown in all three cases in Figure 3.15, 3.16, and 3.17 for D_L=3.5mm, 4mm, and 4.6mm respectively, the results show a good agreement between EM and the circuit model after adding the mutual coupling, while the circuit model without the mutual coupling is quite different from EM results.

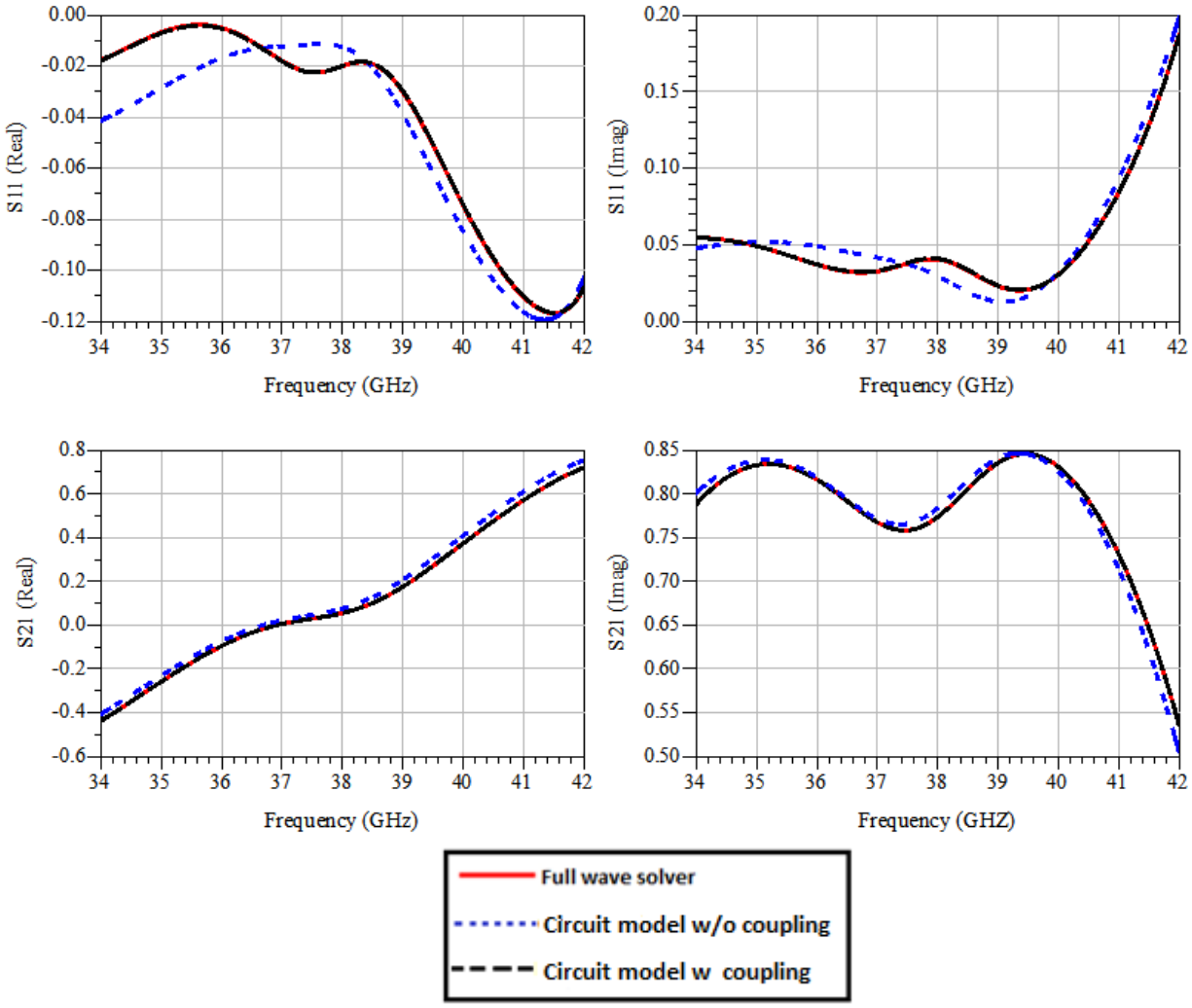

Figure 3.15 S-parameters of the SIW-DRA structure with two elements (D_L=4.6 mm).

B. Four elements SIW series-fed DRA array

This four-element SIW-DRA array with single port as shown in Figure 3.12 is investigated next. Firstly, a piece of SIW with one end short circuited is simulated in the full wave solver and compared to an ideal short-circuited transmission line. The length of the transmission line, X_{sc}, is measured from the center of the last element to the SIW short circuited end. The difference in the S-parameters for the SIW and the ideal short-circuited

transmission line is compensated by adding a correction length ΔL to X_{sc} in the circuit model so that the S-parameters of the EM model and circuit model agree to each other.

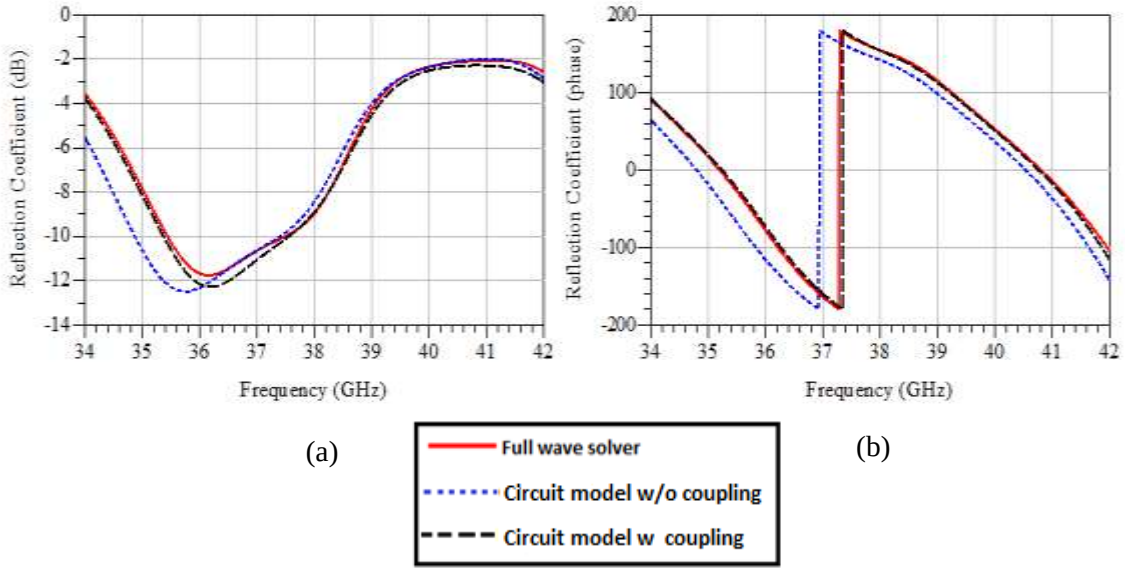

Figure 3.16 Four elements SIW_DRA array single port at D_L=3.5mm and X_{sc}=5mm (a) Reflection coefficient (dB), and (b) phase of Reflection coefficient.

The reflection coefficients of the four-element SIW-DRA array are calculated and compared to the EM simulation results and those of the circuit models with and without mutual coupling. The results using the developed circuit model and the EM simulation agree well as shown in Figure 3.18.

3.3 Development of the Fully Adjustable Circuit Model

The mutual coupling depends on the distance between antenna elements. The extracted coupling for a given structure will not be applicable once the distance changes. In this section, a fully adjustable model is developed.

The total mutual coupling between antenna elements extracted as described in the previous two sections is replaced with a circuit model. As shown in Figure 3.19, the $[S]_{coupling}$ is modeled using two cascaded S-parameters with a piece of lossy transmission line in between. Let the length of the transmission line $L_d = D - D_{ref}$. When $D = D_{ref}$, L_d=0 and $[S]_{coupling}$ is the cascade of $[S]_L$ and $[S]_R$, as shown in Figure 3.20(a). Therefore, $[S]_L$ and $[S]_R$ each represents "half" of the coupling between elements when the distance D is set to be the reference distance D_{ref}. It is assumed that $[S]_L$ and $[S]_R$ do not change with the distance D between antenna elements. The introduction of the transmission line facilitates the tuning of D. The model is therefore valid within a range of D, allowing optimizations of the design parameters. Note that D between each two successive elements is defined to be the distance between the centers of each element. Therefore for longitudinal slots, D is different from D_L as shown in Fig. 3.12.

The transmission line in the mutual coupling model is assumed to have a propagation constant

$$\gamma_c = \alpha_c + j\beta_c. \tag{3.13}$$

The attenuation constant α_c is introduced to model the effect that the coupling between elements diminishes as the distance between them increases. α_c and β_c are obtained through curve fitting. It is found in the simulations that α_c does not have a strong

effect on the accuracy of the results. For the transverse slots, $\beta_c = 2\pi / \lambda$ is found to be a good approximation, where $\lambda = c/f$, c is the speed of light and f is the frequency.

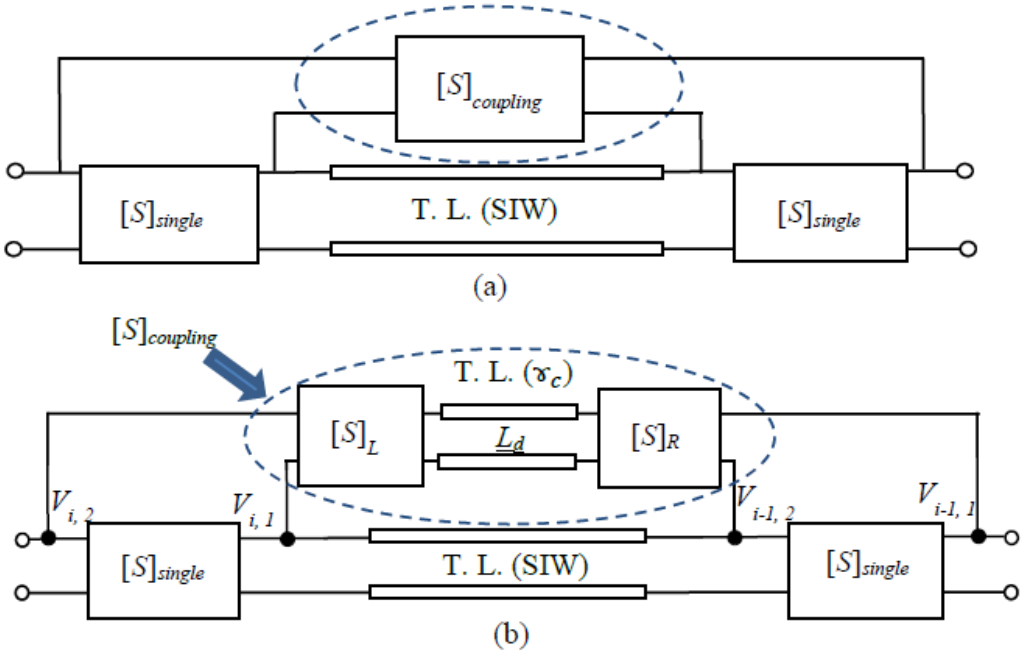

Figure 3.17 The total mutual coupling, $[S]_{coupling}$, circled in (a) is replaced with the equivalent circuit circled in (b), i.e. the cascaded $[S]_L$ and $[S]_R$ with a piece of lossy transmission line (T. L.) in between.

Considering the symmetry of the structure, if

$$[S]_L = \begin{bmatrix} S'_{11} & S'_{12} \\ S'_{21} & S'_{22} \end{bmatrix}$$

$[S]_R$ can be expressed as

$$[S]_R = \begin{bmatrix} S'_{22} & S'_{21} \\ S'_{12} & S'_{11} \end{bmatrix}$$

Therefore the only unknown in the model in Figure 3.19 is $[S]_L$, which can be solved using the mutual coupling of two different antenna separation distances, namely D_{ref} and D_1. As shown in Figure 3.20, let $[S]_A$ represent the $[S]_{coupling}$ for $D = D_{ref}$, and $[S]_B$ represent $[S]_{coupling}$ for $D = D_1$. The difference in $[S]_A$ and $[S]_B$ is caused by the transmission line with

a length of $L_d = D_1 - D_{ref}$. Based on this observation, $[S]_L$ can be derived as detailed in the following. D_{ref} and D_1 can be chosen close to a nominal design value, e.g. λ_g for the transvers slot case. Once $[S]_L$ is known, the model can be used for any D by substituting $L_d = D - D_{ref}$ in the model. For an antenna array with N elements, the building block in Figure 3.20 is repeated.

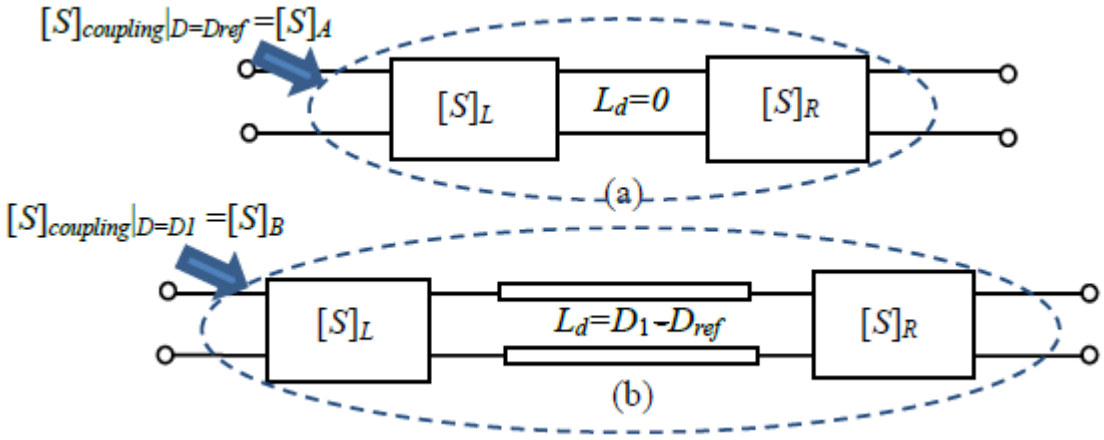

Figure 3.18 Solving for $[S]_L$ using two different antenna separation distance, D_{ref} and D_1. (a) $[S]_{coupling} = [S]_A$ for $D = D_{ref}$, and (b) $[S]_{coupling} = [S]_B$ for $D = D_1$.

Steps for Solving $[S]_{coupling}$

Extract the mutual coupling $[S]_{coupling}$ using the EM simulated data for the two-element DRA array for $D = D_{ref}$ as:

$$[S]_A = \begin{bmatrix} S_{11A} & S_{12A} \\ S_{21A} & S_{22A} \end{bmatrix} \tag{3.14}$$

Extract the mutual coupling $[S]_{coupling}$ using the EM simulated data for the two-element DRA array for $D = D_1$ as:

$$[S]_B = \begin{bmatrix} S_{11B} & S_{12B} \\ S_{21B} & S_{22B} \end{bmatrix} \tag{3.15}$$

For any two networks N' and N'' in cascade connection, if S' is the S-parameters of N', S'' is the S-parameters of N'', the S-parameters of the composite network is [86]

$$\begin{bmatrix} S_{11} & S_{12} \\ S_{21} & S_{22} \end{bmatrix} = \begin{bmatrix} S'_{11} + k.S'_{12}.S'_{21}.S''_{11} & kS'_{12}.S''_{12} \\ k.S'_{21}.S''_{21} & S''_{22} + k.S''_{12}.S''_{21}.S'_{22} \end{bmatrix} \tag{3.16}$$

where,

$$k = \frac{1}{1 - S'_{22}.S''_{11}} \tag{3.17}$$

In Figure 3.13(a), since $S''_{11} = S'_{22}$ and $S''_{21} = S'_{21}$, use the previous equation and substitute *k* value to get S_{11A}, S_{11B}, S_{21A}, and S_{21B}.

$$S_{11A} = S'_{11} + \frac{S'_{12}.S'_{21}.S\prime_{22}}{1 - S\prime_{22}.S\prime_{22}} \tag{3.18}$$

$$S_{11B} = S'_{11} + \frac{S\prime_{12}.S\prime_{21}.e^{-2\gamma.\Delta l}.S\prime_{22}}{1 - S\prime_{22}.e^{-2\gamma.\Delta l}.S\prime_{22}} \tag{3.19}$$

$$S_{21A} = \frac{S\acute{}_{21}.S\acute{}_{12}}{1 - S'_{22}.S'_{22}} \tag{3.20}$$

$$S_{21B} = \frac{S\prime_{21}.S\prime_{12}.e^{-\gamma.\Delta l}}{1 - S\prime_{22}.e^{-2\gamma.\Delta l}.S\prime_{22}} \tag{3.21}$$

Therefore,

$$\frac{S_{21A}}{S_{21B}} = \frac{\left[e^{\gamma\Delta l} - (S\prime_{22})^2.e^{-\gamma.\Delta l}\right]}{1 - (S\prime_{22})^2} \tag{3.22}$$

Then,

$$(S'_{22})^2 = \frac{S_{21A} - S_{21B}.e^{\gamma.\Delta l}}{S_{21A} - S_{21B}.e^{-\gamma.\Delta l}} \tag{3.23}$$

Next, substitute $(S'_{22})^2$ in (3.20) to get $(S'_{21})^2$. Subtract equation (3.19) from equation (3.18), and substitute $(S'_{21})^2$ to get S'_{22}. To get S'_{11}, substitute S'_{22} in equation (3.18). $[S]_L$ and $[S]_R$ are thus solved and the model in Figure 3.19 can be built for any D in the vicinity of D_{ref} and D_1.

Note that even though the 2 element structure with longitudinal slots in 3.13(b) does not seem symmetric, the S_{11} and S_{22} are in fact the same. The steps described above are therefore still valid, as will be shown in the next section.

3.3.1 Simulation Results

The SIW series-fed DRA array as shown in Figure 3.1 and Figure 3.12 are studied. The S-parameters of the mutual coupling are modeled for different values of the distance between antennas elements, following the steps described above to calculate the $[S]_L$ and $[S]_R$ for each design. In all examples of transverse slot, the $[S]_L$ and $[S]_R$ are calculated using the extracted coupling from EM simulated results at D_1=8.2mm and D_{ref}=7mm. On the other hand, all examples of longitudinal slot, the $[S]_L$ and $[S]_R$ are calculated using the extracted coupling from EM simulated results at D_1=5.2mm and D_{ref}=4.6mm.

For two port SIW-DRA fed by transverse slot configuration of two antennas elements, the EM results are compared to the circuit model after considering the new model of the mutual coupling as shown in Figure 3.21 and Figure 3.22. The results of the S-parameters of the adjustable circuit model are very close to the results having total coupling, and both of them are close to the EM simulated results, while the results without mutual coupling is different.

A. Two elements SIW series-fed DRA with two ports

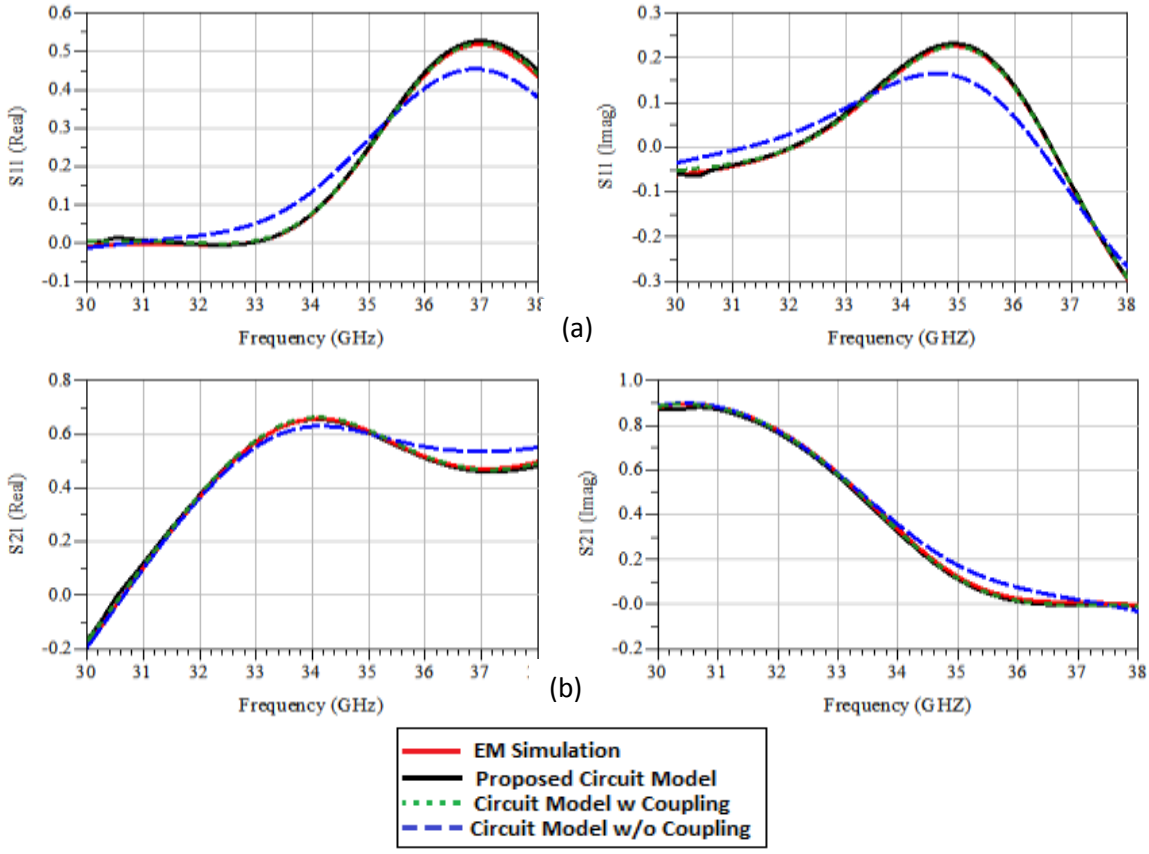

Figure 3.19 S-parameters results of the SIW-DRA fed by transverse slot configuration with two elements at *D*=6.5mm. (a) S_{11} (real and imaginary), and (b) S_{21} (real and imaginary).

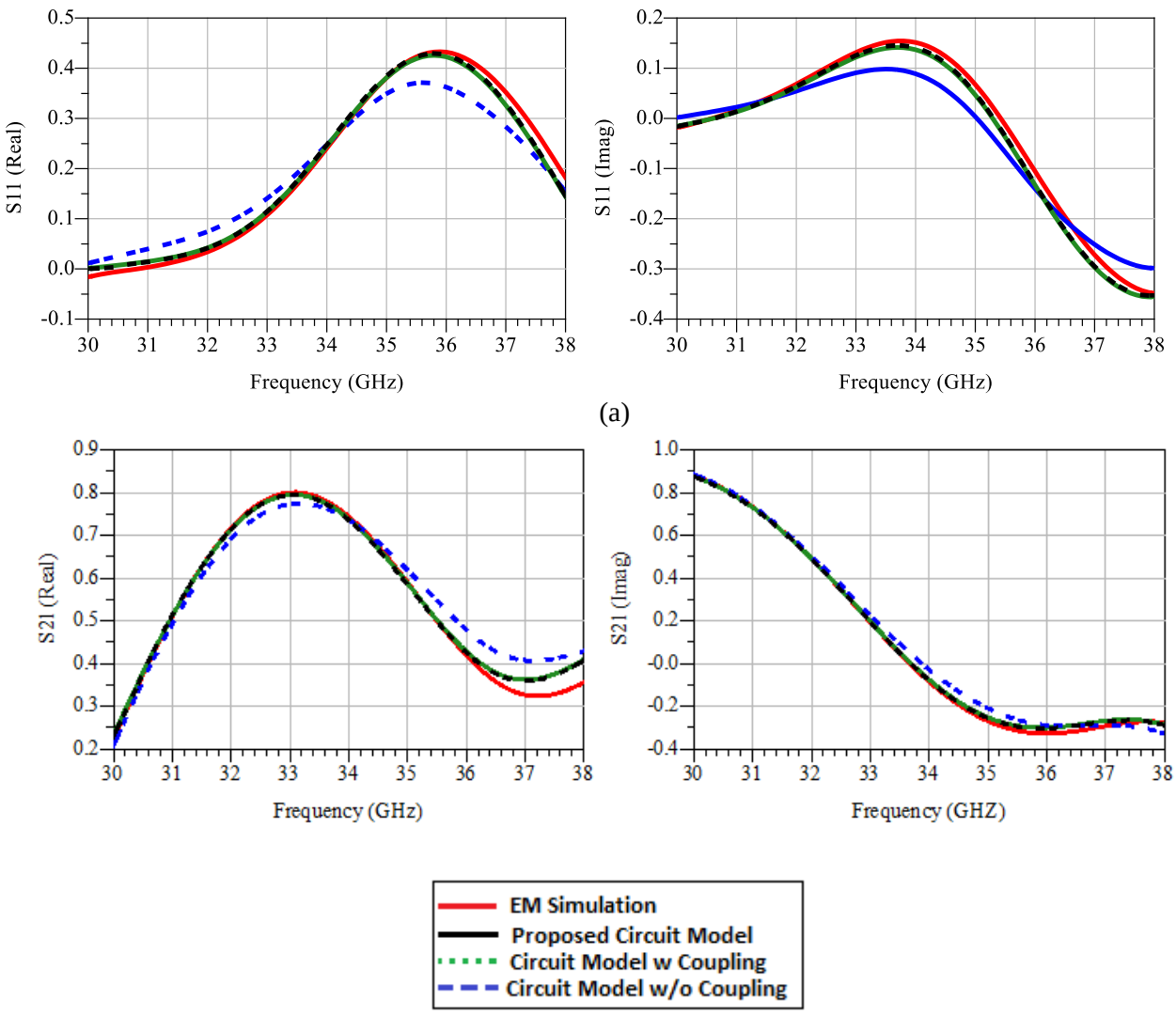

Figure 3.20 S-parameters results of the SIW-DRA fed by transverse slot configuration with two elements at *D*=7.2mm. (a) S_{11} (real and imaginary), and (b) S_{21} (real and imaginary).

The longitudinal slot configuration for the two port SIW-DRA of two antennas elements is modeled, and the EM results are compared to the proposed circuit model as shown in Figure 3.23 and Figure 3.24. From the results of the S-parameters, it is clear that there is a total agreement between the EM solver, the results having the total coupling, and the proposed circuit model results, while the circuit model results without mutual coupling

is different. This proves that the new technique is equivalent to the total mutual coupling extracted before.

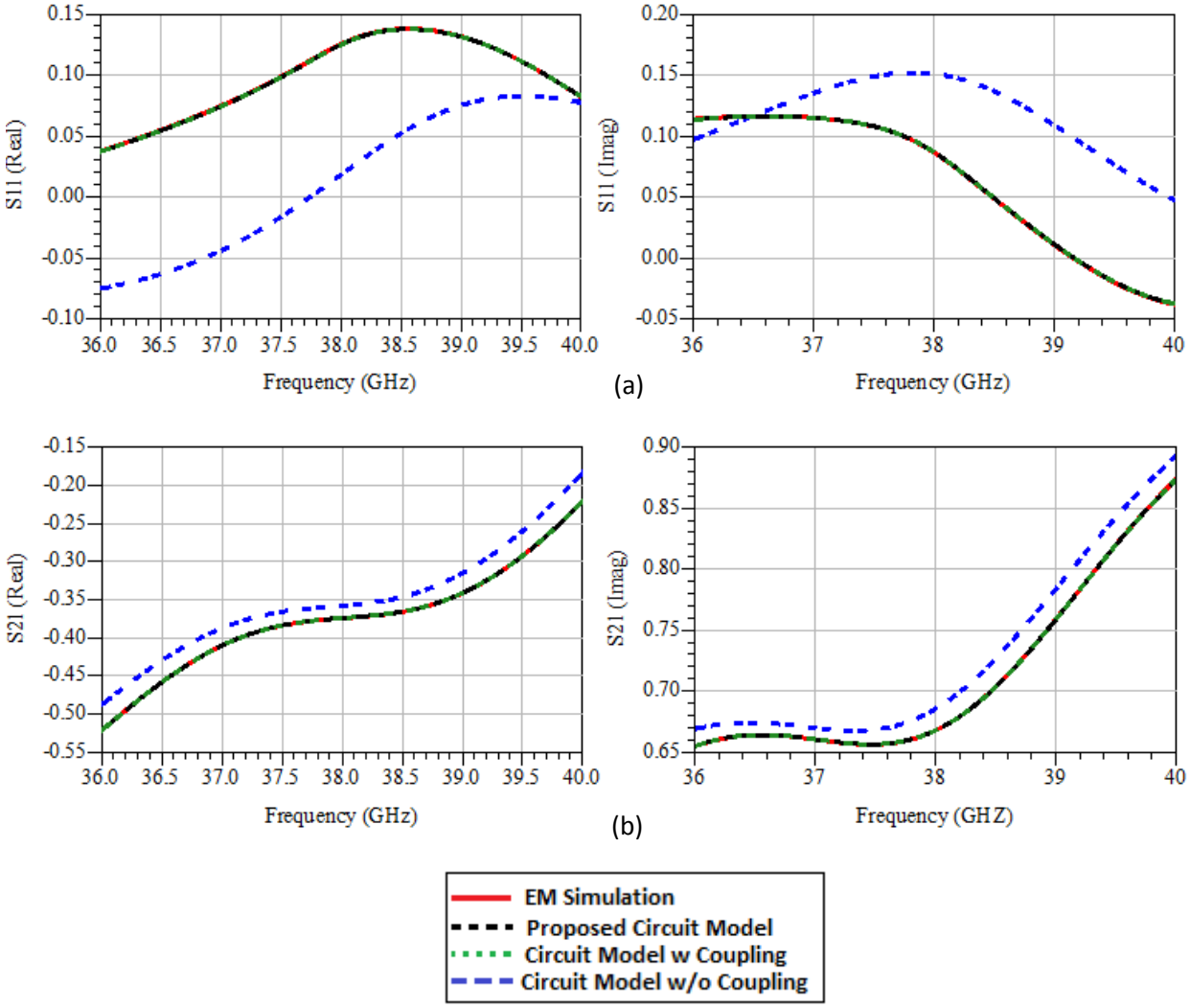

Figure 3.21 S-parameters results of the SIW-DRA fed by longitudinal slot configuration with two elements at D_L=4 mm. (a) S_{11} (real and imaginary), and (b) S_{21} (real and imaginary).

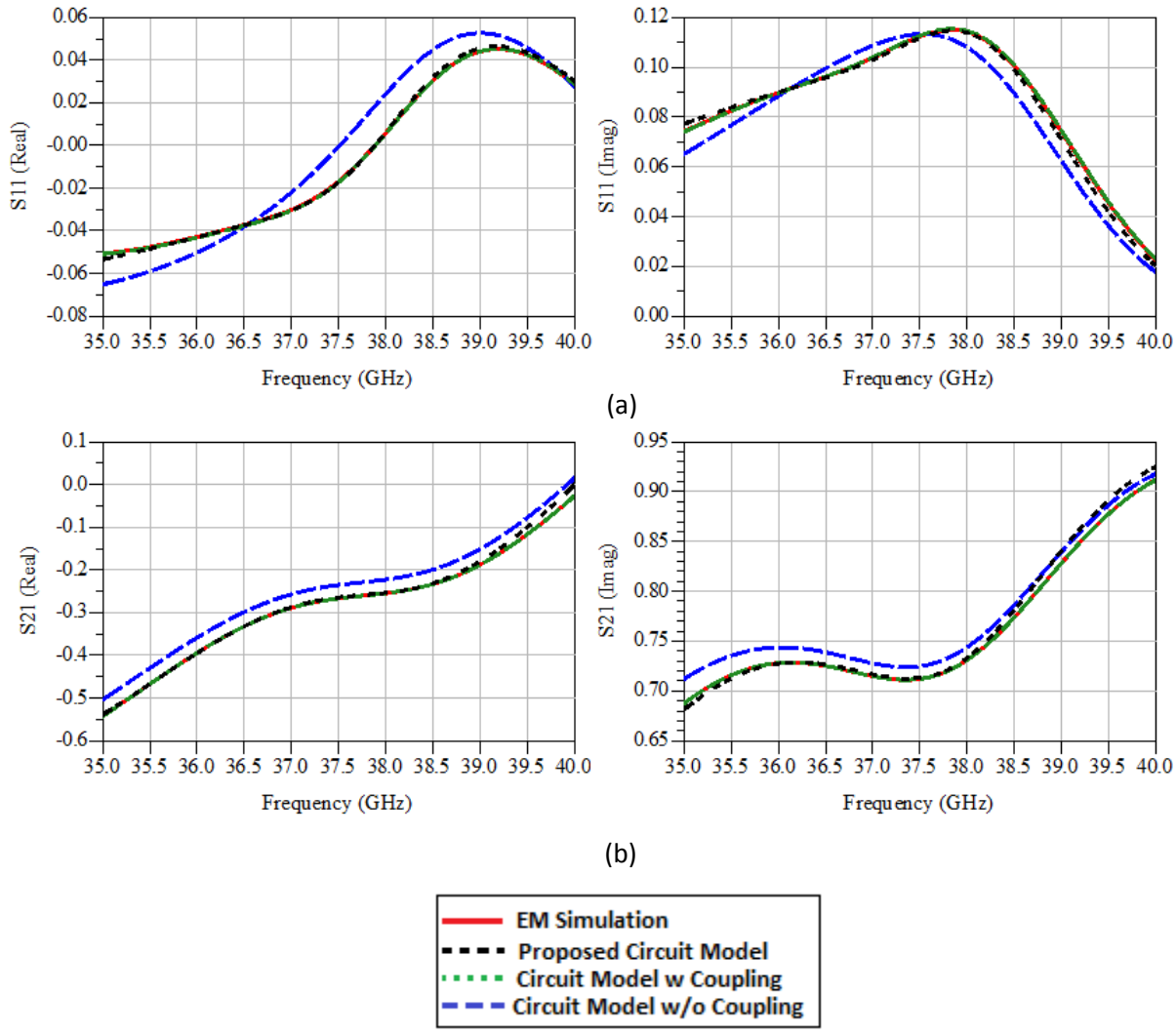

Figure 3.22 S-parameters results of the SIW-DRA fed by longitudinal slot configuration with two elements at D_L=4.2 mm. (a) S_{11} (real and imaginary), and (b) S_{21} (real and imaginary).

B. Four elements SIW series-fed DRA array

The example of the four elements of SIW-DRA single port shown in Figure 3.1 and Figure 3.12 are studied. The reflection coefficients of the four-element SIW-DRA array are calculated at different cases. The EM simulation results are compared to those of the circuit model with the mutual coupling. Firstly, the results of four elements of SIW-DRA

single port fed by transverse slot are illustrated in Figure 3.25 and Figure 3.26 for D= 7.2mm and D=7.6mm, respectively, where X_{sc}=2.5mm for all cases.

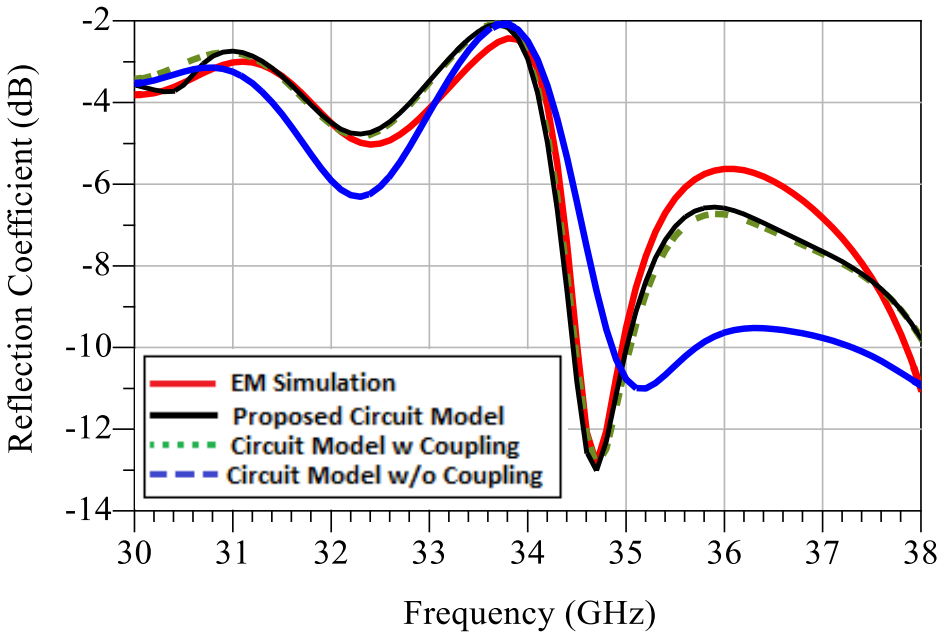

Figure 3.23 The reflection coefficient (S_{11}) in dB of a single port SIW-DRA fed by transverse slot configuration, N=4, D=7.2mm and X_{sc}=2.5mm

In the case of D=7.6mm, the measured results [68] are also compared with the results of the proposed circuit model. The fabricated antenna array is measured over the operating frequency band 33–40 GHz. The comparison with the measured results demonstrates that the new circuit model improves the accuracy of S-parameter. Figure 3.26 shows the reflection coefficient in dB, where an excellent agreement between the proposed circuit model, the measured, and the EM simulation results are achieved. As shown in the figure, the reflection coefficient of the proposed circuit model is very close to the measured results especially around the center of the operating frequency.

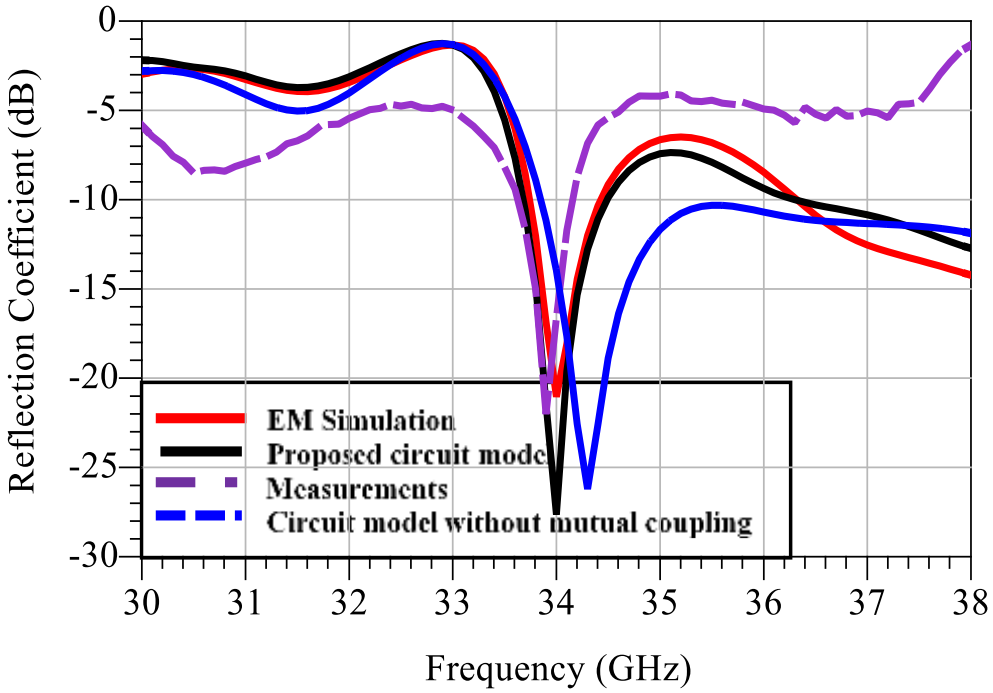

Figure 3.24 The reflection coefficient (S_{11}) in dB of a single port SIW-DRA fed by transverse slot configuration, N=4, D=7.6mm and X_{sc}=2.5mm.

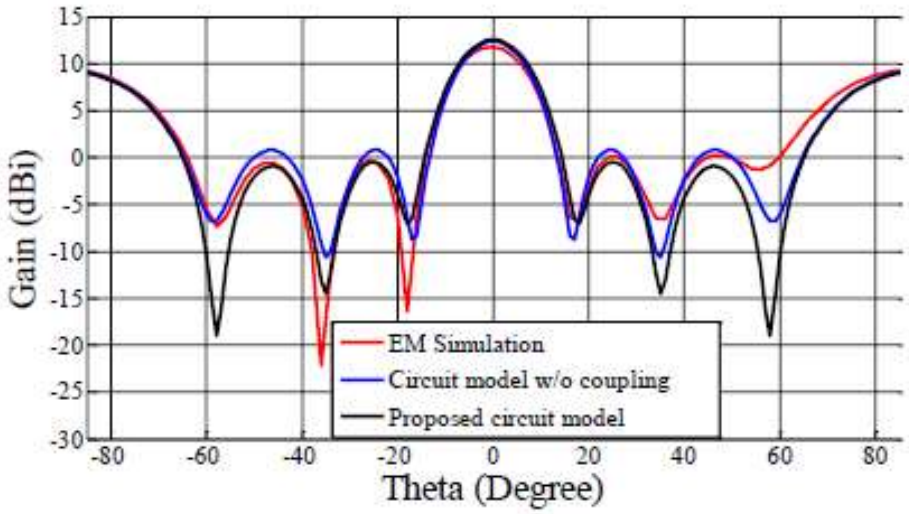

Figure 3.25 The radiation pattern of the antenna array SIW-DRA, N=4, D=7.6mm and X_{sc}=2.5mm.

The voltage across each antenna obtained from the circuit model can also be used to calculate the radiation pattern. The voltages $V_{i,1}$ and $V_{i,2}$, i=1, 2, 3, ..., N, for each antenna are marked in Figure 3.19 (b). These voltages can be found using the circuit model in ADS. The antenna array factor is calculated using [68].

$$AF = \sum_{i=1}^{N} V_i \, e^{j(i-1)k_o D \sin\theta \cos\varphi} \tag{3.24}$$

where $V_i = V_{i,2} - V_{i,1}$ and k_o is the wave number in free space. The radiation pattern is then simulated by multiplying the pattern of a single DRA element (obtained from EM solver) and the array factor in (3.24). The patterns obtained from full EM simulation and the circuit model at ϕ=0 are shown in Figure 3.27, where a maximum gain of 11.79 dBi is shown. For radiation pattern simulation, the results from the proposed circuit model are not significantly different from those of a conventional circuit model. A good agreement between the EM and circuit model results is observed.

Secondly, the results of four elements of SIW-DRA single port fed by longitudinal slot are illustrated in Figure 3.28 and Figure 3.29 for D= 4.2mm and D=3.5mm, respectively, where, X_{sc}=5mm for both cases. The EM results are compared to the proposed circuit model. From the comparison of the S-parameters, it is clear that there is a good agreement between the EM solver, and the proposed circuit model results. However, the mutual coupling in the case of longitudinal slot is weaker than the transverse slot due to the difference in slot orientation. To prove the effect of adding the mutual coupling and the benefits of the adjustable circuit model, an example of parasitic antenna array using longitudinal slot will be shown in the next section.

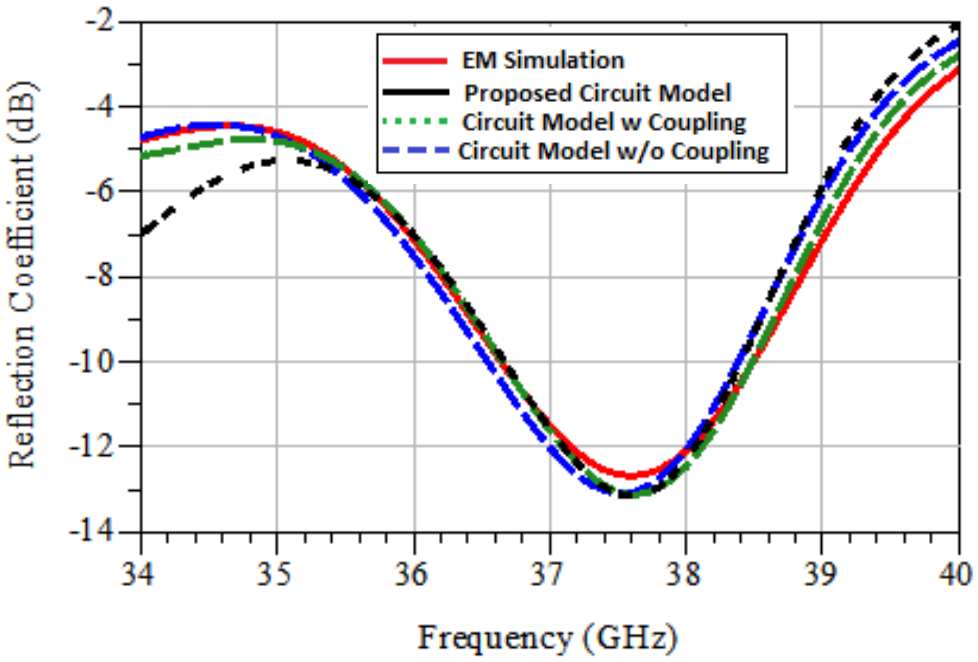

Figure 3.27 The reflection coefficient (S_{11}) in dB of a single port SIW-DRA fed by longitudinal slot configuration, N=4, D_L=4.2 mm, and X_{sc}=5mm

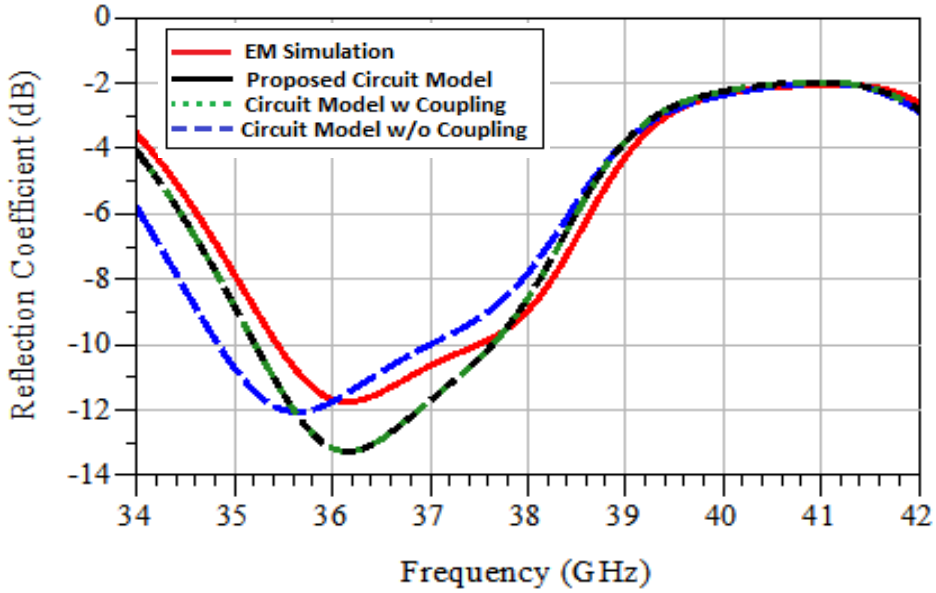

Figure 3.26 The reflection coefficient (S_{11}) in dB of a single port SIW-DRA fed by longitudinal slot configuration, N=4, D_L=3.5 mm, and X_{sc}=5mm.

3.4 SIW-Series Fed DRA Parasitic Array Configuration Using Longitudinal slot

Parasitic (passive) element of an antenna is a directive element that is not connected to a transmitter or receiver either directly or via a feeder, but is coupled to the driven element only by the fields [87]. Parasitic elements in DRA antennas have been investigated to increase the impedance bandwidth of the antenna by Simon, and Antar in [88, 89]. The impedance bandwidth increases in this application, where the parasitic DRs of different dielectric constants and different sizes are positioned next to the active DR. Using parasitic elements for the gain enhancement is shown in [90], by placing parasitic elements on one side of the active element. By comparing the usage of the parasitic elements to the case of feeding each dielectric resonator, this technique has some advantages such as less spurious radiation, low loss, simpler fabrication, and low cost.

In this design, the radiation pattern is improved by using the parasitic elements that are shown in Figure 3.30. An additional parasitic DRA is added on both sides of each active element of the four-element SIW-DRA array fed by longitudinal slots shown in previous section. This array has stronger mutual coupling between the antenna elements compared to the one without parasitic elements.

In this design, active and passive DRAs are made of a dielectric material with ε_{RAD} =10.20 and the dimensions of each element h_{RDRA} (thickness) = 1.27mm, a_{RDRA} (length) = 3.0 mm and W_{RDRA} (width) =1.50 mm. The distance between each active and passive elements is 4.2mm. Each active rectangular DRA element is excited by a narrow slot of length L_{slot}=3.2mm, and width W_{slot}=0.3mm. The SIW is made of two rows of metallic vias of diameter d_{via} =0.3 mm in a substrate, and two neighbouring vias are separated by

s_{via}=0.6mm. The distance between the two rows are considered to be the width of the SIW, W_{SIW}=4.5mm. The substrate material, metalized on both sides, has a permittivity constant of ε_{SIW}=2.94 and a thickness of h_{SIW} = 0.5mm.

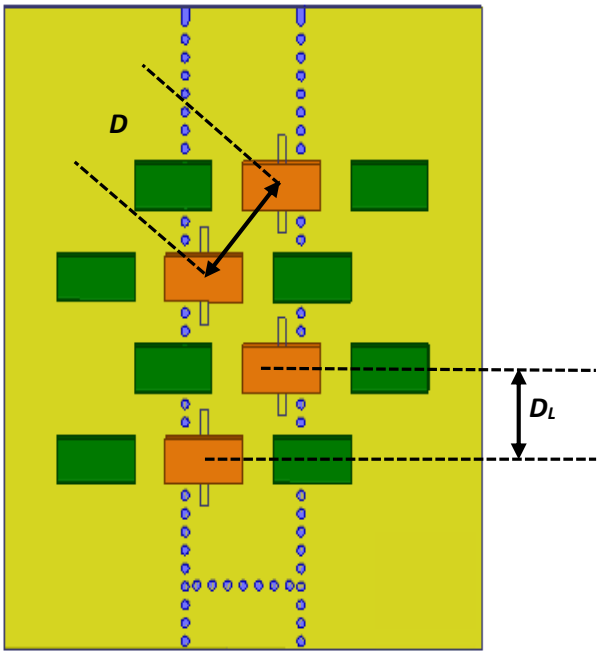

Figure 3.29 A four-element SIW-DRA parasitic array fed by longitudinal slots

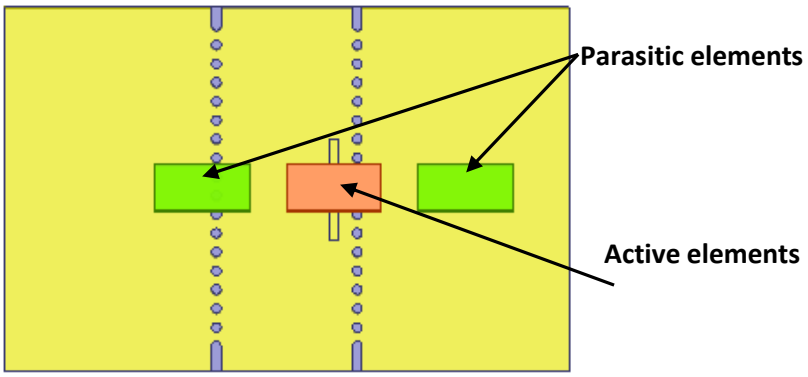

Figure 3.28 A single module of the SIW-DRA parasitic array fed by longitudinal slots

Extraction of the mutual coupling is the same as what has been explained before in section 3.2. Firstly, the circuit model is constructed using the basic cell of the array structure. This basic cell consists of three elements; a single active element of SIW-DRA and passive DRA elements of the same size on both sides of the active element as shown in Figure 3.31. It is simulated using a full-wave solver, to obtain the two-port S-parameters, $[S]_{\text{single}}$. Next, a 2 cell model is EM simulated. Following all the steps mentioned before, $[S]_{coupling}$ is obtained. Finally, the fully adjustable model is developed using the method described in section 3.3. The S-parameters of the mutual coupling are extracted at different values of the distance between antennas elements, namely D_1=4.6 mm and D_{ref}=4.2 mm. $[S]_L$ and $[S]_R$ are then calculated and the adjustable model can then be built. The model is tunable for D_L, and allows optimization of the design parameters.

3.4.1 Simulation Results

The SIW series-fed parasitic DRA array with two and four elements are investigated. The center frequency is at 38 GHz. Simulation results are shown in Figure 3.23 and Figure 3.24 for the two element (two ports) and four element (single port) structures, respectively. As can be seen, there is a good agreement between the proposed circuit model and EM simulation results.

A. Two elements parasitic SIW series-fed DRA with two ports

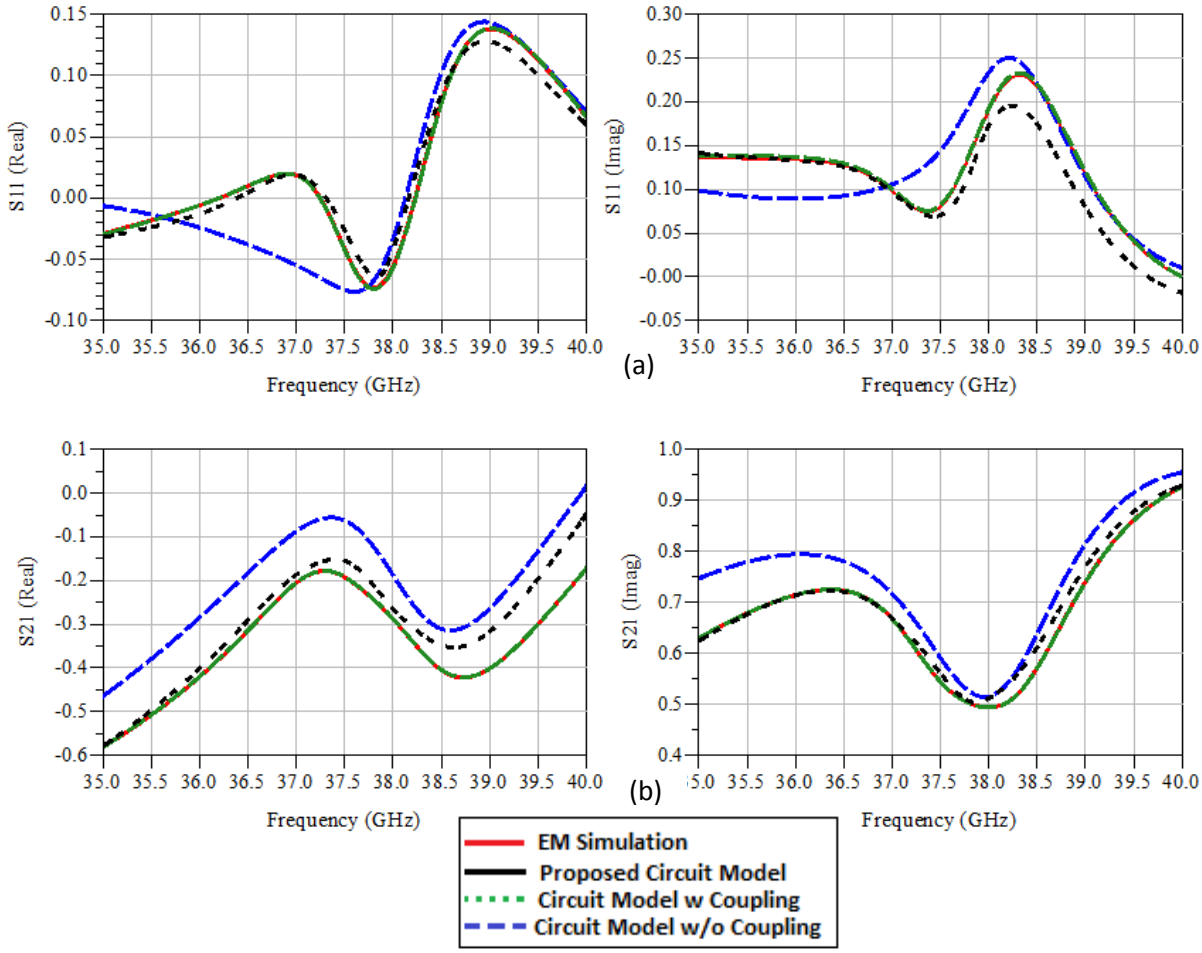

Figure 3.30 S-parameters results of the two elements parasitic SIW-DRA fed by longitudinal slot configuration with D_L=3.5 mm. (a) S_{11} (real and imaginary), and (b) S_{21} (real and imaginary).

B. Four elements SIW series-fed DRA array

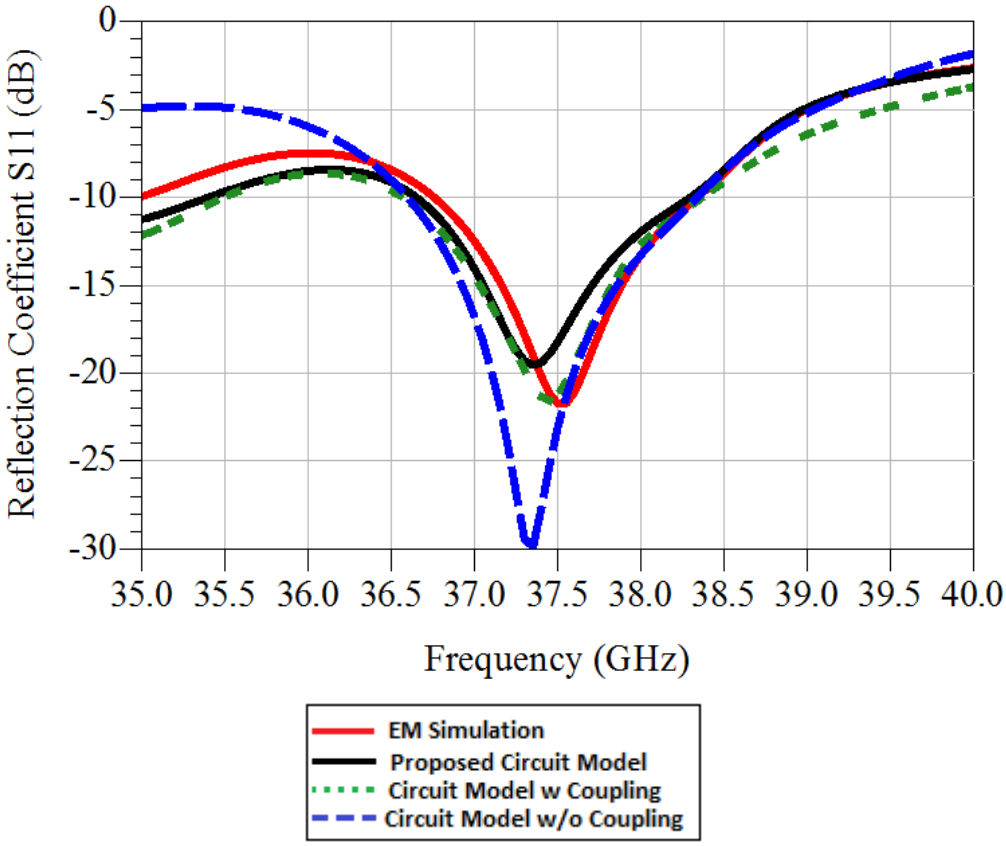

Figure 3.31 The reflection coefficient (S_{11}) in dB of the parasitic SIW-DRA array fed by longitudinal slot configuration, N=4, D_L=3.5 mm, and X_{sc}=4mm

3.5 Conclusion

An efficient and accurate circuit model is presented in this chapter for the modeling of SIW-DRA arrays. For improved model accuracy and flexibility, the mutual coupling between antenna elements is taken into account as a total coupling, then represented by a fully adjustable model, allowing the design parameters to be varied. Development of the circuit model is straightforward, for which only three simple EM simulations are required, and steps are described in detail. Once a model building block is developed, a complete circuit model can be readily built for antenna arrays with different number of elements and different distances between elements. Simulation results with improved accuracy can be obtained very fast. Iterative antenna array design and optimization can therefore be performed much more efficiently, compared to EM-based optimization.

For validation, the developed circuit model is applied to two different structures of SIW series-fed DRA arrays. All results show very good agreement between the proposed circuit model, the measured and/or the EM simulated results.

In addition to, a new design of four elements parasitic SIW-DRA fed by longitudinal slot configuration is presented. This design has stronger mutual coupling between the antenna elements compared to the same design without parasitic elements. In spite of this strong coupling, a good matching is achieved between the proposed circuit model and the simulation results, which indicates the accuracy of the circuit model.

Chapter 4

Design and Optimization of SIW Center Fed Series Rectangular Dielectric Resonator Antenna (DRA) Array with 45° Linear Polarization

In some specific radar applications, such as collision avoidance automotive radar, monopulse tracking radar, and synthesis aperture radar (SAR), a 45° inclined linear polarization (LP) is required to alleviate the interference coming from the opposite direction. Using fundamental shunt and series waveguide-fed slot array antennas can't generate an arbitrary polarization, but generate only the vertical or horizontal LP [91]. There is a proportional relationship between the tilt angle of a centered-inclined series slot, and the corresponding self-impedance. The maximum self-resistance happens when the tilt angle increases to 45° [92]. Moreover, in the case of an arbitrary LP, to achieve impedance matching to the input wave impedance of a given waveguide, the number of series slot

elements for an arbitrary LP should be limited. Various slot array antennas have been presented for the 45°-inclined LP with different operating mechanisms for the traveling-wave excitation [93–95].

In order to avoid these problems of WG-fed slot array antennas, dielectric resonator antennas (DRAs) can be a good replacement. DRAs offer attractive features such as low profile, compact size, low ohmic loss, high radiation efficiency [19]. It is compatible with existing excitation methods [55], and has a good matching with Microwave Integrated Circuits (MICs) [6]. In order to get the best design of DRAs for a specific target, many points should be considered such as size and location of the dielectric resonator (DR), and the dimensions of the feed line and the ground plane [96].

In this chapter, a new design and its equivalent circuit model for the Substrate Integrated Waveguide (SIW) middle fed series dielectric resonator antenna (DRA) array with 45° linear polarization will be described. The S-parameters and the radiation pattern of full-wave simulation are presented and compared with the results from the equivalent circuit model. Furthermore, we propose to optimize the array performance applying the space mapping (SM) optimization technique. The developed circuit model is used as the coarse model. As will be shown, high optimization efficiency is achieved. The input return loss of an eight-element DRA array is optimized within only three iterations.

4.1 SIW-Series Fed DRA Array Configuration

Figure 4.1 shows the structure of an 8-element DRA array with 45° linear polarization and backed by SIW. The basic single element is shown in Figure 4.2, which

is a two port SIW-fed 45°-inclined DRA. It is used as a building block for the 8-element structure in Figure 4.1. The energy into DRA elements is coupled using slots, which are excited by the SIW's fundamental mode, the TE_{10} mode. As we mentioned before, the distance, *D*, between any two neighboring elements, and the distance from the last element to the SIW short circuited end, X_{sc}, are important design parameters.

The rectangular dielectric resonator antenna (RDRA) is preferred over other DRA structures due to the fact that it is simple and easy to fabricate, as mentioned in chapter 3. Regarding the dielectric material, it should have a dielectric constant $5 \leq \varepsilon_r \leq 20$ to have a good bandwidth. Also, the dimension will be smaller for high dielectric constant, which will make the fabrication more difficult. In this design, DRAs are made of a dielectric material with ε_{DRA} =10.20 (Rogers RT/6010 substrate), which is readily available and the cost is low. The dimensions of RDRA should be chosen to excite the correct mode for radiation.

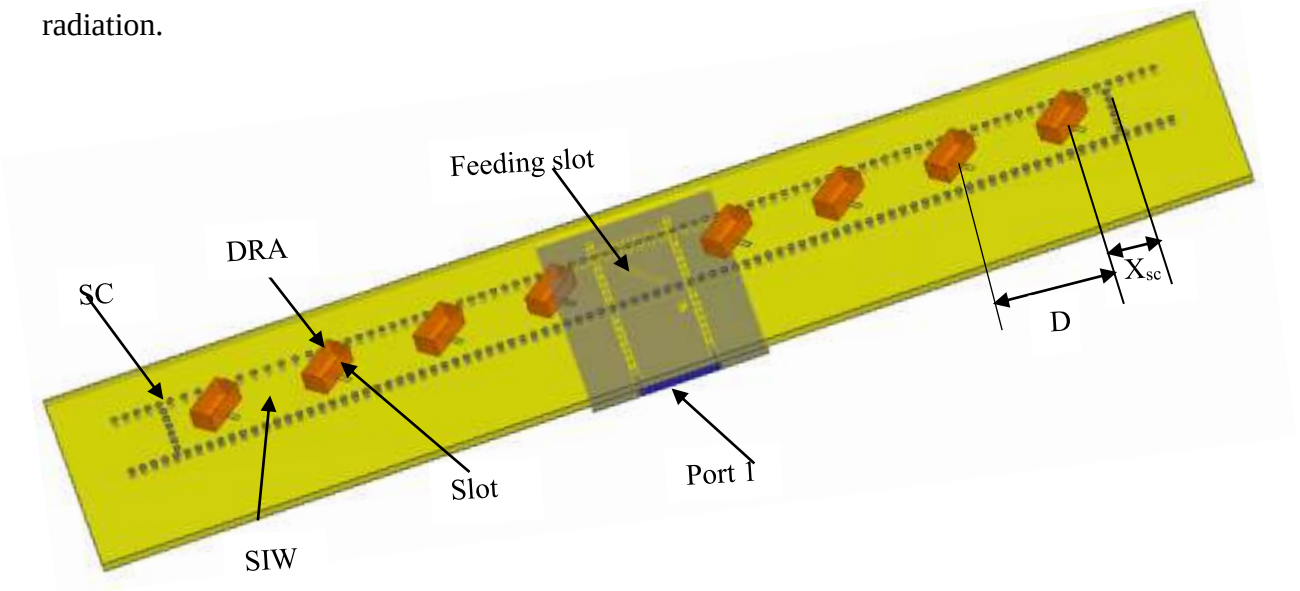

Figure 4.6 An eight-element SIW-middle fed series DRA array with 45° linear polarization

As shown in Figure 4.3, h_{RDRA} (thickness) = 1.27mm, a_{DRA} (length) = 3 mm and W_{RDRA} (width) =1.5 mm. Each rectangular DRA element is excited by a narrow slot of length L_{slot}=3 mm, and width W_{slot}=0.3mm. The SIW is made of two integrated rows of metallic vias of diameter d_{via} =0.4 mm in the substrate, where the distance between the two rows are considered to be the width of SIW W_{SIW}=4.8mm. The substrate material RT/6002 has a permittivity constant of ε_{rSIW}=2.94 and a thickness of h_{SIW} = 0.5mm, metalized on both sides. Any two neighbouring vias are separated by s_{via}=0.6mm. The SIW parameters are designed using the criteria described in [74], where the SIW equivalent rectangular waveguide width is given by equations (2.6) to (2.6c) in chapter 2.

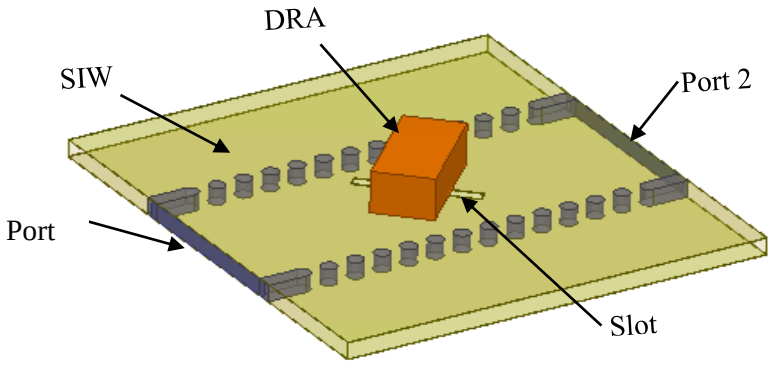

Figure 4.2 A single element of two port SIW- middle fed series dielectric resonator antenna (DRA) with 45° linear polarization

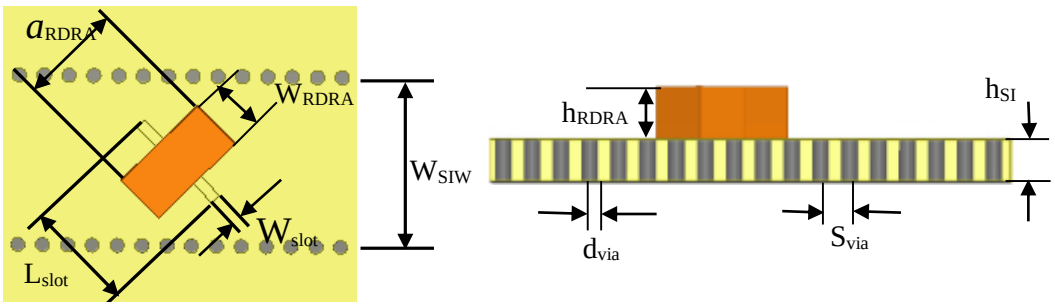

Figure 4.3 Antenna element dimensions. (a)Top view, and (b) side view.

4.2 Design Procedure and Equivalent Circuit Model

4.2.1 Design and Simulation Procedure

The general design and simulation procedure is summarized as the following.

A. Choose the interested operating frequency for mm-wave application.

B. Choose the available material for both RDRA and SIW within the constraints of the dielectric constant.

C. Using the design equations in [2], the initial values of the RDRA at the fundamental mode can be calculated (a_{DRA} and W_{RDRA}).

D. Using full wave Eigen Mode Solver, design the RDRA at the operating frequency with the calculated dimensions (a_{DRA} and W_{RDRA}) for a specific relative permittivity and a standard height h_{DRA}.

E. SIW parameters such as W_{SIW}, d_{via} and s_{via} are calculated using equations (2.1) to (2.6) from chapter two.

F. Choose the initial values of the slot dimensions (L_{slot} and W_{slot}) [70], where

$L_{slot} = \frac{\lambda_o}{\sqrt{2(\varepsilon_r+1)}}$, and $W_{slot} = 0.1\, L_{slot}$

G. Build two port single element RDRA backed by SIW and simulate it using full wave solver to get its S-parameters and then it can be used as a building block for the *N*-element array.

H. Two-element structure with a PEC in the middle is built to extract the S-parameters of the mutual coupling. Then two-element and four-element RDRA arrays backed by SIW are built to check the equivalent circuit model behaviour and the mutual coupling for the 45° LP. The short-circuited end

is simulated using the full wave solver and modeled using the circuit model as a piece of transmission line with a length of X_{sc} and a propagation constant γ with one end short-circuited. The difference in the S-parameters for the SIW and the ideal transmission line is compensated by adding a correction length of ΔL to X_{sc} in the circuit model so that the S-parameters of the EM model and circuit model agree to each other.

I. Similarly, the junction in the middle, which has the feeding slot as shown in Figure 4.4, is modeled as a three port network. Its EM simulated S-parameters are used in the circuit model.

J. Finally, built the circuit model of the entire structure and compare the results of the S-parameters with the EM simulated results for the eight-element array in Figure 4.1

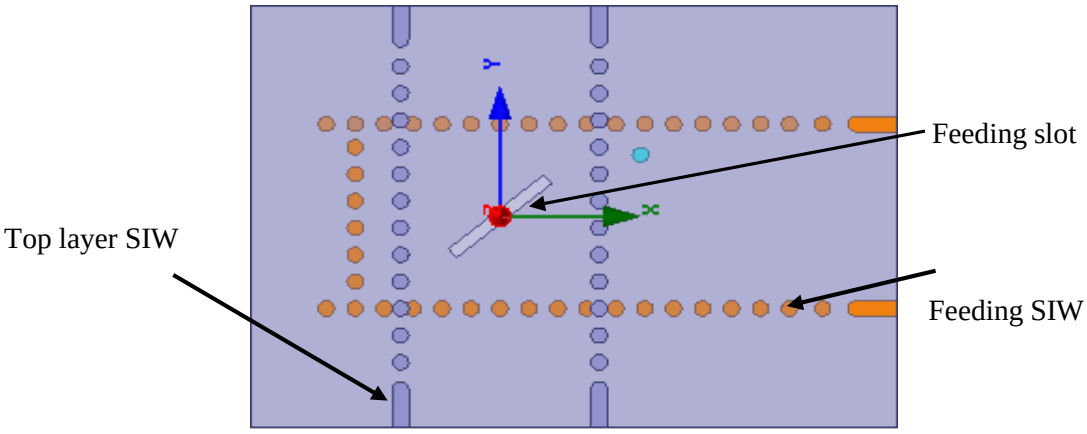

Figure 4.4 The center feeding slot

An effective width of a_{eff} =4.397mm for the transmission line model is used to give the same propagation constant extracted from EM results of the unloaded SIW. In addition, the difference in the S-parameters for a short circuit SIW and the ideal transmission line model is checked, where a correction length of ΔL of -0.128 mm is added to X_{sc} of 3mm in the circuit model so that the S-parameters of the EM model and circuit model agree to each other. After adding a correction of ΔL to transmission line circuit model, the S-parameters circuit model results agree well with the EM results as shown in Figure 4.5, before and after correction. The values of D and X_{sc} are initially set to be the guided wavelength in SIW, λ_g, and $\lambda_g/2$, respectively.

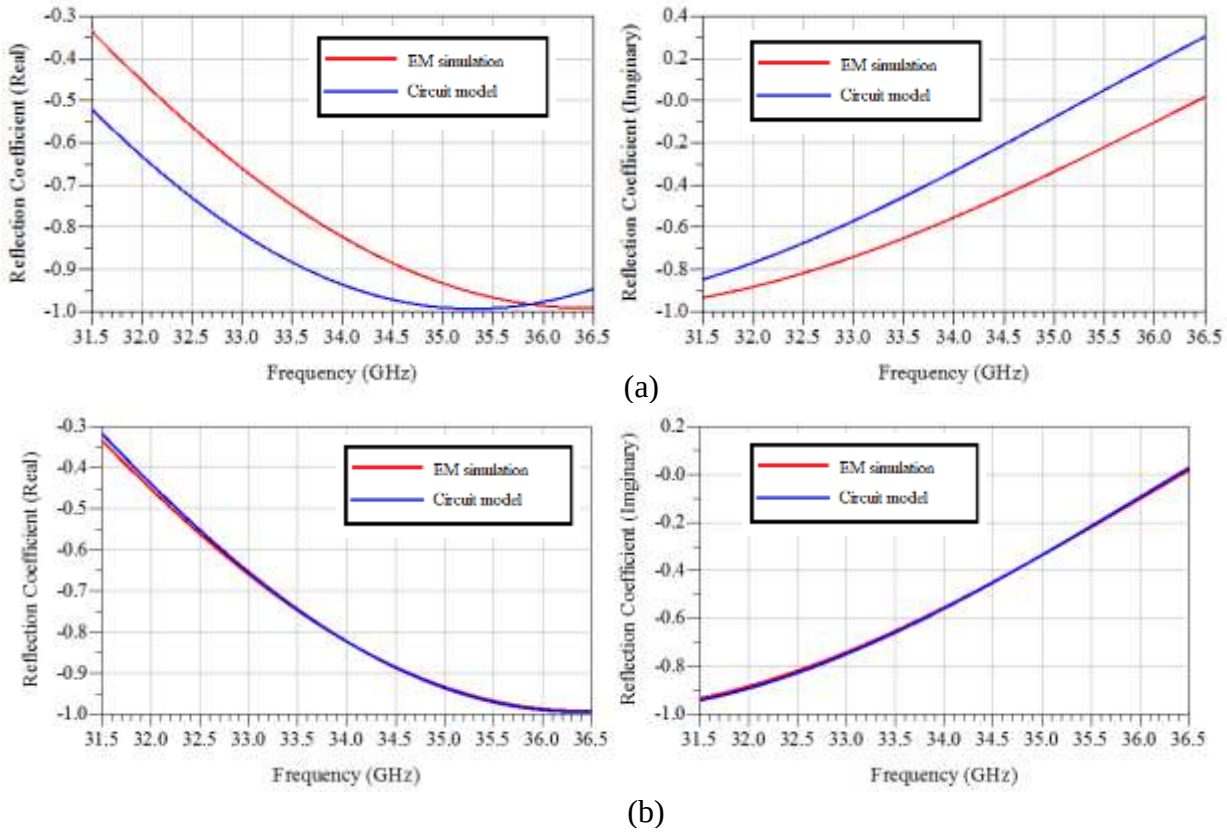

Figure 4.5 The SIW with one end short-circuited, (a) before correction (ΔL=0 mm), and (b) after correction (ΔL=-0.128 mm), where EM simulated results and the circuit model results agree.

The reflection coefficients of the proposed circuit model and the EM simulation are compared in Figure 4.6. As can be seen, the circuit model with mutual coupling shows good accuracy. However due to the complexity of the design, there is still difference comparing to the EM results. The design is further optimized as described in the next section.

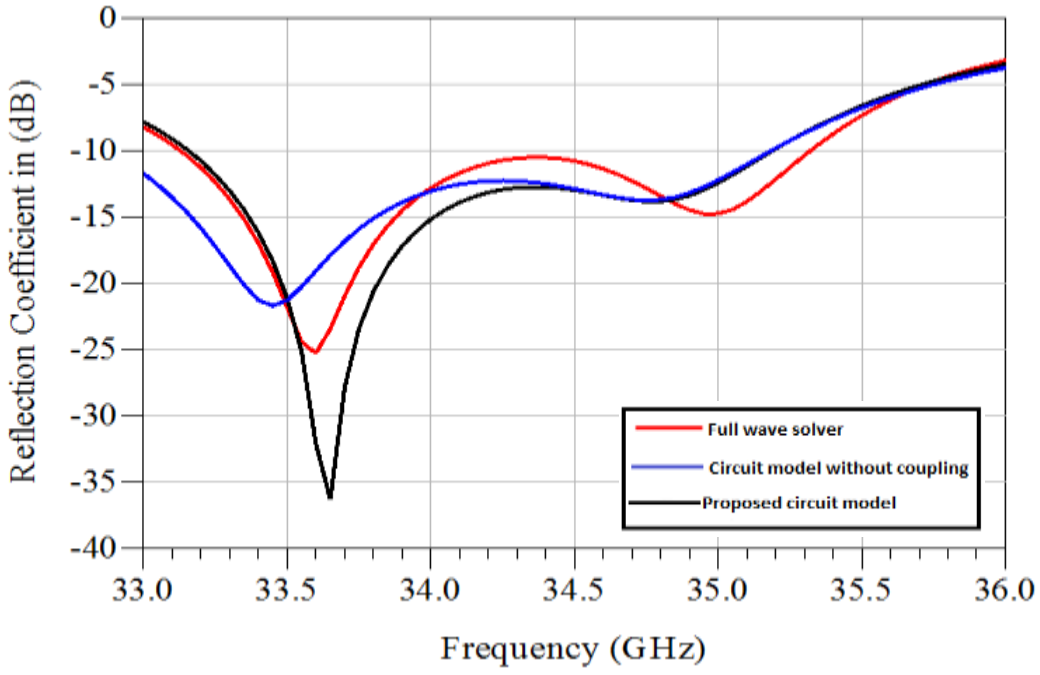

(a)

Figure 4.6 The reflection coefficient of the eight-element SIW series-middle fed DRA array with 45° LP. In the circuit model *aeff* =4.397mm and ΔL= -0.128mm.

4.3 Design Optimization using Implicit Space Mapping (ISM)

As mentioned in chapter 2, space mapping has been proven to be a very effective optimization technique. It combines the speed of circuit models, and the accuracy of EM solvers. Implicit space mapping (ISM), one of the SM techniques, is very easy to implement. The mapping between the coarse model and the fine model is achieved by defining an auxiliary set of parameters, which are not actual design parameter. These selected preassigned parameters are extracted in each iteration to match the coarse model responses with those of the fine model.

Based on the space mapping framework in [77], we optimize the eight elements SIW middle fed series DRA array with 45° linear polarization using ISM. The fine model is one of the most powerful EM solvers, HFSS. The coarse model is based on the proposed circuit model built using the Agilent ADS.

In the coarse model, the S-parameters of single antenna element, the center feed junction, $[S]_L$, and $[S]_R$ are built in as a dataset. Transmission line lengths between antennas, D, and between antenna and the short-circuited end, X_{sc} are defined as design variables. The PE procedures are also performed within ADS, for which the fine model S-parameters are imported as a dataset and matched to the circuit model (coarse model) responses by varying the pre-assigned parameters $\boldsymbol{x}$, where $\boldsymbol{x}=[a_{eff}\ \Delta L]^T$ in the coarse model. The following general steps are used.

1 Set up the coarse model, and select the suitable pre-assigned parameters.

2 Initialize the pre-assigned parameters for good coarse model.

3 Optimize the coarse model according to the design specification.

4 Apply the design parameters in the coarse model from step 3 to the parameterized fine model (HFSS).

5 Simulate the fine model (HFSS) and save the responses in Touchstone format. This is the first iteration.

6 Check the stopping criteria; if satisfied, stop.

7 Import the responses to the ADS schematic using the *SnP* component. Set up ADS (calibrated) coarse-model to match the *SnP* component and run the ADS optimization algorithm to perform PE. The pre-assigned parameters are extracted to match coarse model responses to those of the fine model.

8 Predict the next fine-model solution by re-optimizing the design parameters using calibrated coarse model according to design specifications.

9 Update the fine-model design and go to Step 5.

SM optimization process is built in the ADS schematic using three schematic designs:

a) Coarse-model for steps 1 and 2.

b) PE for step 7.

c) Surrogate model for re-optimization (step 8).

In the following, the eight-element antenna array of rectangular DRA backed by SIW with middle fed and 45° linear polarization is optimized. There are two sets of parameters. The design parameters and the pre-assigned parameters. The design parameters

are variables in both the fine model and coarse model, which are D and X_{sc} for this case. The pre-assigned parameters, namely a_{eff} and ΔL, are coarse model parameters only. a_{eff} and ΔL are selected based on the result after tuning of the 8-element structure with single port, as shown in Figure 4.7 (b). Figure 4.7 (a) is the same as Figure 4.6, redrawn here for comparison. As discussed earlier, due to the complexity of the structure, there is still noticeable difference between the circuit model and EM responses. As shown in Figure 4.7(b), if the effective width a_{eff} is further tuned in the circuit model from 4.397mm to 4.428mm, and ΔL is changed from -0.128 mm to -0.038 mm, even better matching between the circuit model and the EM simulation can be achieved. These two parameters, a_{eff} and ΔL, are therefore used as pre-assigned parameters in the optimization process.

Table 4.1 shows the initials values of the pre-assigned and the design parameters for our design. Starting with the initial values of all parameters, a coarse model is built in ADS, and design parameters are optimized according design specification. Then, the new values of the design parameters are applied to the full wave solver. As the simulation is finished, the fine model data is saved in touchstone file format, which is the end of the first iteration. After checking the design specification, the procedure may be ended or another iteration may be needed. In this example, only three iterations are needed to meet the specifications.

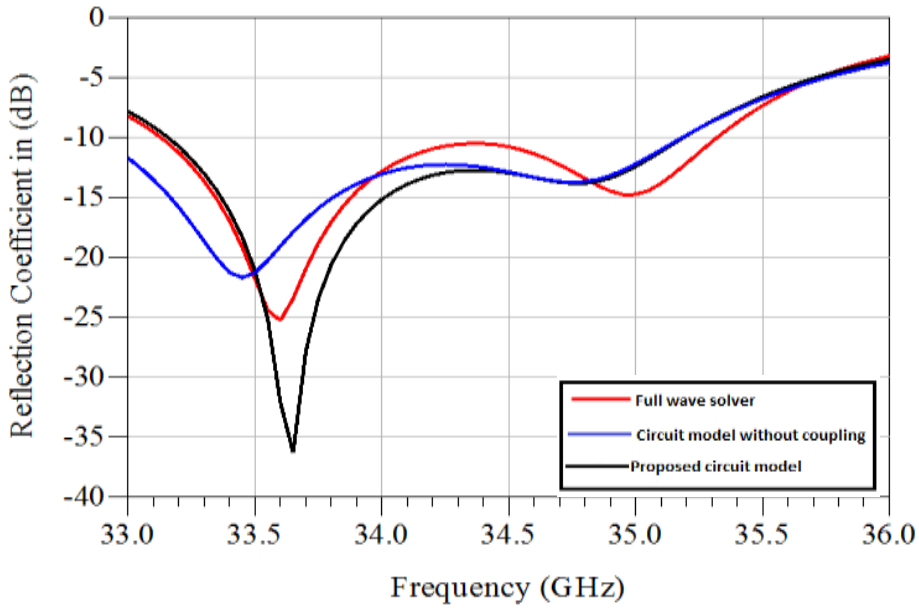

(a)

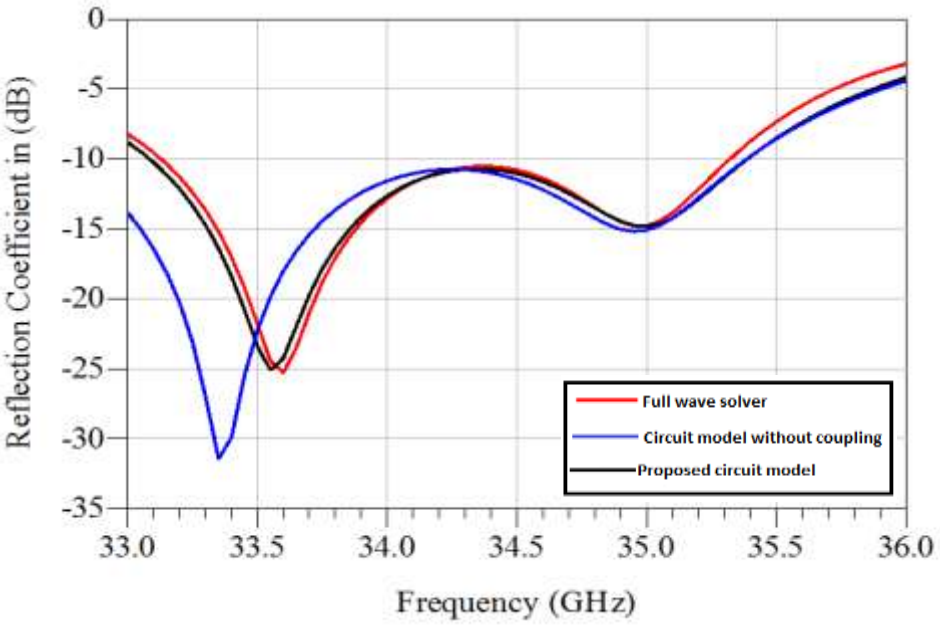

(b)

Figure 4.7 The reflection coefficient of the eight-elements SIW series-middle fed DRA array with 45° LP. (a) a_{eff} =4.397mm and ΔL= -0.128mm, and (b) a_{eff} =4.428mm and ΔL= -0.038 mm.

Table 4.1 The definition and initial values of pre-assigned parameters and design parameters

Pre-assigned parameters *(x)*		
Parameter Name	**Definition**	**Initial value**
a_{eff}	The equivalent width of the SIW in the circuit model. It is a coarse model parameters only.	4.428 mm
short circuit correction (ΔL)	It is a small length of transmission line to match the fine and coarse model responses of a piece of SIW with one end short-circuited. It is a coarse model parameters only.	-0.038 mm
Design Parameters *(x_f)*		
Parameter Name	**Definition**	**Initial value**
D	The distance between each two neighboring antenna elements, which is initially set to be the guided wavelength in SIW, λ_g.	6.3 mm
X_{sc}	The distance from the center of the last element to the short-circuited end, which is initially set to be $\lambda_g/2$.	3.15 mm

The design specifications are to obtain a wide bandwidth at -10dB return loss level with the frequency centered at 34.5 GHz. The design parameters and pre-design parameters are shown in Table 4.1. An extra step of PE to obtain the pre-defined parameters before SM is taken to ensure that the coarse model can match the fine model very well as shown in Figure 4.7. Next, the coarse model design parameters are optimized as shown in Figure

4.8 to achieve the design specifications. Once the new values achieve the goal, apply these values to the fine model. Table 4.2 summarizes the values of all parameters from the first step to the end of last iteration, where three iterations are needed. The gray cells indicates that these parameters are fixed in this step.

Table 4.2 The pre-assigned parameters and design parameters after each iteration

	Coarse Model				Fine Model	
All values in mm	a_{eff}	ΔL	D	X_{sc}	D	X_{sc}
Initial values	4.397	-0.128	6.3	3.15		
Improved coarse model	4.428	-0.038	6.3	3.15		
Optimization of Coarse model	4.428	-0.038	6.17	2.75	6.17	2.75
End of the first Iteration						
Parameter extraction	4.44	-0.119	6.17	2.75		
Optimization of Coarse model	4.44	-0.119	6.19	2.76	6.19	2.76
End of the second Iteration						
Parameter extraction	4.49	-0.239	6.19	2.76		
Optimization of Coarse model	4.49	-0.239	6.16	2.84		
End of the third Iteration						
Final Design					**6.16**	**2.84**

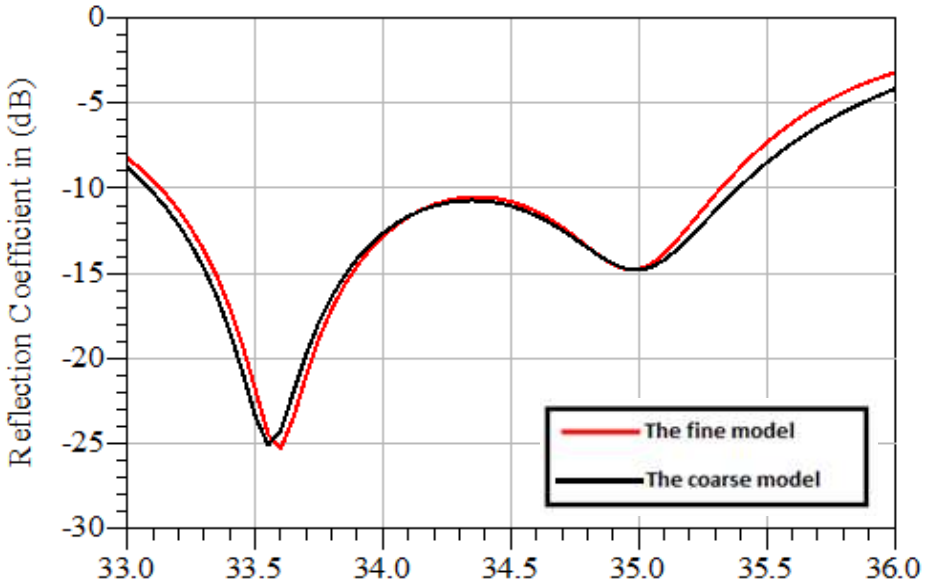

Figure 4.8 The fine model and the coarse model before Space Mapping optimization at the initial step.

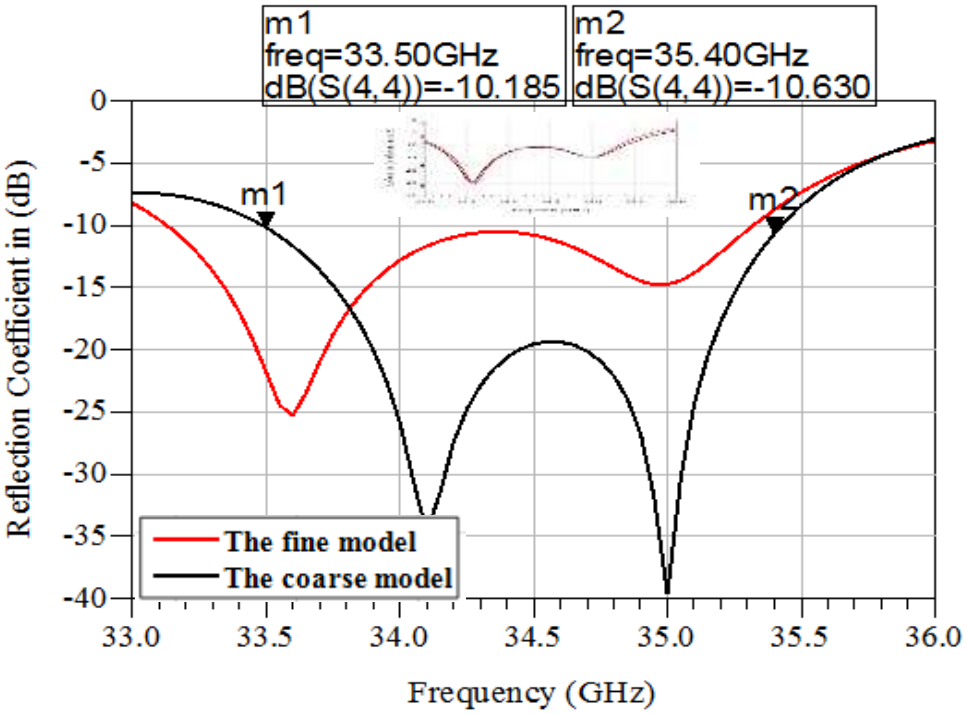

Figure 4.9 The coarse model response after the optimization of the coarse model to achieve a wide bandwidth. The fine model is still the initial response, showing shifted passband

As shown from Figure 4.9, the coarse model can be optimized to achieve a wide bandwidth of 2GHz at -10 dB. After applying the design parameter values to HFSS, we obtained the fine-model response, which is saved as *S*1*P* file (single-port S-parameter file). The reflection coefficient S_{11} for the coarse model and the fine model is shown in Figure 4.10. There is a difference between the response of the coarse model and the fine model, which means a second iteration is needed to match exactly. In this step, the pre-assigned parameters of the coarse model are calibrated (PE) to match the fine- and coarse-model responses as shown in Figure 4.11.

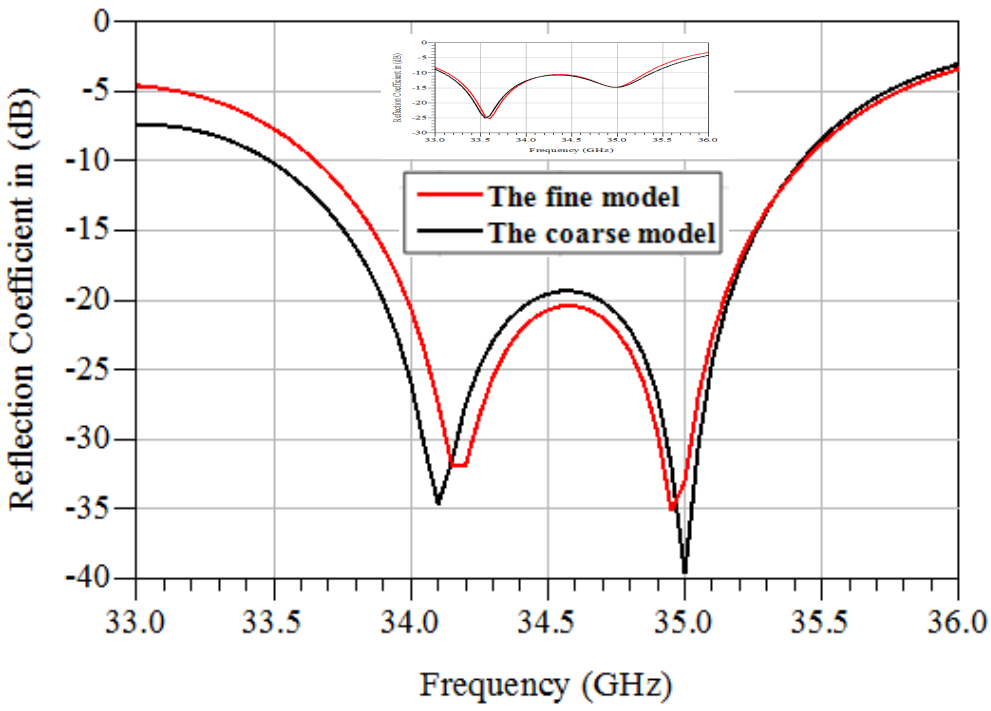

Figure 4.10 The fine and the coarse model responses after the first iteration and before the PE. The fine model shows a slight shift in frequency

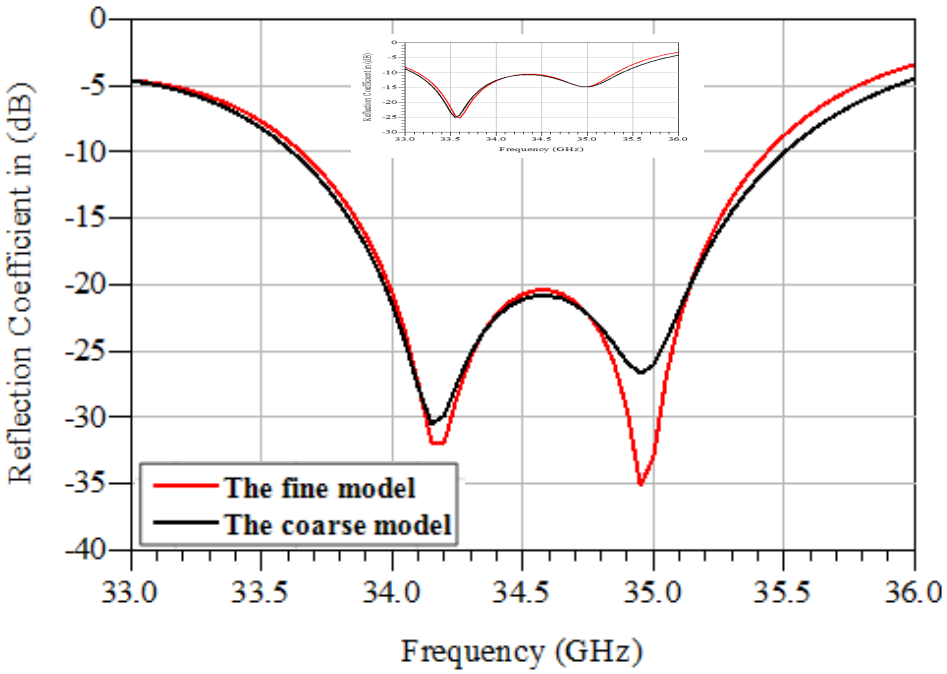

Figure 4.11 The fine and the coarse model responses after the first PE.

Once we obtain a good matching between the fine and coarse models by calibrating the pre-assigned parameters (PE), we proceed to the optimization step. By fixing the pre-assigned parameters from the previous step, the new coarse model (surrogate) is re-optimized with respect to the original specification. A new set of design parameters are thus found to achieve the goal. We apply the design parameters to the fine model again. Another two iterations are done to give a satisfactory result of the fine model simulations as shown in Figure 4.12, and Figure 4.13 proving that the design specification are achieved. In addition, a high gain of 14.24 dBi is calculated using equation (3.24) as mentioned before. with a good agreement between the fine model and the coarse model as shown in Figure 4.14, where a slight difference in the *SLL* can be noted.

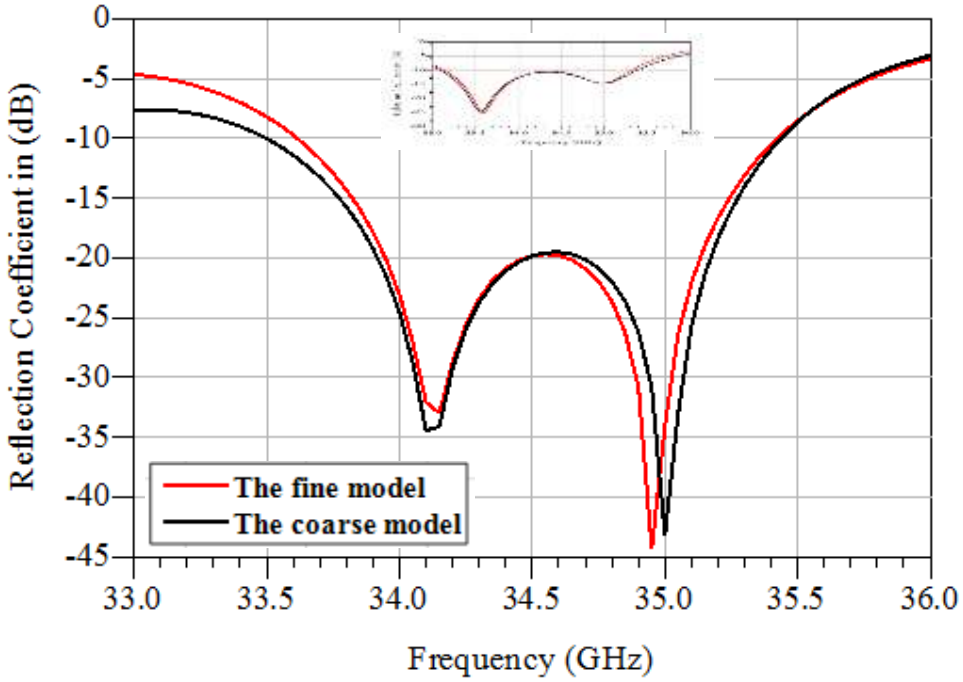

Figure 4.12 The fine and the optimum coarse model responses after the second iteration.

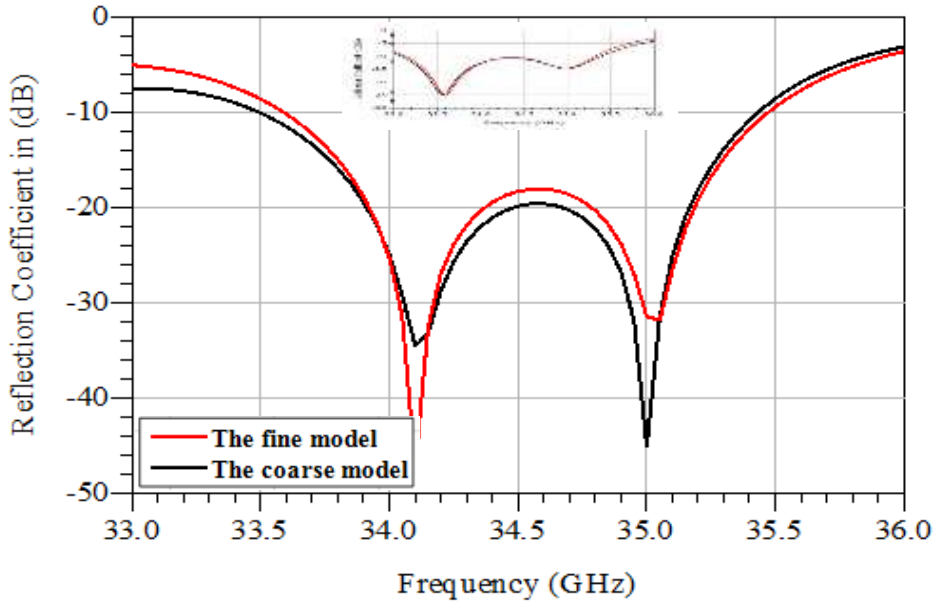

Figure 4.13 The fine and the optimum coarse model responses after the third (last) iteration.

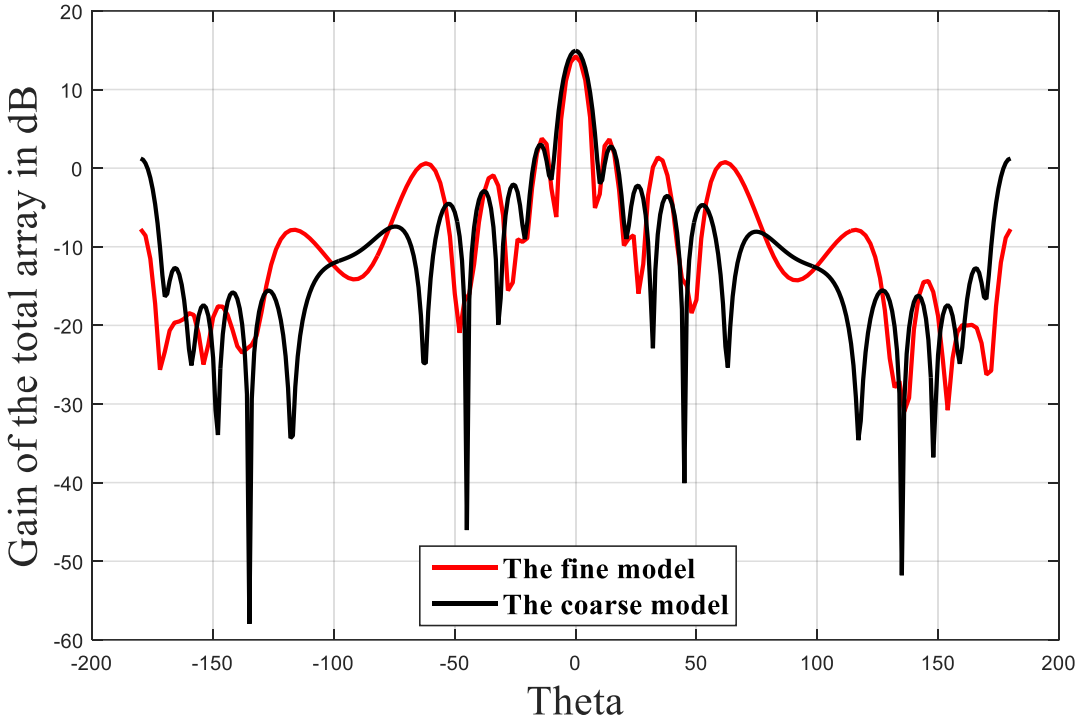

Figure 4.14 The radiation pattern of the optimum design for both fine model and coarse model.

4.4 Fabrication and Experimental Results

4.4.1 Coaxial line to SIW Transition

The transition between the SIW and the planar circuits, such as MSL, CPW, or SL circuits can be built on the same substrate. Several types of transitions between the coaxial line and the RWG have been reported in [97-99]. A transition between the coaxial line and the SIW has been presented in [100].

A coaxial line to SIW transition is designed to give a wide bandwidth at a reflection coefficient less than -10dB through the design frequency range from 33 to 36 GHz. A back-to-back design is shown in Figure 4.15. Good results is achieved using the full wave solver by optimizing three important parameters. These parameters are the distance between the short circuit and the center of the coaxial d_{sc}, the distance from the center of the two matching vias to the center of the coaxial d_y, and the distance between the two centers of the matching vias d_x as shown in Figure 4.15. After applying the transition to the optimum design in figure 4.13, the simulated result is changed as shown in Figure 4.19.

The back-to-back design of coaxial line to SIW transition is fabricated. Figure 4.16 shows a comparison between the measured results and the simulated results over the frequency band of 33 to 36 GHz. It shows that the frequency shifts up by approximately 1GHz in the measurement results, with a worst case reflection coefficient of -12dB in the frequency band of interest comparing to -25 dB in the simulated results. It is speculated that the difference between the measured and the simulated results is due to fabrication tolerances, inaccuracy in the dielectric constant and connector contacts.

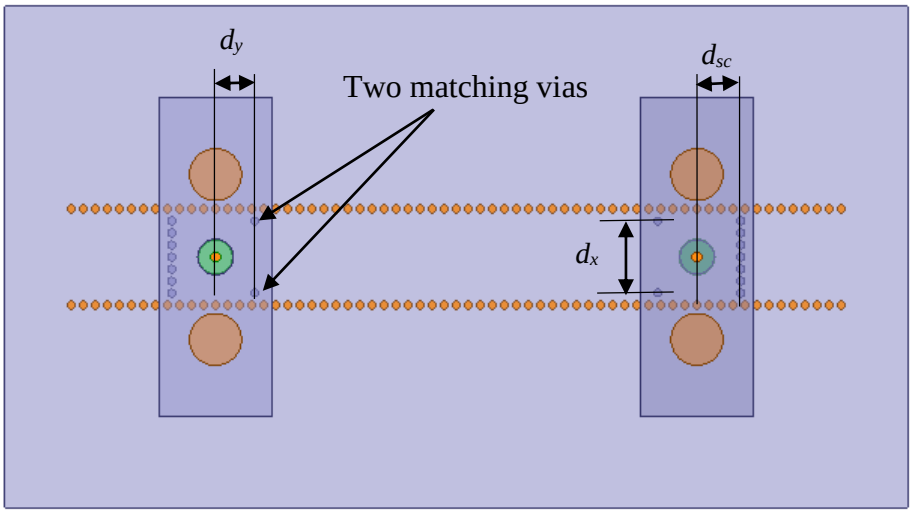

Figure 4.15 A back-to-back design of the coaxial line to SIW transition.

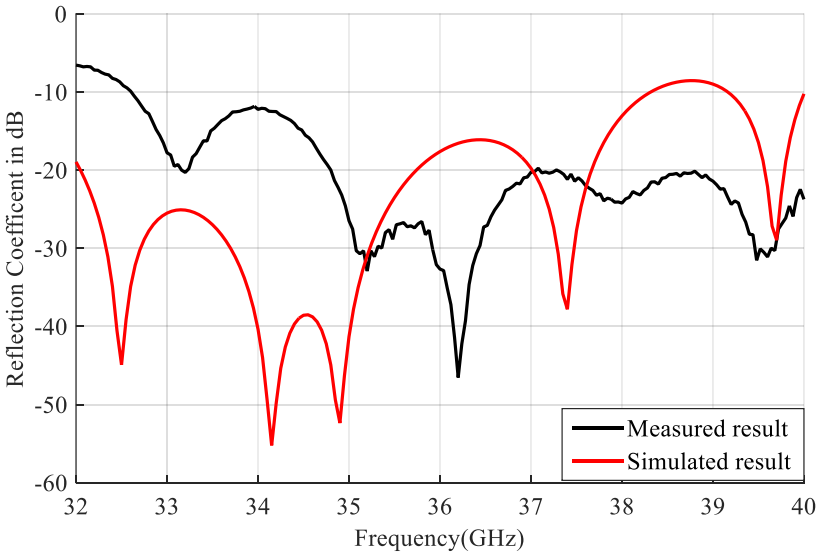

Figure 4.16 The simulated and measured reflection coefficient S_{11} (dB) of the coaxial line to SIW transition in Figure 4.15.

A tolerance analysis is done to match the measurement result of the transition by changing the dielectric constant ε_r.. The material used for the SIW substrate is Rogers RT/6002 with the nominal value of ε_r = 2.94. Different values of the relative permittivity are used in the simulations as shown in Figure 4.17. In addition, some dimensions in the fabricated transition are found to slightly deviate from the design, and the measured dimensions are included in the simulations. It can be observed from Figure 4.17 that the actual value of ε_r is close to 2.9.

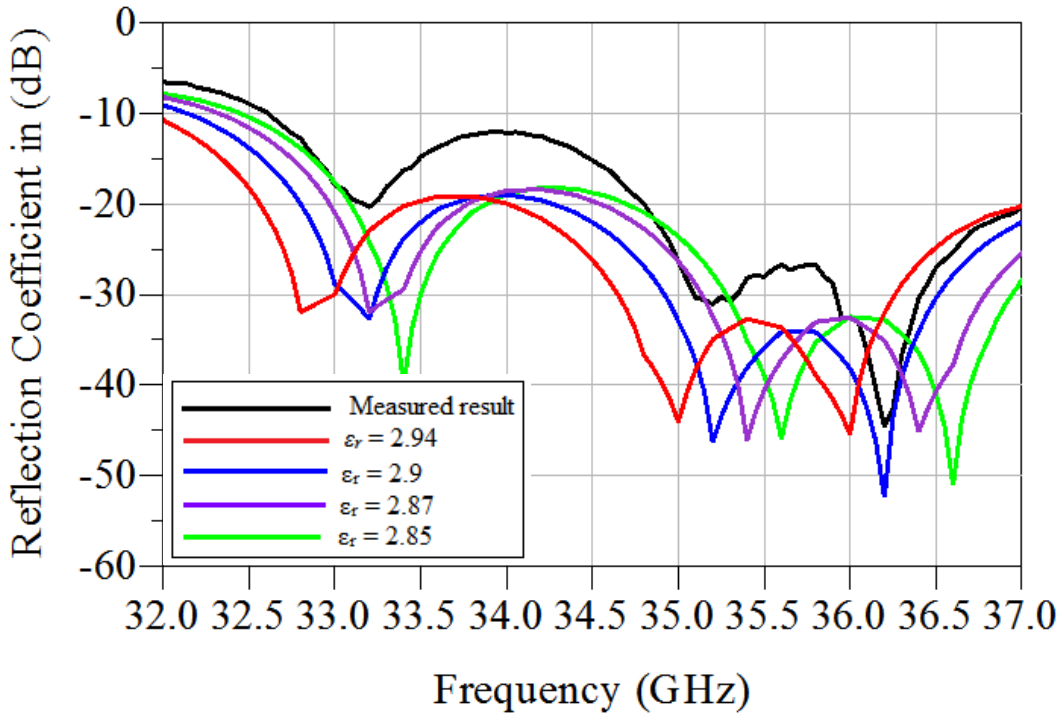

Figure 4.17 Tolerance analysis for the reflection coefficient S_{11}(dB) of the coaxial line to SIW transition.

4.4.2 Antenna Measurements

The SIW-RDRA is fabricated using a multi-layer PCB fabrication process. The fabricated structure consists of a three layers, two dielectric layers for the SIW-fed layer, and DRA element(s), respectively. The fabrication process is similar to the one described in [101]. The DRAs are bonded to one side of the SIW using low loss thin adhesive bonding material.

The first fabricated antenna prototypes is shown in Figure 4.18. It is measured to determine the reflection coefficient S_{11}(dB) and the radiation pattern (gain) of the antenna.

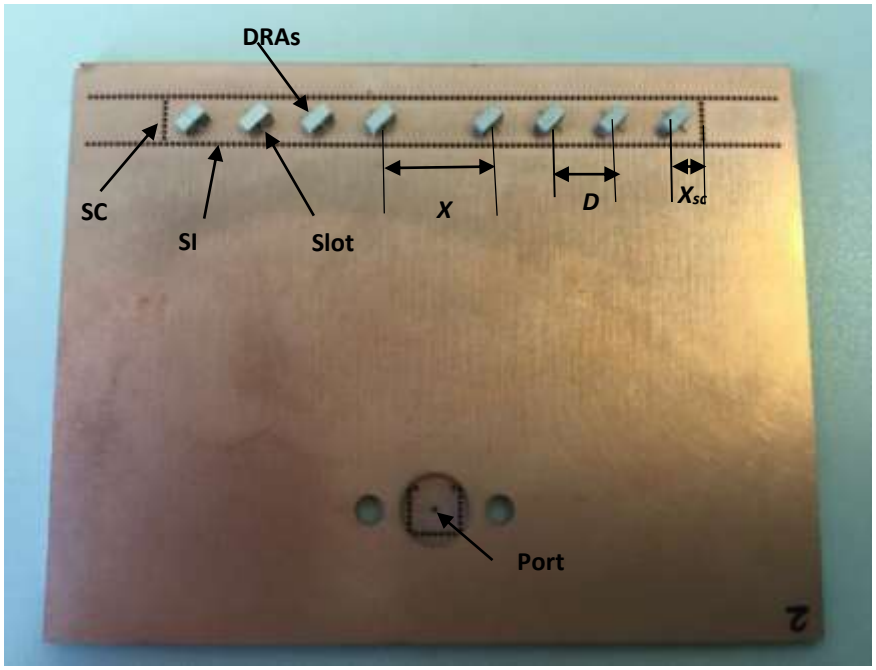

Figure 4.18 The first fabricated prototype of SIW middle fed series rectangular dielectric resonator antenna (DRA) array with 45° LP. The array dimensions D=6.16mm, X_{sc} = 2.84mm and X_s = 5.3mm.

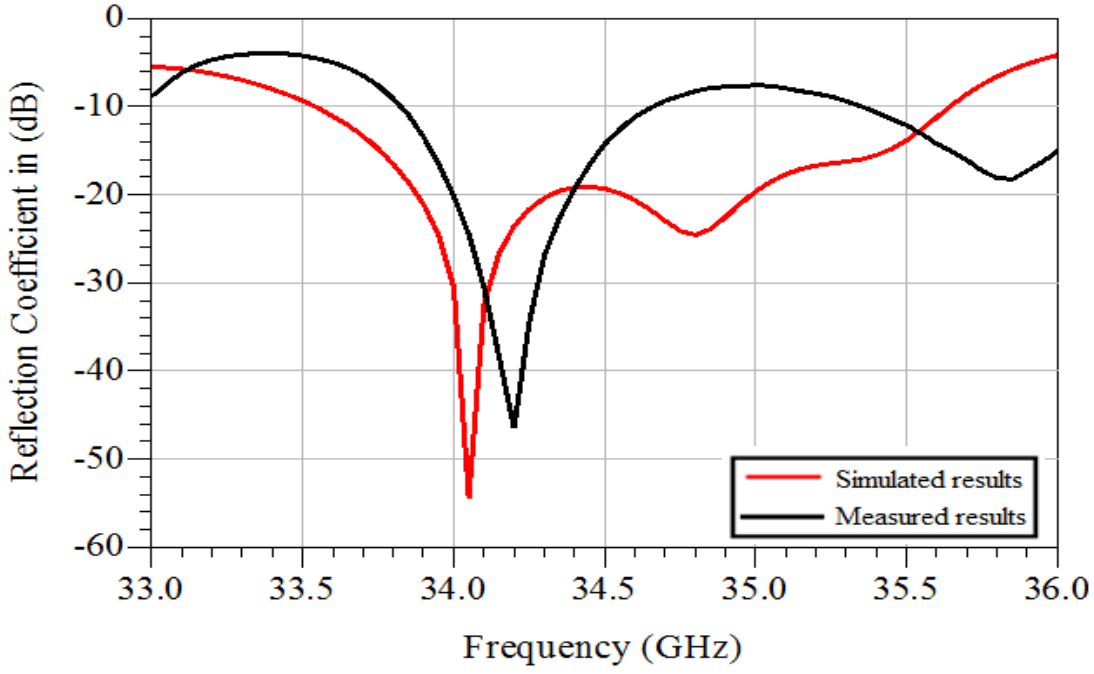

Figure 4.19 The simulated and measured reflection coefficient S_{11}(dB) of SIW middle fed series rectangular dielectric resonator antenna (DRA) array with 45° LP shown in Figure 4.18

Figure 4.19 shows a comparison between the measured reflection coefficients S_{11} (dB) and the simulated results over the frequency band of 33 to 36 GHz. The antenna prototype shows a good agreement between the measured and simulated results taking into account the inaccuracy in the dielectric constant, and manufacturing tolerances. In addition, the shift of resonance frequency in the measured results is partly due to the addition of adhesive material between the substrate and the DRA layers. The multi-layer fabrication method affects the coupling to the RDRA. The connector contact and misalignment also affect the measured responses. The reflection coefficient at the center frequency is shifted up to -8dB.

The radiation pattern (gain) for the antenna prototypes in Figures 4.18 is tested at 34.5 GHz within scanning angle range of $-90° \leq \theta \leq 90°$ in two orthogonal planes. Figure 4.20 shows the measured and simulated radiation patterns (gain) for the antenna prototype. The simulated and the measured results are in a very good agreement, showing a boresight (θ=0°) radiation pattern with a *SLL* of -10.79 dB (simulated results) and -10dB (measured results). The proposed SIW series fed RDRA prototype presents a high overall efficiency of 85% (simulated) as shown in Figure 4.21, over the operating frequency bandwidth. In addition, the gain versus frequency is measured and compared to the simulated results as shown in Figure 4.22. A good agreement between the measured and simulated gain is achieved with a max gain value of 15 dB (simulated) at the center frequency. The difference between the measured and the simulated gain is for the most part caused by connector losses. The adapter used in the horn antenna has 0.9 dB loss, and there is approximately 0.4 dB losses caused by other connectors used for the measuring process. The gain of the horn antenna is measured from 34 GHz to 36 GHz, and the fabricated design is measured through the same frequency range to obtain the gain of the fabricated prototypes.

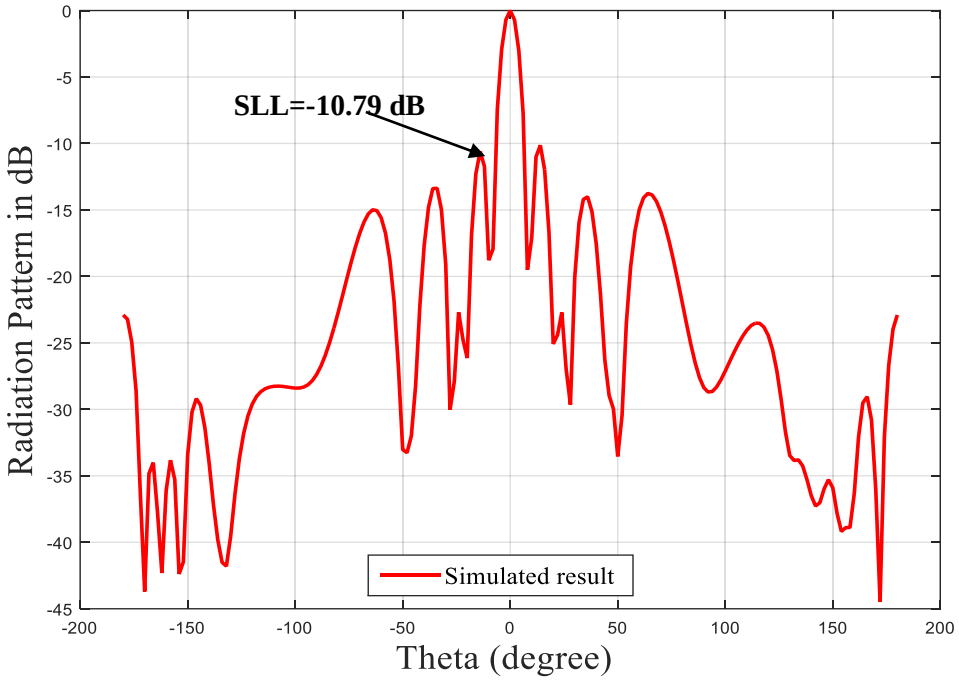

(a)

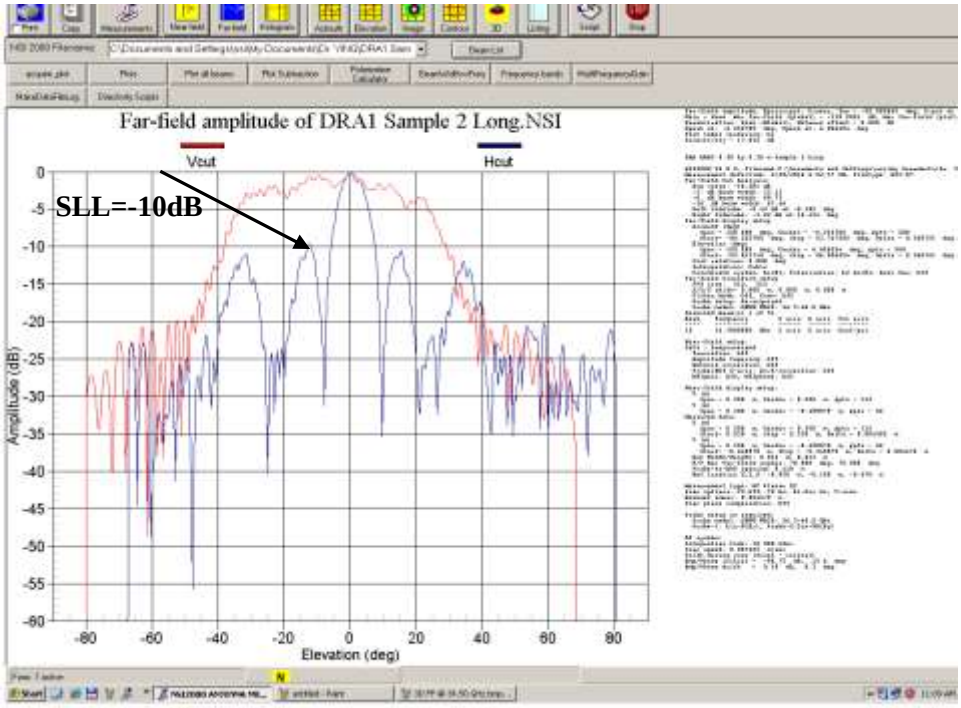

(b)

Figure 4.20 (a) The simulated and (b) the measured radiation pattern of the optimum design shown in Figure 4.18.

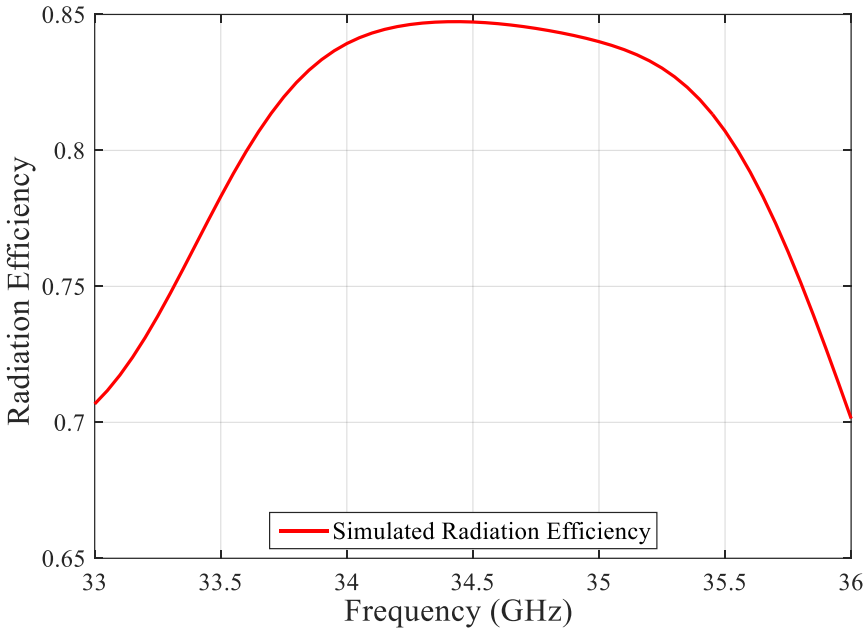

Figure 4.21 The radiation efficiency versus the frequency of the SIW-RDRA array.

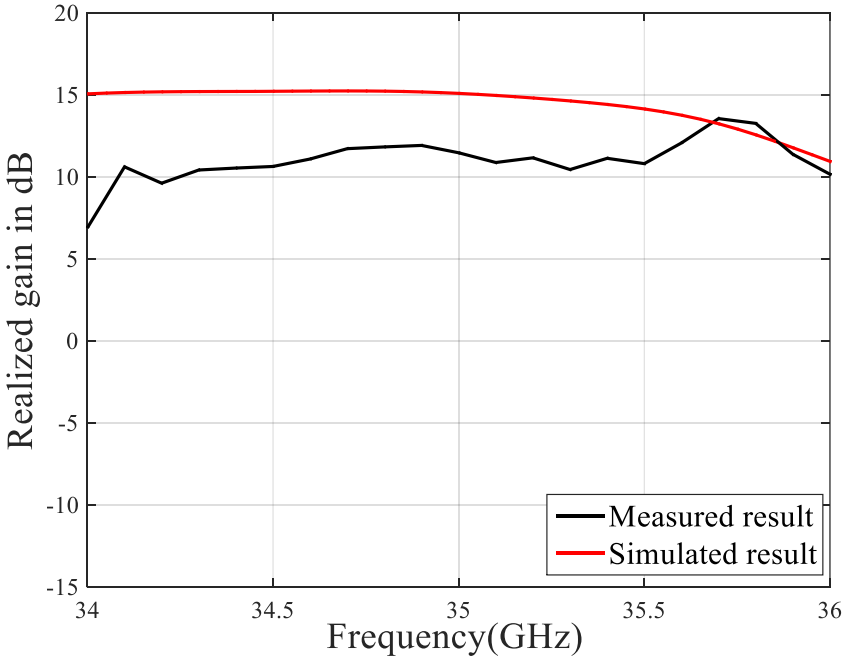

Figure 4.22 The realized gain in dB of SIW middle fed series rectangular dielectric resonator antenna (DRA) array with 45° LP shown in Figure 4.18.

As one of the main targets in the antenna design problem is to reduce the relative side lobe level (RSLL), the first antenna prototypes is modified. The modified fabricated antenna shown in Figure 4.23 has a smaller distance between the two middle elements X_s to reduce the *SLL*. A half waveguide wavelength is subtracted from the previous distance X_s to reduce from 5.3mm to 2.15mm. The antenna reflection coefficient S_{11}(dB) of the second fabricated SIW-fed RDRA prototype in Figure 4.23 is measured. A comparison between the measured results and the simulated results over the frequency band of 33-36 GHz is shown in Figure 4.24. The antenna prototype shows a good agreement between the measured and simulated results taking into account manufacturing tolerances.

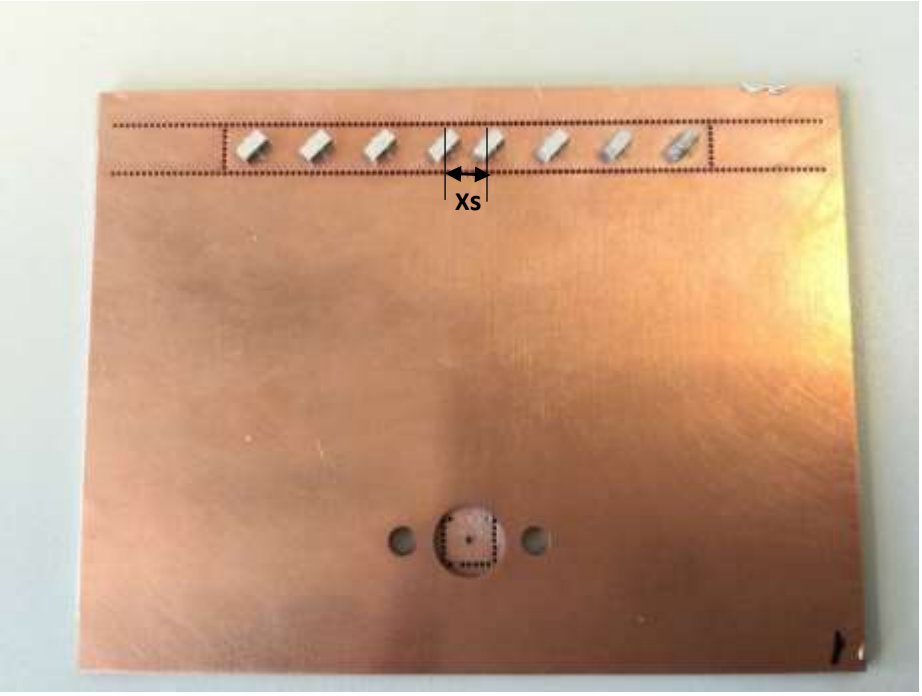

Figure 4.23 The second fabricated prototype of SIW middle fed series rectangular dielectric resonator antenna (DRA) array with 45° LP. The array dimensions D=6.16mm, X_{sc} = 2.84mm and X_s = 2.15 mm.

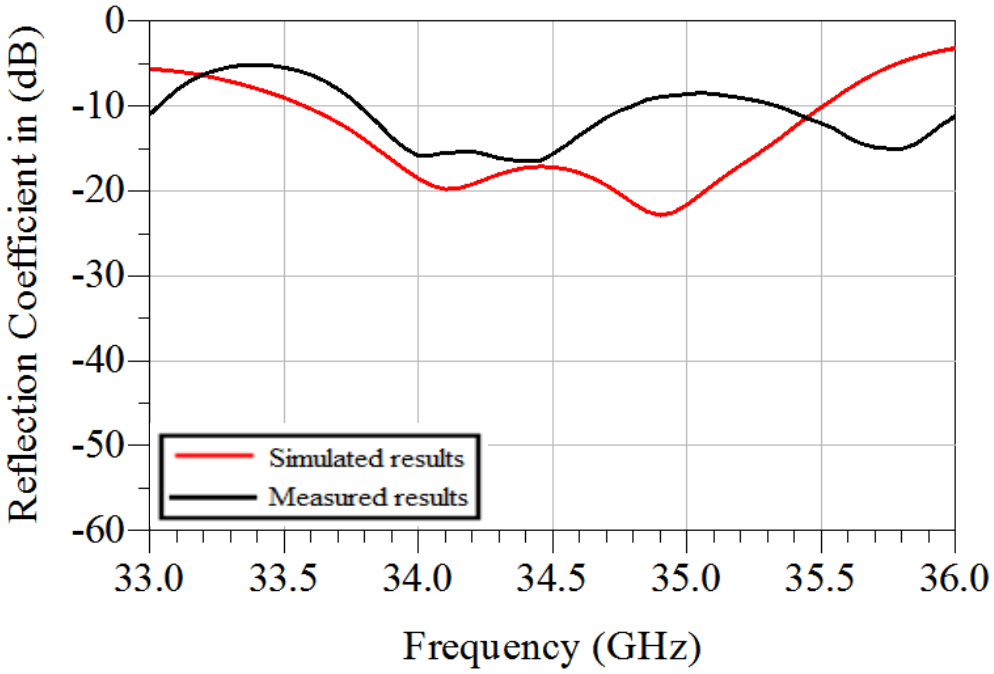

Figure 4.24 The simulated and measured reflection coefficient S_{11}(dB) of SIW middle fed series rectangular dielectric resonator antenna (DRA) array with 45° LP shown in Figure 4.23.

There is a shift in the resonance frequency in the measured results due to inaccuracy of the dielectric constant and fabrication tolerances as discussed earlier. The reflection coefficient at the center frequency is worse than -10 dB.

The radiation pattern for the first and second prototype is compared using the simulated results, a reduction in the *SLL* from -10.79dB to -12.25dB is achieved as shown in Figure 4.25 (a).The radiation pattern (gain) measurements for the antenna prototypes in Figures 4.23 was tested as before at 34.5 GHz within scanning angle range of $-90° \leq \theta \leq 90°$ in two orthogonal planes. Figure 4.25 (b) shows the measured radiation pattern for the second antenna prototypes at boresight (θ=0°) with *SLL* around -12 dB, where the

reduction of *SLL* is achieved. In addition, the measured and simulated results of the peak gain and directivity are compared in Figure 4.26 and 4.27, respectively. All measurements are performed using a planar near field system.

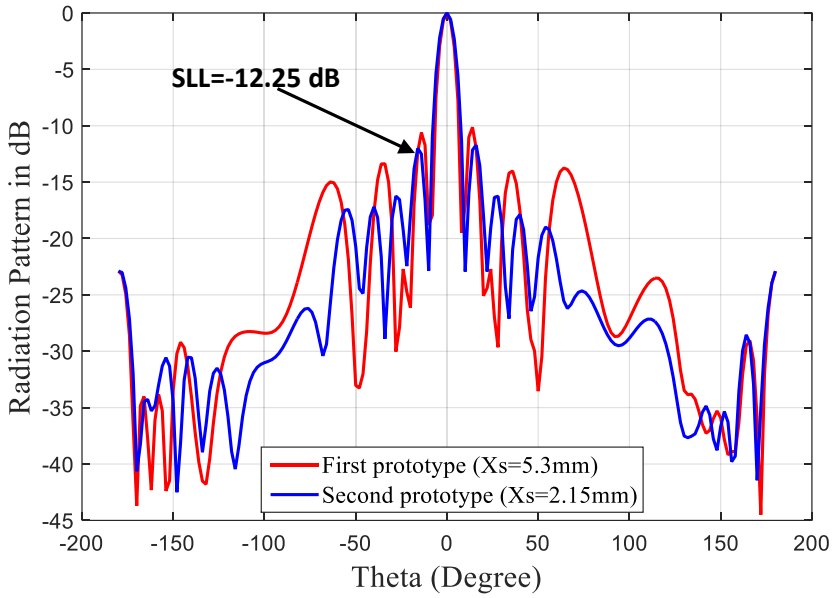

(a)

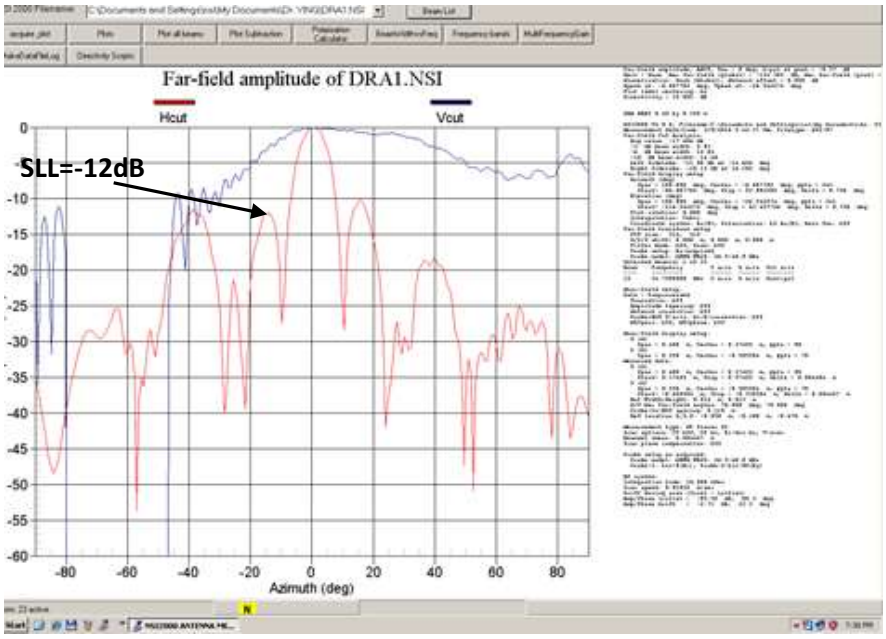

(b)

Figure 4.25 (a) The simulated radiation pattern of the first and second prototype, (b) the measured radiation pattern for the second prototype shown in Figure 4.23.

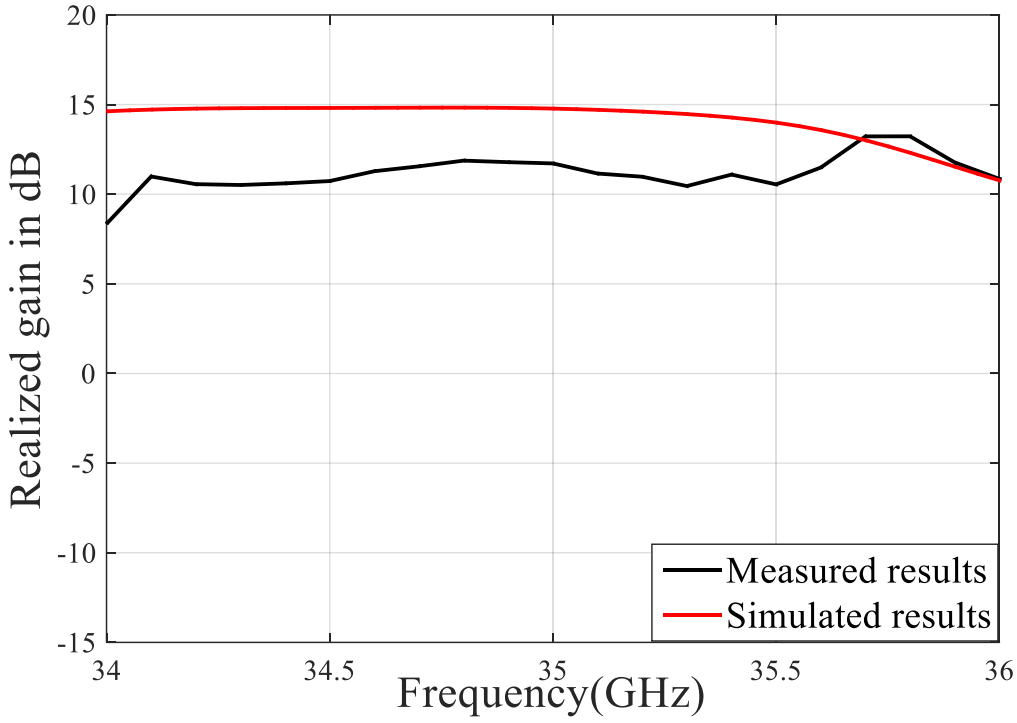

Figure 4.26 The realized gain in dB of SIW middle fed series rectangular dielectric resonator antenna (DRA) array with 45° LP shown in Figure 4.23.

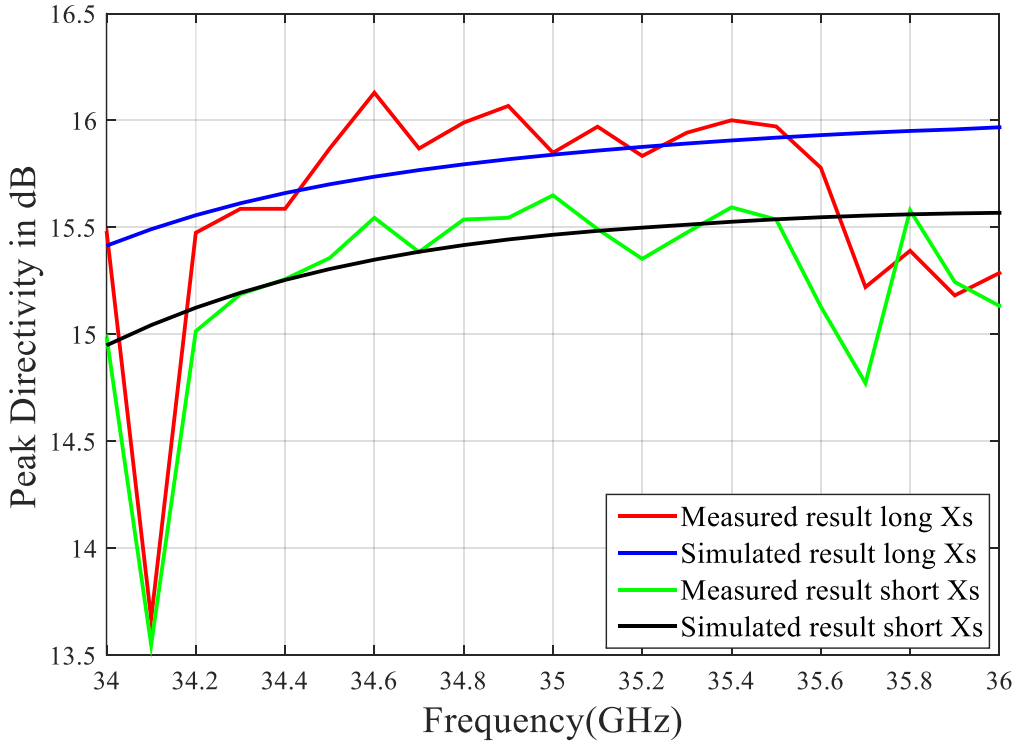

Figure 4.27 Peak directivity comparison between the measured and the simulated results for both first (long X_s) and second prototype (short X_s).

Table 4.3 summarizes the main antenna radiation pattern (gain) and efficiency characteristics. As mentioned before, the difference between the simulated and measured gain is mostly caused by adaptor and connector losses, which are not included in the simulated results. The reduction in the impedance bandwidth is caused by inaccuracy of the dielectric constant and tolerances, which cannot be properly assessed using the measured data.

Table 4.3 The basic characteristics of SIW middle fed series rectangular dielectric resonator antenna (DRA) array with 45° LP

Antenna Characteristics	EM Simulation (HFSS)	Measurements
The first fabricated prototype (X_s=5.3mm)		
f_0 at minimum reflection coefficient (GHz)	34.05	34.2
Impedance Bandwidth (GHz) (-10 dB reflection coefficient)	2.2	< 2
S_{11} (dB) at f_0	-20	-8
G_{max} (dB) at f_0	15	13
SLL (dB)	-10.79	-10
The second fabricated prototype (X_s=2.15mm)		
f_0 at minimum reflection coefficient (GHz)	34.9	34.4
Impedance Bandwidth (GHz) (-10 dB reflection coefficient)	2	< 2
S_{11} (dB) at f_0	-22	-8
G_{max} (dB) at f_0	13.8	12
SLL (dB)	-12.25	-12

4.5 Conclusion

A new design of SIW middle fed series rectangular DRA array with 45° Linear Polarization is presented in this chapter. Extraction of the mutual coupling S-parameters is applied using the proposed method in Chapter 3. This mutual coupling is plugged into the circuit model to improve the model accuracy.

Based on the proposed circuit model, the design parameters are optimized to enhance the performance of the antenna array using space mapping. The space mapping is a powerful optimization tool to connect between the accurate fine model and the fast and trusted coarse model. The implicit space mapping is used in our case as it is preferred when pre-assigned parameters are part of the parameter set in the problem. Good results are achieved using SM, where only three iterations are needed to get the optimal solution. EM simulations show that a max gain of 15 dBi is achieved with a max impedance bandwidth of 2 GHz.

Furthermore, high design efficiency has been demonstrated through the combination of the developed circuit model with space mapping technique in the optimization of antenna arrays.

The designs are fabricated using low cost PCB fabrication process. A good agreement between the measured results and the simulated results is obtained. Difference in simulation and measurement is investigated.

Chapter 5

Conclusion and Future Work

Dielectric resonator antennas (DRAs) have shown good performance for millimeter wave applications. It overcomes the drawbacks of conventional antennas, such as microstrip antennas. Substrate integrated waveguide (SIW) has been proven to be a good alternative for the future generation of microwave and millimeter wave components. Due to these advantages of DRAs and SIW, they are an excellent candidate for millimeter wave applications when combined together.

Design and optimization of an antenna array usually depend on accurate full wave solvers. Full wave electromagnetic (EM) simulations can be very time consuming, especially in the case of large size antenna arrays. On the other hand, circuit models are fast and much less computationally intensive, but without the required accuracy. Space mapping (SM) is a powerful and unique optimization method that combines the strength

of coarse model (such as circuit models) and full wave simulations. However high quality coarse models are not readily available, especially for complex radiating structures.

The objective of this work is to investigate, design and optimize dielectric resonator antenna (DRA) arrays based on SIW technology for millimeter-wave applications, with the help of highly efficient computer aided modeling and optimization techniques.

An efficient and accurate circuit model is presented in this thesis for the modeling of SIW-DRA arrays. Taking into account the mutual coupling between antenna elements, a fully adjustable model is built, allowing the design parameters to be varied. A complete circuit model can be easily built for antenna arrays with different numbers of elements and different design parameters once the basic building block is developed. Optimization of antenna array can therefore be performed much more efficiently compared to conventional EM-based optimization.

For validation, the developed circuit model is applied to three different structures of SIW series-fed DRA arrays. All results show very good agreement between the proposed circuit model, the measured and/or the EM simulated results.

A new design of eight-element SIW middle fed series rectangular DRA array with 45° linear polarization is presented, which can be used for radar applications. For the optimization of the complex structure, we propose to apply implicit space mapping (ISM) technique. The implicit space mapping is preferred when pre-assigned parameters are part of the parameter set in the problem. The new circuit model plays an important role in the optimization method serving as the coarse/surrogate mode. The accuracy of the coarse model is critical in the space mapping to guarantee fast convergence. Good results are

achieved combining the developed circuit model with ISM technique. Only three iterations are needed to get the optimized solution.

The design is fabricated using a low cost PCB-based technology. Good agreement between the measured results and the simulated results is obtained. The first prototype shows a maximum gain of 13 dBi, and a side lobe level (*SLL*) of -10 dB. The distance between the two middle elements around the center feeding slot affects the *SLL*. After reducing this distance in the second fabricated prototype, the *SLL* is improved to -12 dB.

In this work, important contributions to the development of SIW-based DRA for millimeter wave applications are achieved. To the best our knowledge, this is the first attempt to extract and model the mutual coupling in a fully adjustable circuit model. The simple and fast model is further combined with full wave solver for space mapping optimization of complex antenna arrays. New designs of SIW-DRA arrays are developed using the modeling and optimization techniques.

The future work of this thesis can be carried out in the following aspects.

1. Both the design concept and the modeling techniques can be extended to two dimensional SIW-DRA arrays operating in the millimeter wave frequency range. Although promising, challenges in the modeling/optimization and experimental verifications are expected due to the significantly increased complexity in a two dimensional structure.
2. The modeling and optimization techniques developed in the thesis can be applied to other types of antenna arrays, and other frequency ranges. The

methodologies presented here is not limited to DRA or SIW technologies. Applications in certain types of arrays can be straightforward.

3. As discussed earlier, DRAs offer many advantages in the millimeter frequency range. Other configurations of DRA and designs of array can be further explored for various applications.

References

[1] Petosa and A. Ittipiboon, "Dielectric Resonator Antennas: A Historical Review and the Current State of the Art," *IEEE Antennas Propag. Mag.*, vol. 52, no. 5, pp. 91-116, 2010.

[2] K. Wu, D. Deslandes, and Y. Cassivi, "The substrate integrated circuits-a new concept for high-frequency electronics and optoelectronics," *Telecommunications in Modern Satellite, Cable and Broadcasting Service, TELSIKS*, vol. 1, pp. P-III-P-X, 2003.

[3] W. M. Abdel-Wahab, S. Safavi-Naeini, and D. Busuoic, "A Simple Circuit Model for Milliemeter-Wave Substrate Integrated Waveguide (SIW) Series-Fed Dielectric Resonator Antenna Arrays," in *IEEE Int. Antennas Propag. Symp. Dig., Jun. 2009,Charleston, SC, USA,*.

[4] Robert Bains. "On the Usage of Parasitic Antenna Elements in Wireless Communication Systems," PhD. thesis, Dep. of Electronics and Telecomm., Norwegian University of Science and Technology, Trondheim, May 2008.

[5] H. Wenxin. "Analysis and Design of Substrate Integrated Waveguide Cavity Filter for Microwave & Millimeter Wave Applications." PhD. thesis, École polytechnique, Montreal, Quebec, 2005.

[6] F. Xu, and K. Wu, "Guided-wave and leakage characteristics of substrate integrated waveguide," *IEEE Trans. Microw. Theory Tech.*, vol. 53, pp. 66–73, 2005.

[7] D. M. Pozar, *Microwave Engineering*. New York:Wiley, 2005, pp. 113.

[8] Y. Cassivi, L. Perregrini, P. Arcioni, M. Bressan, K. Wu, and G. Conciauro, "Dispersion characteristics of substrate integrated rectangular waveguide," *IEEE Microw. Wireless Components Lett.*, vol. 12, pp. 333-335, 2002.

[9] W. Che, X. Ji and K. Wu, "Characteristics comparison of substrate-

integrated rectangular waveguide (SIRW) and its equivalent rectangular waveguide," *Microw., Optical Tech. Lett.*, vol. 46, no. 6, pp. 588-592, 2005.

[10] X. Chen, and K. Wu, "Low-loss ultra-wideband transition between conductor-backed coplanar waveguide and substrate integrated waveguide," *in IEEE MTT-S Int. Microw.Symp. Dig.*, pp. 349-352, 2009.

[11] F. Xu, Y. Zhang, W. Hong, K. Wu, and T. Cui, "Finite-difference frequency-domain algorithm for modeling guided-wave properties of substrate integrated waveguide," *IEEE Trans. Microw. Theory Tech.*, vol. 51, no. 11, pp. 2221–2227, 2003.

[12] D. Deslandes, and K. Wu, "Accurate modeling, wave mechanisms, and design considerations of a substrate integrated waveguide," *IEEE Trans. Microw. Theory Tech.*, vol. 54, no. 6, pp. 2516–2526, 2006.

[13] D. Deslandes, and K. Wu, "Design Consideration and Performance Analysis of Substrate Integrated Waveguide Components," *in Europ. Microw. Conf.*, Milan, Italy, 2002, pp. 1-4.

[14] M. Bozzi, M. Pasian, L. Perregrini, and K. Wu, "On the losses in substrate integrated waveguides," in *Europ. Microw. Conf.*, Munich, 2007, pp. 384-387.

[15] R. E. Collin, *Field Theory of Guided Waves*. Piscataway, NJ: IEEE Press, 1990, pp. 441.

[16] M. Bozzi, L. Perregrini, and K. Wu, "Modeling of conductor, dielectric, and radiation losses in substrate integrated waveguide by the boundary integral-resonant mode expansion method," *IEEE Trans. Microw. Theory Tech.*, vol. 56, no. 12, pp. 3153–3161, 2008.

[17] *IEEE Standard Definitions of Terms for Antennas*. IEEE, 1993.

[18] C. A. Balanis, *Antenna theory: analysis and design*. Wiley series in microwave and optical Engineering, 3nd Edition, 2005, pp. 5.

[19] C. G. Christodoulou, and P. F. Wahid, *Fundamentals of Antennas: Concepts and Applications*. vol. 50, SPIE Press, 2001.

[20] A. W. Rudge, *The Handbook of Antenna Design* vol. 2. London: Peter Peregrinus Ltd, 1983.

[21] S. R. Best,"Antenna properties and their impact on wireless system performance," *Cushcraft Corporation, Manchester*, 1998.

[22] M.G. Keller, D. Roscoe, Y.M.M. Antar and A. Ittipiboon, "Active millimetre-wave aperture-coupled microstrip patch antenna array," *Electronics lett.*, vol. 31, no. 1, pp. 2-4, 1995.

[23] D. J. Roscoe, J. Carrie, M. Cuhaci, A. Ittipiboon, L. Shafai, and A. Sebak, "A 30 GHz transmit array for portable communications terminals," *in IEEE Int. Antennas Propag. Symp. Dig.*, 1996, vol. 2, pp. 1116-1119,

[24] R. K. Mongia, and P. Bhartia, "Dielectric resonator antennas-A review and general design relations for resonant frequency and bandwidth," *Int. Journal of Microw. and Millimeter-Wave Computer- Aided Eng.*, vol. 4, pp. 230-246, 1994.

[25] D. Soren, R. Ghatak, R. K. Mishra, and D. R. Poddar, "Dielectric resonator antennas: designs and advances," *Progress In Electromagnetics Research B*, vol. 60, pp. 195–213, 2014.

[26] R. K. Mongia, A. Ittibipoon, and M. Cuhaci, "Low profile dielectric resonator antennas using a very high permittivity material," *Electronics lett.*, vol. 30, no. 17, pp. 1362-1363, 1994.

[27] A. Petosa, and R. Larose. A. Ittipiboon, and M. Cuhaci, "Low profile phased array of dielectric resonator antennas," *in IEEE Int. Phased Array Syst. Tech. Symp. Dig.*,Boston, Massachusetts, USA, pp. 182-185, 1996.

[28] A. Petosa, A. Ittipiboon, and M. Cuhaci, "Low Profile Dielectric Resonator Antenna Arrays for Reflector Feeds," *in Europ. Microw. Conf.*, Munich, 1999, no. 3, pp. 171-174.

[29] Nasimuddin, and K. P. Esselle., "A low-profile compact microwave antenna with high gain and wide bandwidth," *IEEE Trans. Antennas Propag.*, vol. 55, no. 6, pp. 1880-1883, June 2007.

[30] R. Chair, A. A. Kishk and K. F. Lee, "Wideband low profile eye shaped dielectric resonator antennas," *in IEEE Int. Antennas Propag. Symp. Dig.*, Jul. 2005, vol. 3, pp. 582-585,.

[31] R. K. Mongia, "Reduced size metallized dielectric resonator antennas," *in*

IEEE Int. Antennas Propag. Symp. Dig, Montreal, Canada, vol. 4, 1997.

[32] M.T.K. Tam and R.D. Murch, "Half volume dielectric resonator antenna designs," *Electronics Lett.,* vol. 33, no. 23, pp. 1914-1916, 1997.

[33] A. Abumazwed and A.R. Sebak, "Compact dielectric resonator antenna for broadband applications (5.2/5.8 GHz)," *in Europ. Antennas Propag.. Conf.,*, Berlin, pp. 433- 436, 2009.

[34] R. K. Mongia, A. Ittibipoon, and M. Cuhaci, "Measurement of radiation efficiency of dielectric resonator antennas," *IEEE Microw. Guided Wave Lett.,* vol 4, no. 3, pp. 80-82, 1994.

[35] Petosa, Aldo, *Dielectric Resonator Antenna Handbook*. Artech House Publishers, 2007.

[36] D. Cormos, A. Laisne, R. Gillard, F. Le Bolzer, and C. Nicolas, "Compact dielectric resonator antenna for WLAN applications," *Electronics Lett.,* vol. 39, no. 7, pp. 588-590, 2003.

[37] A. Petosa, A. Ittipiboon, Y. M. M. Antar, D. Roscoe, and M. Cuhaci, "Recent advances in dielectric-resonator antenna technology," *IEEE Antennas Propag. Mag.,* vol. 40, no. 3, pp. 35-48,1998.

[38] W. M. Abdel Wahab,S. S. Naeini, and D. Busuioc, "Low cost low profile dielectric resonator antenna (DRA) fed by planar waveguide technology for millimeter-wave frequency applications," *in the Proceeding of the 4th International Conference on Radio and Wirless,*San Diego,USA, 2009.

[39] W. M. Abdel Wahab,S. S. Naeini, and D. Busuioc, "Modeling and Design of Millimeter-Wave High-Factor Parallel Feeding Scheme for Dielectric Resonator Antenna Arrays," *IEEE Antennas Wireless Propag. Lett.,* vol. 10, pp. 53-55, 2011.

[40] A. Rashidian, and L. Shafai, "Low-profile dielectric resonator antennas for millimeter-wave applications," *in IEEE Int. Antenna Tech. Applied Electrom. Symp. Dig., Toulouse,* 2010, pp. 1-2.

[41] K. Gong, and Xue Hui Hu., "Low-Profile Substrate Integrated Dielectric Resonator Antenna Implemented With PCB Process," *IEEE Antennas and Wireless Propag. Lett.,* vol. 13, pp. 1023-1026, 2014.

[42] M. S. Iqbal, K. P. Esselle, "A low-profile dielectric resonator antenna for wideband applications," *in IEEE Int. Antennas Propag. Symp. Dig*., Vancouver, BC, Jul. 2015, pp. 440 – 441.

[43] S. A. Long, M. W. McAllister, and L. C. Shen, "The resonant cylindrical dielectric cavity antenna," *IEEE Trans. Antennas Propag.,* vol. 31, no. 3, pp. 406-412, 1983.

[44] M. W. McAllister, S. A. Long, and G. L. Conway, "Rectangular Dielectric Resonator Antenna," *Electronics Lett.,* vol. 19, pp.218-219, 1983.

[45] K. M. Luk, and K. W. Leung, *Dielectric Resonator Antennas*. Baldock, Hertfordshire, England: Research Studies Press Ltd., 2002.

[46] K.W. hung, K. M. Luk, E. K.Yung, and S. Lai, "Characteristics of a low-profile circular disk DR antenna with very high permittivity," *Electronics Lett.,* vol. 31, no. 6, pp. 417-418, 1995.

[47] B.J. Fasenfest, A.G. Walsh, C.S. De Young, T.F. Kennedy, S.A. Long and J.T. Williams, "Investigation of low profile, conformable, dielectric resonator antennas," *Electronics Lett.,* vol. 39, no. 1, p. 1, 2003.

[48] K.W. Leung, K.Y. Chow, K. M. Luk, and E. K. Yung, "Low-profile circular disk DR antenna of very high permittivity excited by a microstripline," *Electronics Lett.,* vol. 33, no. 12, pp. 1004-1005, 1997.

[49] H. Y. Lo, K.W. Leung, K. M. Luk, and E. K. Yung, "Low profile equilateral-triangular dielectric resonator antenna of very high permittivity," *Electronics Lett.,* vol. 35, no. 25, pp. 2164-2166, 1999.

[50] R. K. Mongia,and A. Ittipiboon, "Theoretical and experimental investigations on rectangular dielectric resonator antennas," *IEEE Trans. Antennas Propag.,*vol. 45, no. 9, pp. 1348-1356, 1997.

[51] K. P. Esselle,"A low-profile rectangular dielectric-resonator antenna,"*IEEE Trans. Antennas Propag.,*vol. 44, no. 9, pp. 1296-1297, 1996.

[52] C. D. Young, and S. A. Long, "Wideband Cylindrical and Rectangular Dielectric Resonator Antennas," *IEEE Antennas and Wireless Propagation Lett.,* vol. 5, pp. 426-429, 2006.

[53] G. P. Junker, A. A. Kishk, and A. W. Glisson, "Input impedance of aperture-

coupled dielectric resonator antennas," *IEEE Trans. Antennas Propag.*, vol. 44, no. 5, pp. 600, 1996.

[54] G. P. Junker, A. A. Kishk, and A. W. Glisson,"Input impedance of dielectric resonator antennas excited by a coaxial probe," *IEEE Trans. Antennas Propag.*, vol. 42, no. 7, pp. 960-966, 1994.

[55] L. Huitema and T. Monediere, "Dielectric Materials for Compact Dielectric Resonator Antenna Applications," INTECH. Available: http://www.intechopen.com/books/dielectric-material/dielectric-materials-for-compact-dielectric-resonator-antenna-applications[2012].

[56] K. W. Leung, K. M. Luk, K. Y. A. Lai, and D. Lin, "Theory and experiment of a coaxial probe fed hemispherical dielectric resonator antenna," *IEEE Trans. Antennas Propag.*,vol. 41, no.10, pp. 1390-1398, 1993.

[57] R. A. Kranenburg, and S. A. Long,"Microstrip transmission line excitation of dielectric resonator antennas," *Electronics Lett.*, vol. 24, no. 18, pp. 1156-1157, 1988.

[58] A. Petosa, R.K. Mongia, A. Ittipiboon and J.S. Wight, "Design of microstrip-fed series array of dielectric resonator antennas," *Electronics lett.*, vol. 31, no. 16, pp. 1306-1307, 1995.

[59] R. A. Kranenburg, S. A. Long, and J. T. Williams, "Coplanar waveguide excitation of dielectric resonator antennas," *IEEE Trans. Antennas Propag.*, vol. 39, no. 1, pp. 119-122, 1991.

[60] S. M. Deng, T. W. Chen, and H. H. Kan, "A CPW-fed rectangular dielectric resonator antenna," *IEEE Microw. Conf. Asia-Pacific, APMC.*, Taipei, Taiwan, 2001, vol. 2, pp. 954-957.

[61] S. Lin, S. Gigoyan, J. Wilson, and A. E Fathy, "Dielectric Resonator Antennas fed by Image Guide Lines," *in IEEE Int. Antennas Propag. Symp. Dig.,* Albuquerque, NM, 2006, pp. 2205-2208.

[62] A. S. Al-Zoubi, A. A. Kishk, and A. W. Glisson, 'Aperture coupled rectangular dielectric resonator antenna array fed by dielectric image guide," *IEEE Trans. Antennas Propag.*, vol. 57, no. 8, pp. 2252-2259, 2009.

[63] M. T. Birand, and R. V. Glesthorpe, "Experimental millimetric array using

dielectric radiators fed by means of dielectric waveguide," *Electronics Lett.*, vol. 17, no. 18, pp. 633 – 635, 1981.

[64] Z. C. Haol, W. Hong, A. Chen, J. Chen, K. Wu, "SIW fed dielectric resonator antennas (SIW-DRA)," *in IEEE Int. Microw. Symp. Dig.*, San Francisco, CA, 2006, pp. 202 – 205.

[65] Q. Lai, C. Fumeaux, W. Hong, and R. Vahldieck, "60 GHz aperture-coupled dielectric resonator antennas fed by a half-mode substrate integrated waveguide," *IEEE Trans. Antennas Propag.*, vol. 58, no. 6, pp. 1856-1864, 2010.

[66] W. M. Abdel-Wahab, S. Safavi-Naeini, and D. Busuoic, "SIW-series fed RDRA array system for millimeter-wave applications," *in the Proceeding of the 3rd European Conf. Antenna Propag.*, March,Berlin, Germany 2009.

[67] W. M. Abdel-Wahab, S. Safavi-Naeini, and D. Busuoic, "Low cost planar waveguide technology-based dielectric resonator antenna (DRA) for millimeter-wave applications: Analysis, design, and fabrication," *IEEE Trans. Antennas Propag.*,vol. 58, no. 8, pp. 2499-2507, 2010.

[68] W. M. Abdel-Wahab, S. S. Naeini, and D. Busuoic, "Millimeter-wave high radiation efficiency planar waveguide series-fed dielectric resonator antenna (DRA) array: analysis, design, and measurements," *IEEE Trans. Antennas Propag.*,vol. 59, no. 8, pp. 2834-2843, 2011.

[69] J. W. Bandler, R. M. Biernack, S. H. Chen, P. A. Grobelny, Ronald H. Hemmers,"Space mapping technique for electromagnetic optimization," *IEEE Trans. Microw. Theory Tech.*, vol. 42, no. 12, pp. 2536-2544, 1994.

[70] M. H. Bakr, J. W. Bandler, R. M. Biernack, S. H. Chen, K. Madsen, "A trust region aggressive space mapping algorithm for EM optimization," *IEEE Trans. Microw. Theory Tech.*, vol. 46, no. 12, pp. 2412-2425, 1998.

[71] J. W. Bandler, Q. Cheng, D. H. Gebre-Mariam, K. Madsen, F. Pedersen and J. Sondergaard, "EM-based surrogate modeling and design exploiting implicit, frequency and output space mappings," *in IEEE Int. Microw. Symp. Dig.*, Philadelphia, USA, vol. 2, 2003, pp. 1003–1006.

[72] S. Koziel, J. W. Bandler, A. S. Mohamed, and K. Madsen, "Enhanced

surrogate models for statistical design exploiting space mapping technology," *in IEEE Int. Microw. Symp. Dig.*, 2005.

[73] J. Zhu, J. W. Bandler, N. K. Nikolova,and S. Koziel, "Antenna optimization through space mapping," *IEEE Trans. Antennas Propag.*,vol. 55, no. 3, pp. 651-658, 2007.

[74] S. Amari, C. LeDrew, and M. Menzel, "Space-mapping optimization of planar coupled-resonator microwave filters," *IEEE Trans. Microw. Theory Tech.*, vol. 54, no. 5, pp. 2153-2159, 2006.

[75] G. Minatti, M. Faenzi, E. Martini,F. Caminita, P. De Vita, D. González-Ovejero,M. Sabbadini, and S. Maci, "Modulated metasurface antennas for space: synthesis, analysis and realizations," *IEEE Trans. Antennas Propag.*,vol. 63, no. 4, pp. 1288-1300, 2015.

[76] Q. Cheng, J. W. Bandler, and S. Koziel, "Combining coarse and fine models for optimal design," *IEEE Microw.Mag.*,vol. 9, no. 1,pp. 79-88, 2008.

[77] M. H. Bakr, J. W. Bandler, K. Madsen, and J. Ssndergaard,"An introduction to the space mapping technique," *Optimization and Engineering*, vol. 2, no. 4, pp. 369-384, 2001.

[78] M. H. Bakr, J. W. Bandler, K. Madsen, J. E. Rayas-Sánchez, and J. Ssndergaard, "Space-mapping optimization of microwave circuits exploiting surrogate models," *IEEE Trans. Microw. Theory Tech.*, vol. 48, no. 12, pp. 2297-2306, 2000.

[79] Jie Meng. "Microwave circuit optimization exploiting tuning space mapping," M.A. thesis, McMaster University, Hamilton, Ontario, 2008.

[80] J. W. Bandler, Q. Cheng, Sameh A. Dakroury, A. S. Mohamed, M. H. Bakr, K. Madsen, and J. Sondergaard,"Space mapping: the state of the art," *IEEE Trans. Microw. Theory Tech.*,vol. 52, no. 1, pp. 337-361, 2004.

[81] J. W. Bandler, Q. Cheng, N. K. Nikolova,and M. A. Ismail, "Implicit space mapping optimization exploiting preassigned parameters," *IEEE Trans. Microw. Theory Tech.*,vol. 52, no. 1, pp. 378-385, 2004.

[82] J. W. Bandler, and Q. Cheng, "New developments in space mapping CAD technology," *Proc. China-Japan Joint Microw. Conf*. 2006.

[83] M. Abdallah, Y. Wang, W. Abdel-Wahab, S. Safavi-Naeini, and J. Liu, "A simple circuit model including mutual coupling for dielectric resonator antenna array," *in IEEE Int. Antennas Propag. Symp. Dig. (APS/URSI),* Memphis, TN, pp. 1944-1945, July 2014.

[84] M. Abdallah, Y. Wang, W. Abdel-Wahab, and S. Safavi-Naeini, "Modeling of substrate integrated waveguide series fed dielectric resonator antenna array with longitudinal slots excitation," *in IEEE Int. Antennas Propag. Symp. Dig. (APS/URSI),* Vancouver, BC, pp. 35-36, July 2015.

[85] M. Abdallah, Y. Wang, W. Abdel-Wahab, and S. Safavi-Naeini, "A Tunable Circuit Model for the Modeling of Dielectric Resonator Antenna Array," *IEEE Antennas Wireless Propag. Lett.*, vol. 15, pp. 830-833, 2016.

[86] J.-S. Hong, and M. J. Lancaster, *Microstrip Filters for RF/Microwave Applications*, Wiley series in microwave and optical Engineering, Wily-Inter science, 2nd Edition, 2001, pp. 17.

[87] M. R. Nikkhah, J. R. Mohassel, and A. A. Kishk, "Compact wideband rectangular dielectric resonator antenna with parasitic elements and air gaps," *Progress In Electromagnetics Research Lett.*, vol. 42, pp. 129-139, 2013.

[88] R. N. Simons, and R. Q. Lee, "Effect of parasitic dielectric resonators on CPW/aperture-coupled dielectric resonator antennas," *Proc. IEE Microw., Antennas, Propag.*,vol. 140, no. 5, pp 336-338, 1993.

[89] Z. Fan, Y.M.M. Antar, A. Ittipiboon and A. Petosa, "Parasitic coplanar three-element dielectric resonator antenna subarray," *Electronics Lett.*, vol. 32, no. 9, pp. 789-790, 1996.

[90] M. R. Nikkhah, J. R. Mohassel, and A. A. Kishk, "High-gain aperture coupled rectangular dielectric resonator antenna array using parasitic elements," *IEEE Trans. Antennas Propag.*,vol. 61, no. 7, pp. 3905-3908, 2013.

[91] L.Yan, W. Hong, , G. Hua, , J. Chen, , K. Wu, and T. J. Cui, "Simulation and experiment on SIW slot array antennas," *IEEE Microwave Wireless Compon. Lett.*,vol. 14, no. 9, pp. 446-448, 2004.

[92] D. Y. Kim, W. S. Chung, C. H. Park, S. J. Lee, and S. Nam, "A series slot array antenna for 45º-inclined linear polarization with SIW technology," *IEEE Trans. Antennas Propag.*,vol. 60, no. 4, pp. 1785-1795, 2012.

[93] H. Zhou,and W. Hong, "45º Linearly Polarized Resonant Slot Array Antenna Based on Substrate Integrated Waveguide," *Asia-Pacific Microw. Conf.*, 2007.

[94] S. Park, Member, Y. Okajima, J. Hirokawa, and M. Ando, "A slotted post-wall waveguide array with interdigital structure for 45 linear and dual polarization," *IEEE Trans. Antennas Propag.*, vol. 53, no. 9, pp. 2865-2871, 2005.

[95] D. Y. Kim, W. Chung, C. Park, S. Lee, and S. Nam,"Design of a 45-Inclined SIW Resonant Series Slot Array Antenna for *Ka* Band," *IEEE Antennas Wireless Propag. Lett.*, vol. 10, pp. 318-321, 2011.

[96] M. Saed and R. Yadla,"Microstrip-Fed Low Profile And Compact Dielectric Resonator Antennas*,"Progress In Electromagnetics Research, PIER*, vol. 56, pp. 151–162, 2006.

[97] A. G. Williamson, "Coaxially fed hollow probe in a rectangular waveguide," *Proc. IET Microw., Antennas, Propag.*,vol. 132, no. 5, pp. 273 – 285, 1985.

[98] A. G. Williamson, "Analysis and modelling of a coaxial-line/rectangular-waveguide junction," *Proc. IEE Microw., Optics, Antennas,*vol. 129, no. 5, pp. 262-270, 1982.

[99] R. B. Keam, and A. G. Williamson, "Broadband design of coaxial line/rectangular waveguide probe transition," *Proc. IEE Microw., Antennas, Propag.*,vol. 141, no. 1, pp. 1350-2417, 1994.

[100] T. Kai, J. Hirokawa, M. Ando, H. Nakano, Y. Hirachi, "ACoaxial Line to Post-Wall Waveguide Transition for a Cost-Effective Transformer between a RF-Device and a Planar Slot-Array Antenna in 60-GHz Band," *IEICE Trans. Commun.*, vol. E89–B, no. 5, pp. 1646-1653, 2006.

[101] W. Abdel-Wahab, Y. Wang, and S. Safavi-Naeini, "SIW Hybrid Feeding Network-Integrated 2D DRA Array: Simulations and Experiments," *IEEE*

Antennas and Wireless Propag. Lett., vol. 15, pp. 548-551, 2016.